OF COLLEGE ENGINEERING

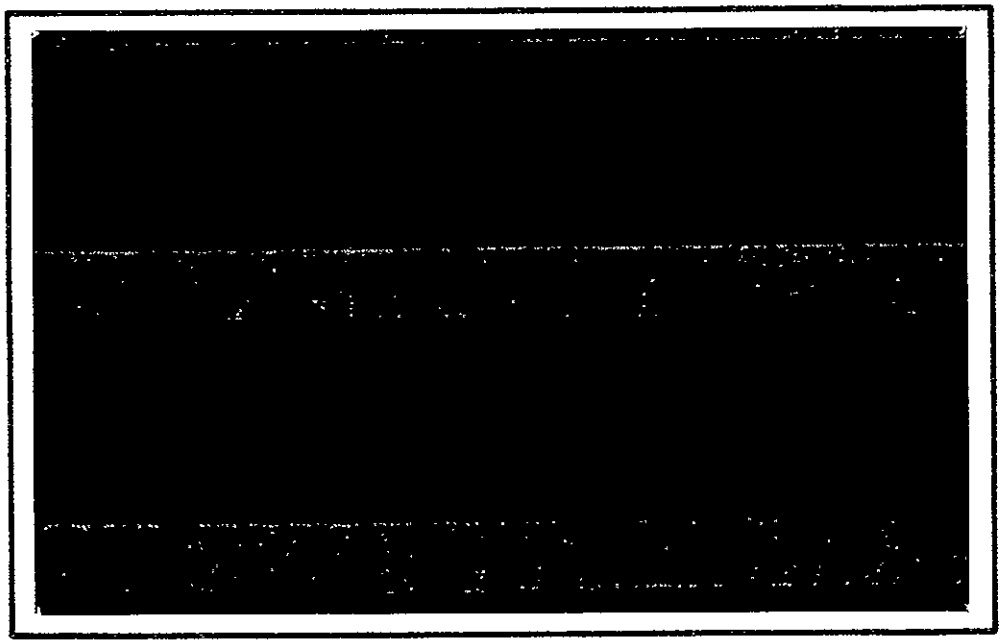

VIRGINIA POLYTECHNIC INSTITUTE AND STATE UNIVERSITY

BLACKSBURG, VIRGINIA

BIBLIOGRAPHIC DATA SHEET	1. Report No. VPI-E-75-7	2.	3. Recipient's Accession No. N76-24407
4. Title and Subtitle RATE AND TIME DEPENDENT BEHAVIOR OF STRUCTURAL ADHESIVES			5. Report Date April, 1976 6.
7. Author(s) Michael P. Renieri, Carl T. Herakovich & Halbert F. Brinson			8. Performing Organization Rept. No. VPI-E-76-7
9. Performing Organization Name and Address Virginia Polytechnic Institute and State University Engineering Science and Mechanics Blacksburg, Virginia 24061			10. Project/Task/Work Unit No. 11. Contract/Grant No. NGR 47-004-090
12. Sponsoring Organization Name and Address National Aeronautics & Space Administration Langley Research Center Hampton, Virginia .23665			13. Type of Report & Period Covered 14.

15. Supplementary Notes

16. Abstracts

see page i

17. Key Words and Document Analysis. 17a. Descriptors

adhesive
rate effects
stress-whitening
elastic
visco-elastic
plastic
visco-plastics creep
relaxation
Ramberg-Osgood
Bingham model
unloading behavior

17b. Identifiers/Open-Ended Terms

17c. COSATI Field/Group

18. Availability Statement	19. Security Class (This Report)	21.
Distribution unlimited	UNCLASSIFIED	
	20. Security Class (This Page) UNCLASSIFIED	22.

INSTRUCTIONS FOR COMPLETING FORM NTIS-35 (Bibliographic Data Sheet based on COSATI Guidelines to Format Standards for Scientific and Technical Reports Prepared by or for the Federal Government, PB-180 600).

1. **Report Number.** Each individually bound report shall carry a unique alphanumeric designation selected by the performing organization or provided by the sponsoring organization. Use uppercase letters and Arabic numerals only. Examples FASEB-NS-73-87 and FAA-RD-73-09.

2. Leave blank.

3. **Recipient's Accession Number.** Reserved for use by each report recipient.

4. **Title and Subtitle.** Title should indicate clearly and briefly the subject coverage of the report, subordinate subtitle to the main title. When a report is prepared in more than one volume, repeat the primary title, add volume number and include subtitle for the specific volume.

5. **Report Date.** Each report shall carry a date indicating at least month and year. Indicate the basis on which it was selected (e.g., date of issue, date of approval, date of preparation, date published).

6. **Performing Organization Code.** Leave blank.

7. **Author(s).** Give name(s) in conventional order (e.g., John R. Doe, or J.Robert Doe). List author's affiliation if it differs from the performing organization.

8. **Performing Organization Report Number.** Insert if performing organization wishes to assign this number.

9. **Performing Organization Name and Mailing Address.** Give name, street, city, state, and zip code. List no more than two levels of an organizational hierarchy. Display the name of the organization exactly as it should appear in Government indexes such as Government Reports Index (GRI).

10. **Project/Task/Work Unit Number.** Use the project, task and work unit numbers under which the report was prepared.

11. **Contract/Grant Number.** Insert contract or grant number under which report was prepared.

12. **Sponsoring Agency Name and Mailing Address.** Include zip code. Cite main sponsors.

13. **Type of Report and Period Covered.** State interim, final, etc., and, if applicable, inclusive dates.

14. **Sponsoring Agency Code.** Leave blank.

15. **Supplementary Notes.** Enter information not included elsewhere but useful, such as: Prepared in cooperation with . . . Translation of . . . Presented at conference of . . . To be published in . . . Supersedes . . . Supplements . . . Cite availability of related parts, volumes, phases, etc. with report number.

16. **Abstract.** Include a brief (200 words or less) factual summary of the most significant information contained in the report. If the report contains a significant bibliography or literature survey, mention it here.

17. **Key Words and Document Analysis. (a). Descriptors.** Select from the Thesaurus of Engineering and Scientific Terms the proper authorized terms that identify the major concept of the research and are sufficiently specific and precise to be used as index entries for cataloging.
(b). Identifiers and Open-Ended Terms. Use identifiers for project names, code names, equipment designators, etc. Use open-ended terms written in descriptor form for those subjects for which no descriptor exists.
(c). COSATI Field/Group. Field and Group assignments are to be taken from the 1964 COSATI Subject Category List. Since the majority of documents are multidisciplinary in nature, the primary Field/Group assignment(s) will be the specific discipline, area of human endeavor, or type of physical object. The application(s) will be cross-referenced with secondary Field/Group assignments that will follow the primary posting(s).

18. **Distribution Statement.** Denote public releasability, for example "Release unlimited", or limitation for reasons other than security. Cite any availability to the public, other than NTIS, with address, order number and price, if known.

19 & 20. **Security Classification.** Do not submit classified reports to the National Technical Information Service.

21. **Number of Pages.** Insert the total number of pages, including introductory pages, but excluding distribution list, if any.

22. **NTIS Price.** Leave blank.

SECURITY CLASSIFICATION OF THIS PAGE *(When Data Entered)*

REPORT DOCUMENTATION PAGE

READ INSTRUCTIONS BEFORE COMPLETING FORM

1. REPORT NUMBER: VPI-E-76-7	2. GOVT ACCESSION NO.
3. RECIPIENT'S CATALOG NUMBER: N76-24407	
4. TITLE *(and Subtitle)*: RATE AND TIME DEPENDENT BEHAVIOR OF STRUCTURAL ADHESIVES	5. TYPE OF REPORT & PERIOD COVERED
	6. PERFORMING ORG. REPORT NUMBER: VPI-E-76-7
7. AUTHOR(s): Michael P. Renieri, Carl T. Herakovich, Halbert F. Brinson	8. CONTRACT OR GRANT NUMBER(s): NGR-47-004-090
9. PERFORMING ORGANIZATION NAME AND ADDRESS: Virginia Polytechnic Institute and State University, Engineering Science and Mechanics, Blacksburg, Virginia 24061	10. PROGRAM ELEMENT, PROJECT, TASK AREA & WORK UNIT NUMBERS
11. CONTROLLING OFFICE NAME AND ADDRESS: National Aeronautics & Space Administration, Langley Research Center, Hampton, Virginia 23665	12. REPORT DATE: April, 1976
	13. NUMBER OF PAGES: 140
14. MONITORING AGENCY NAME & ADDRESS *(if different from Controlling Office)*: Virginia Polytechnic Institute and State University, Engineering Science and Mechanics, Blacksburg, Virginia 24061	15. SECURITY CLASS. *(of this report)*: Unclassified
	15a. DECLASSIFICATION/DOWNGRADING SCHEDULE

16. DISTRIBUTION STATEMENT *(of this Report)*

Approved for public release; distribution unlimited

17. DISTRIBUTION STATEMENT *(of the abstract entered in Block 20, if different from Report)*

Approved for public release; distribution unlimited

18. SUPPLEMENTARY NOTES

19. KEY WORDS *(Continue on reverse side if necessary and identify by block number)*

adhesive, rate effects, stress-whitening, elastic, visco-elastic, plastic, visco-plastics creep, relaxation, Ramberg-Osgood, Bingham model, unloading behavior.

20. ABSTRACT *(Continue on reverse side if necessary and identify by block number)*

See page i

DD FORM 1 JAN 73 1473 EDITION OF 1 NOV 65 IS OBSOLETE

SECURITY CLASSIFICATION OF THIS PAGE *(When Data Entered)*

College of Engineering
Virginia Polytechnic Institute and State University
Blacksburg, Virginia 24061

VPI-E-76-

April, 1976

Rate and Time Dependent Behavior of Structural Adhesives

Michael P. Renieri
Carl T. Herakovich
Halbert F. Brinson

Department of Engineering Science and Mechanics

This work constituted Dr. Renieri's Ph.D. dissertation.

Supported by NASA Grant NGR 47-004-090

(ABSTRACT)

Studies on two adhesives (Metlbond 1113 and 1113-2) identified as having applications in the bonding of composite materials are presented. Constitutive equations capable of describing changes in material behavior with strain rate are derived from various theoretical approaches. It is shown that certain unique relationships exist between these approaches. It is also shown that the constitutive equation derived from mechanical models can be used for creep and relaxation loading.

Modifications to the constitutive equations for constant strain rate loading are proposed. Nonlinear constitutive equations are derived using a nonlinear perturbation technique in conjunction with a modified Bingham model. Using the modified Bingham model, constitutive equations describing loading-unloading behavior are also proposed.

The stress-strain behavior of the adhesives is shown to be significantly rate dependent. Further it is shown that a rate dependent stress-whitening (crazing) phenomenon occurs prior to the maximum stress. A region of elastic behavior, a rate and time dependent region, and a region of perfectly plastic flow are identified in the stress-strain behavior. Information regarding variations of Poisson's ratio with rate and time is also presented.

The elastic limit stress and strain, and maximum stress are shown to be rate dependent and agree well with an empirical equation pro-

posed by Ludwik. Analytical predictions based on modified Ramberg-Osgood equations are shown to agree well with experimental stress-strain-strain rate results. It is shown that the coefficients of these equations are different before and after stress-whitening due changes in the properties of the adhesives. Analytical predictions based on the modified Bingham model are shown to agree well with the constant strain rate results. It is also shown that the nonlinear model indicates that the coefficients of the modified Bingham model may vary due to the change in material properties before and after stress-whitening.

A creep to failure phenomenon is shown to exist and is correlated with a delayed yield equation proposed by Crochet. Loading-unloading results are presented and are shown to correlate well with the proposed form of the loading-unloading equations for the modified Bingham model.

Experimental results obtained for relaxation tests above and below the glass transition temperature are presented. It is shown that the adhesives obey the time-temperature superposition principle.

ACKNOWLEDGEMENT

This work was supported by NASA's Langley Research Center under NASA Grant NGR 47-004-090. Dr. John G. Davis, Jr. was the NASA technical monitor and his assistance in the conduct of this work is gratefully acknowledged.

The authors also appreciate and acknowledge Mr. Dale Black of Narmco Whittaker for supplying adhesive materials and Messers. Kenneth McCauley, Robert Davis and Archie Montgomery of the Engineering Science and Mechanics Shop for their helpful suggestions and assistance in the experimental phase of the research. Finally, thanks are due to Mrs. Peggy Epperly for typing the manuscript.

TABLE OF CONTENTS

LIST OF FIGURES

LIST OF TABLES

LIST OF SYMBOLS

A, B, C, C'	material constants
C_1, C_2	constants in WLF equation
E	elastic modulus
E_o	linear coefficient of elastic modulus
F	yield condition
G	shear modulus
$H(t)$	unit step function
J_2	second invariant of the stress deviation
$\overline{K}$	bulk modulus
K, K_1, K_2	material constants
R	constant
S_{ij}, $\dot{S}_{ij}$	deviatoric stress and deviatoric stress rate tensors
S_1	perturbation coefficient
T	temperature
T_o	reference temperature
T_g	glass transition temperature
Y	maximum stress
Y', Y''	material constants
a, b, c, d	material constants
a_T	shift factor
e_{ij}, $\dot{e}_{ij}$	deviatoric strain and deviatoric strain rate tensors
$\dot{e}_{ij}^{E}$	deviatoric elastic strain rate
$\dot{e}_{ij}^{P}$	plastic strain rate (viscoplastic component)

k	yield stress in simple shear
n, n_1, n_2	material constants
t	time
t'	time at temperature T_o
γ, γ^o, $\bar{\gamma}$	material constants
γ_E, γ_μ	dimensionless constants
δ_{ij}	Kronecker delta
ε, $\dot{\varepsilon}$	one-dimensional strain and strain rate
ε_{ij}, $\dot{\varepsilon}_{ij}$	strain and strain rate tensors
ε_{ij}^E, ε_{ij}^P	elastic and plastic strains
ε_E, ε_p	one-dimensional elastic and plastic strains
ε_μ	strain in viscous element (dashpot)
$\dot{\varepsilon}_E$, $\dot{\varepsilon}_\mu$	one-dimensional elastic and viscous strain rates
ε_o	elastic limit strain
ε_o', ε_o'', $\dot{\varepsilon}'$	material constants
$\bar{\varepsilon}_o$	level of constant strain in relaxation test
θ	elastic limit stress (yield stress) in simple tension
θ', θ''	material constants
λ	inverse of τ
μ	viscosity coefficient
μ_o	linear coefficient of viscosity coefficient
ν	Poisson's ratio
ρ	density
σ_{ij}	stress tensor
σ	one-dimensional stress

σ^*	as defined on page 58
σ_0, σ_1	perturbation coefficients
$\bar{\sigma}_0$	level of constant stress in creep test
τ	relaxation time
$\Phi(F)$	generalized yield function
ϕ	scalar function of the invariants of the stress tensor
χ	as defined by Eq. (6.1.3)
Ψ, ψ	scalar functions of the invariants of the stress tensor

Chapter 1

INTRODUCTION

Adhesives are currently being used in a wide variety of structural applications. This is especially true for structures made using advanced composites. Adhesive bonding has proven to be a viable method of assembling composite joints, however the overall performance of an adhesively bonded structural composite cannot be predicted accurately unless the role of the adhesive joint is fully understood.

It has been pointed out that the process of adhesion can be divided into two types; mechanical adhesion and specific adhesion [1].* The former describes the process of the adhesive solidifying in the pores of the two adherent surfaces and the latter describes the process of attractive intermolecular forces between molecules of even the smoothest solids. For mechanical adhesion, Bowers and Zisman [1] state that if ideal conditions (i.e., complete wetting and freedom from the formation of gas pockets and inclusions) prevail, the joint must fail in cohesion rather than adhesion. That is, failure is in the bulk phase rather than at the adherend/adhesive interface. Since bulk or cohesive failure is a likely failure mode, the present study is an effort to identify bulk or cohesive stress-strain, strain-rate, creep, relaxation, yield and/or failure properties of typical structural

---

*Numbers in brackets [ ] refer to the references listed in the Bibliography.

adhesives. This is in contrast to the work of others regarding the viscoelastic behavior of adhesives [2] where the adhesives were tested in the bonded state.

A complete analysis of the stress distribution in adhesively bonded structural composite joints must include rate and time dependent material properties when these are significant. Adhesive materials, which are frequently molecular high polymers, generally exhibit significant rate and time dependence that must be considered in a reliable failure analysis. The phenomenological behavior of the adhesives in bulk form is considered to be of prime importance in this study. The extent to which bulk properties can be related to properties in the bonded state is as yet undetermined. However, it is reasonable to assume that if adhesive materials exhibit rate and time dependent properties in bulk form, time effects will also be important in the bonded state. In addition, this study may give insight into rate and time dependent behavior of some matrix materials used in advanced composites as they are frequently similar in composition to the adhesives investigated herein.

With the advent of computer oriented analytical techniques to study the behavior of complex structural problems, it is now possible to observe the effects of the plastic and viscoelastic properties of the constituent materials. The performance of a structural system is predicted from the mechanical properties of the materials employed. If the environment causes strain rates above the static rate, the resulting effects on modulus, strength, and ductility must be understood.

An analytical description of mechanical behavior by a suitable constitutive equation accounting for property changes with strain rate becomes necessary for accurate response calculations.

The materials under investigation in this study are Narmco Whittaker's Metlbond 1113 and 1113-2 adhesives. These adhesives are currently being used in composite bonding applications. Initial investigations indicated that the adhesives exhibited strain rate effects with respect to elastic limit stress and maximum stress. For a given strain rate, a region of linear elasticity and a region of inelastic behavior followed by perfectly plastic flow at the maximum stress to failure was observed for both adhesives (these results can be found in Reference 3). It was also observed that a "stress-whitening" phenomenon occurred prior to failure. The constitutive equations describing these materials should include as many of these rate and time dependent properties as possible.

The second chapter of this dissertation is devoted to selecting the final constitutive forms to be further analyzed. A review of constitutive equations derived from various theoretical approaches is presented. These are deformation theories, incremental theories, and mechanical models. It is shown that certain unique relationships exist between these approaches. The final section of this chapter concerns the use of the constitutive equation derived from mechanical models for creep and relaxation loading.

Chapter three outlines proposed modifications to the constitutive equations. A nonlinear perturbation technique developed by Davis [4]

used in conjunction with the constitutive equation derived from mechanical models is reviewed. The use of this same mechanical model for loading-unloading considerations is also reviewed.

Chapter four describes the experimental considerations. The materials selected for study and specimen features are reviewed. A description is also given of the experimental apparatus used for the various types of tests conducted.

The fifth chapter is concerned with the constant strain rate results and the ability of the constitutive equations selected to model this behavior. It will be shown that during the constant strain rate testing a "stress-whitening" or "crazing" phenomenon occurs prior to the maximum stress. The effect of this phenomenon on the constitutive equations is reviewed. It is also shown that the perturbation technique developed by Davis yields significant information relative to the behavior of the adhesives above and below the "stress-whitening" point.

Chapter six concerns the ability of the constitutive equation derived from mechanical models to predict the behavior of Metlbond 1113 and 1113-2 for creep and relaxation as well as other more complex loading histories. This chapter includes comparisons between theoretical predictions and experimental results for two different loading histories.

Since bonded composite structures are often subjected to high temperature environments, the behavior of the adhesive at high temperatures is also important. Chapter seven presents the experimental results obtained for relaxation tests above and below the glass

transition temperature. Theoretical considerations relative to the time-temperature superposition principle are presented.

The final chapter presents the conclusions and indicates areas for future research.

Chapter 2

CONSTITUTIVE EQUATIONS

This chapter reviews the development of constitutive equations which have been used previously to model rate and time dependent material behavior. These equations were derived from several approaches; deformation theories, incremental theories, and mechanical models.

It is shown that certain unique relationships exist between the final form of the constitutive equations derived from incremental theories and that derived from mechanical models. It is also shown that constitutive equations proposed on the basis of experimental observations by early investigators can be derived from recent theories and mechanical models. The final section of this chapter concerns the constitutive equation derived from mechanical models for creep and relaxation loading.

2.1 Terminology

During the development of the constitutive equations certain terms such as viscoelastic, viscoplastic, yield stress, and work-hardening are used. Therefore, before proceeding into the various approaches these terms are discussed.

The stress-strain diagram shown in Fig. 1(a) is representative of the materials studied herein. It is assumed that this response

would be obtained if the material were loaded or unloaded at a constant rate. Several different types of analytical approaches to the characterization of such stress strain response are given. In each, the parameters θ and Y have different meaning and the general approach to the representation of the region beyond θ is different in each case.

The modified Bingham model or linear viscoelastic-plastic mechanical model of Fig. 1(b) is used in which θ is an elastic limit stress and Y is a yield stress. The material is linear elastic below θ, linearly viscoelastic between θ and Y and perfectly plastic above Y.

A non-linear viscoelastic modified Bingham model is also discussed. For this model the material is elastic below θ, nonlinearly viscoelastic between θ and Y and perfectly plastic above Y.

In all other instances (i.e., the Ramberg-Osgood approach and much of the discussion of literature), the material is assumed to be elastic below θ, strain hardening plastic (including time effects) between θ and Y and perfectly plastic beyond Y.

Without exception all comparisons between theory and experiment are made using either the linear viscoelastic-plastic modified Bingham model or the non-linear modified Ramberg-Osgood model.

The term viscoplastic will refer to rate effects occuring in the plastic region. Perzyna [5] defined an "elastic-viscoplastic" material as having rate effects in both the elastic and plastic regions. In contrast an "elastic/viscoplastic" material was defined as having rate effects in the plastic region only. This terminology has been adopted for this study.

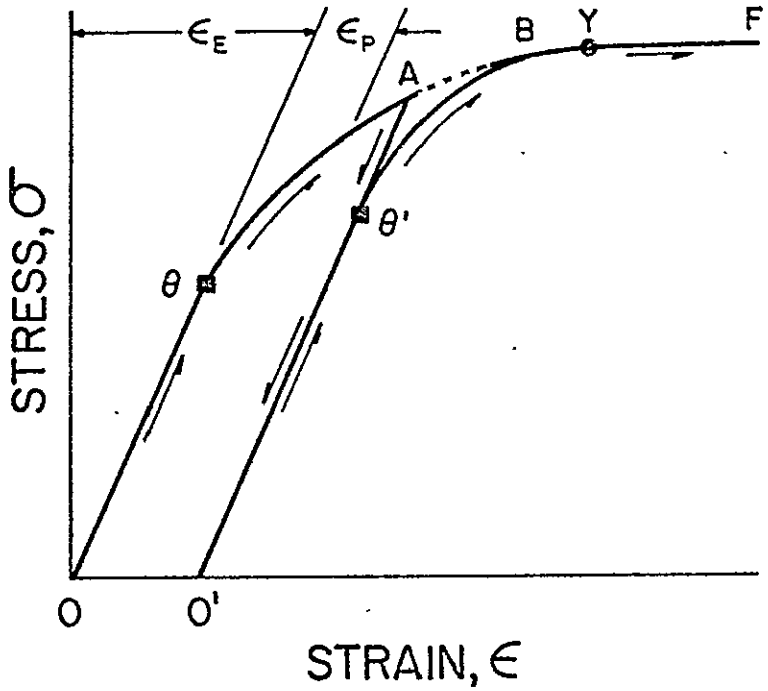

a. STRESS - STRAIN CURVE

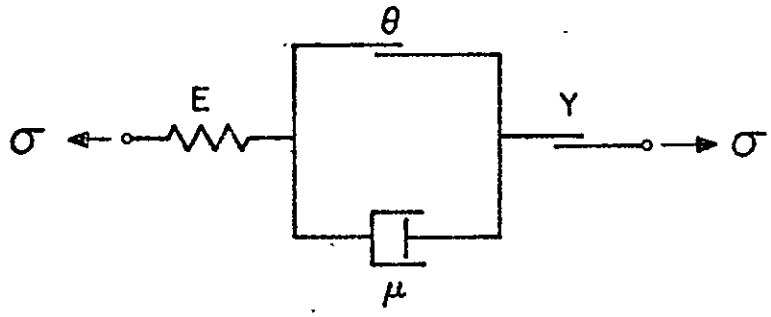

b. MODIFIED BINGHAM MODEL

Figure 1. Stress-Strain Curve and Modified Bingham Model

2.2 Deformation Theories

In 1924, Hencky [6] proposed stress-stress relations whereby the plastic strains are functions of the current state of stress and are independent of the loading history. Such theories are called total or deformation theories. Hencky's relations, as given by Kachanov [7] are,

$$\varepsilon_{ij} = \frac{\sigma_{mm}}{9\bar{K}} \delta_{ij} + \Psi S_{ij} \tag{2.2.1}$$

where $\bar{K} = E/3(1 - 2\nu)$ is the bulk modulus and E and ν are the elastic modulus and Poisson's ratio, respectively. The term Ψ is a scalar function of the invariants of the stress tensor as indicated by Hill [8]. The parameters σ_{ij}, ε_{ij}, and S_{ij} represent the stress, strain, and deviatoric stress tensors, respectively.

For Ψ = constant = $1/2G$, where $G = E/2(1 + \nu)$ is the shear modulus, Eq. (2.2.1) reduces to the elastic stress-strain relations. However, if $\Psi = 1/2G + \psi$, the strain components are then the sum of elastic components, ε_{ij}^{E}, and plastic components, ε_{ij}^{P}, and Eq. (2.2.1) becomes,

$$\varepsilon_{ij} = \frac{\sigma_{mm}}{9\bar{K}} \delta_{ij} + \frac{S_{ij}}{2G} + \psi S_{ij} \tag{2.2.2}$$

or

$$\varepsilon_{ij} = \varepsilon_{ij}^{E} + \varepsilon_{ij}^{P} \tag{2.2.3}$$

where

$$\varepsilon_{ij}^{E} = \frac{\sigma_{mm}}{9\bar{K}} \delta_{ij} + \frac{S_{ij}}{2G} \tag{2.2.4}$$

$$\varepsilon_{ij}^{P} = \psi S_{ij} \tag{2.2.5}$$

and ψ is a scalar function of the invariants of the stress tensor.

For the case of uniaxial tension, Eq. (2.2.2) reduces to,

$$\varepsilon = \frac{\sigma}{E} + \phi\sigma \tag{2.2.6}$$

where the subscripts have been dropped and $\phi = \frac{2}{3}\psi$.

The function ϕ in Eq. (2.2.6) is often determined empirically in order to fit experimental results.

2.2.1 Ramberg-Osgood Equation

From uniaxial tension and compression results on various metal alloys, Ramberg and Osgood [9] in 1943 proposed an analytical expression of the form,

$$\varepsilon = \frac{\sigma}{E} + K\sigma^{n} \tag{2.2.7}$$

where K and n are material constants. It is evident that Eq. (2.2.7) may be considered as a special case of Eq. (2.2.6) since ϕ is a function of σ.

2.2.2 Modified Ramberg-Osgood Equation

In 1960 McLellan [10] modified Eq. (2.2.7) for rate dependent materials by observing that for many materials n is invariant with strain rate and K and E are simple functions of the strain rate such that,

$$E(\dot{\varepsilon}) = c\dot{\varepsilon}^{d} \tag{2.2.8}$$

and

$$K(\dot{\varepsilon}) = a\dot{\varepsilon}^{b} \qquad (2.2.9)$$

where a, b, c, and d are material constants. Variations in E, K, and n (if such exists for n) indicate different types of material sensitivity to strain rate. Changes in E denote viscoelastic behavior. Both parameters K and n of the plastic strain term represent work-hardening characteristics and variations in these parameters with strain rate can be considered viscoplastic phenomenon. Changes in K show that the relative magnitude of strength is affected by strain rate, whereas changes in the plastic flow behavior are indicated by variations in n.

Substituting Eqs. (2.2.8) and (2.2.9) into Eq. (2.2.7) McLellan obtained the form,

$$\varepsilon = \frac{\sigma}{c\dot{\varepsilon}^{d}} + a\dot{\varepsilon}^{b}\sigma^{n} \qquad (2.2.10)$$

McLellan and Eichenberger [11] in 1967 used an equation of this form to predict the behavior of aluminum in uniaxial compression at various strain rates. McLellan [12], also in 1967, was able to modify Eq. (2.2.10) in order to predict the behavior of many metals, various phenolics, and plexiglass at various strain rates and temperatures. In 1971 Zabora, et al. [13] used a form of Eq. (2.2.10) to describe the shear behavior of structural adhesives in the bonded state.

Eq. (2.2.7) and its respective rate form, Eq. (2.2.10), were selected for further consideration in this study.

2.3 Incremental Theories

In the incremental theory of plasticity the strains are in general not uniquely determined by the stresses, but depend on the entire history of loading. The equations describing plastic flow cannot in general be finite relations between the components of stress and strain, but must be incremental relations.

The equations of incremental theory establish relations between stress and infinitesimal increments of strain. Equations of this form were proposed in 1925 by Prandtl [14] and later in 1930 by Reuss [15] and are known as the Prandt-Reuss equations (textbook presentation can be found in Mendelson [16]).

Reuss assumed that the plastic strain increments are at any instant of loading above yield proportional to the instantaneous stress deviation,

$$d\varepsilon_{ij}^{P} = d\lambda S_{ij} \tag{2.3.1}$$

where $d\lambda$ is a non-negative parameter which may vary throughout the loading history. To determine the actual magnitudes of the plastic strain increments a yield criterion is required.

In incremental theory the total increments of deviatoric strain, Δe_{ij}, are the sum of elastic components, Δe_{ij}^{E}, and plastic components, Δe_{ij}^{P}. In rate form (i.e., dividing by Δt and taking the limit as Δt approaches zero) this becomes,

$$\dot{e}_{ij} = \dot{e}_{ij}^{E} + \dot{e}_{ij}^{P} \tag{2.3.2}$$

For an elastic/viscoplastic material, the elastic strain rate, $\dot{e}_{ij}^{E}$, is given by,

$$\dot{e}_{ij}^{E} = \frac{\dot{S}_{ij}}{2G} \tag{2.3.3}$$

The plastic strain rate, $\dot{e}_{ij}^{P}$, represents combined viscous and plastic effects and thus is often called the "viscoplastic component." Possible constitutive forms for the viscoplastic component were given by Hohenemser and Prager [17] in 1932 in the form,

$$2\mu\dot{e}_{ij}^{P} = 2k\langle F\rangle \frac{\partial F}{\partial \sigma_{ij}} \tag{2.3.4}$$

where

$$F = \frac{J_2^{1/2}}{k} - 1 \tag{2.3.5}$$

is the yield function, k is the yield stress in simple shear, μ is the viscosity coefficient, J_2 represents the second invariant of the stress deviation given by,

$$J_2 = \frac{1}{6}[(\sigma_{11} - \sigma_{22})^2 + (\sigma_{22} - \sigma_{33})^2 + (\sigma_{33} - \sigma_{11})^2 + 6(\sigma_{12}^2 + \sigma_{23}^2 + \sigma_{31}^2)] \tag{2.3.6}$$

and the symbol <F> is defined,

$$\langle F\rangle = \begin{cases} 0 & \text{for } F \leq 0 \\ F & \text{for } F > 0 \end{cases} \tag{2.3.7}$$

The yield function, Eq. (2.3.5), implies von Mises yield criteria. That is, yield is said to occur when $J_2^{1/2} = k$. The total strain rate below yield is the elastic strain rate. Above yield, the

total strain rate is composed of elastic and viscoplastic components. Combining Eqs. (2.3.2) through (2.3.5) the following relations are obtained,

$$\begin{aligned} \dot{e}_{ij} &= \frac{\dot{S}_{ij}}{2G} && J_2^{1/2} \leq k \\ \dot{e}_{ij} &= \frac{\dot{S}_{ij}}{2G} + \frac{1 - kJ_2^{-1/2}}{2\mu} S_{ij} && J_2^{1/2} > k \end{aligned} \qquad (2.3.8)$$

Equations of this form were studied by Freudenthal [18] in 1958.

In 1963 Perzyna [19] generalized Eqs. (2.3.8) by replacing $2k\langle F\rangle$ by $\gamma^{\circ}\Phi(F)$, where γ° denotes a material constant, F is the yield function (not necessarily given by Eq. (2.3.5)), and the function Φ satisfies the conditions,

$$\begin{aligned} \Phi(F) &= 0 && \text{for } F \leq 0 \\ \Phi(F) &\neq 0 && \text{for } F > 0 \end{aligned} \qquad (2.3.9)$$

Perzyna's generalized form was,

$$\begin{aligned} \dot{e}_{ij} &= \frac{\dot{S}_{ij}}{2G} && F \leq 0 \\ \dot{e}_{ij} &= \frac{\dot{S}_{ij}}{2G} + \gamma\Phi(F)\frac{\partial F}{\partial \sigma_{ij}} && F > 0 \end{aligned} \qquad (2.3.10)$$

where $\gamma = \gamma^{\circ}/2\mu$ is a material constant.

The relations in Eqs. (2.3.10) involve the assumption that the viscoplastic component be a function of the over-stress above the yield condition. This assumption is the same as that introduced by Malvern [20] earlier in 1951 from experimental investigations of one-

dimensional problems.

2.3.1 Sokolovsky's Equation

During the same era as Malvern's work, Sokolovsky [21] (1948) determined from experimental observations that the viscoplastic component can be written as a function of the over-stress above the elastic limit, $g(\sigma - \theta)$. Sokolovsky's equations had the form,

$$\begin{aligned} \dot{\varepsilon} &= \frac{\dot{\sigma}}{E} && \sigma \leq \theta \\ \dot{\varepsilon} &= \frac{\dot{\sigma}}{E} + \frac{1}{E} g(\sigma - \theta) && \sigma > \theta \end{aligned} \tag{2.3.11}$$

It is interesting to note that the form of Sokolovsky's equations can be determined from that proposed by Perzyna, Eqs. (2.3.10), if the yield condition is taken as Eq. (2.3.5). The function $\Phi(F)$ is then written as,

$$\Phi(F) = \begin{cases} 0 & \text{for } F \leq 0 \quad \text{or } J_2^{1/2} \leq k \\ F & \text{for } F > 0 \quad \text{or } J_2^{1/2} > k \end{cases} \tag{2.3.12}$$

and Eqs. (2.3.10) become,

$$\begin{aligned} \dot{e}_{ij} &= \frac{\dot{S}_{ij}}{2G} && J_2^{1/2} \leq k \\ \dot{e}_{ij} &= \frac{\dot{S}_{ij}}{2G} + \gamma \left[\frac{J_2^{1/2}}{k} - 1 \right] \frac{S_{ij}}{J_2^{1/2}} && J_2^{1/2} > k \end{aligned} \tag{2.3.13}$$

For one-dimensional loading (and dropping the subscripts), Eqs. (2.3.13) become,

$$\begin{aligned} \dot{\varepsilon} &= \frac{\dot{\sigma}}{E} && \sigma \leq \sqrt{3}k \\ \dot{\varepsilon} &= \frac{\dot{\sigma}}{E} + \frac{2\sqrt{3}}{3}\left(\frac{\gamma}{\sqrt{3}k}\right)(\sigma - \sqrt{3}k) && \sigma > \sqrt{3}k \end{aligned} \tag{2.3.14}$$

For von Mises criteria, the yield stress in pure shear is $1/\sqrt{3}$ times the yield stress in simple tension. That is, $\sqrt{3}k = \theta$, and hence Eqs. (2.3.14) have the form,

$$\begin{aligned} \dot{\varepsilon} &= \frac{\dot{\sigma}}{E} && \sigma \leq \theta \\ \dot{\varepsilon} &= \frac{\dot{\sigma}}{E} + \frac{\bar{\gamma}}{\theta}(\sigma - \theta) && \sigma > \theta \end{aligned} \tag{2.3.15}$$

where $\bar{\gamma} = \frac{2}{3}\sqrt{3}\gamma$ is a material constant. These are essentially Sokolovsky's equations.

The form of Eqs. (2.3.15) was selected for further consideration in this study. The final equations investigated are actually derived in the following section using a mechanical model. However, Eqs. (2.3.15) yielded information relative to the coefficient of the over-stress term which was not readily recognizable in the mechanical model. The elastic limit or yield stress of the adhesives was found to be rate dependent (i.e., $\theta = \theta(\dot{\varepsilon})$). This then indicates that the coefficient of the over-stress term in Eqs. (2.3.15) may be rate dependent.

2.4 Mechanical Models

An alternate approach to the development of suitable constitutive forms is the use of discrete mechanical models. Recent investigators

[22, 23, 24] have attempted to use such models to describe the rate dependency observed in various polymers.

2.4.1 Modified Bingham Model

In 1972, Brinson [23] proposed a modified Bingham model, Fig. 1(b), to describe the rate behavior of various polymeric materials. The constitutive equations for this model are,

$$\dot{\varepsilon} = \frac{\dot{\sigma}}{E} \qquad \sigma \leq \theta$$
$$\dot{\varepsilon} = \frac{\dot{\sigma}}{E} + \frac{1}{\mu}(\sigma - \theta) \qquad \theta < \sigma < Y \tag{2.4.1}$$

Once the maximum stress, Y, is reached, perfectly plastic flow to failure is assumed. It can be readily observed that Eqs. (2.4.1) are similar to those proposed by Sokolovsky, Eqs. (2.3.11), and that derived from the work of Perzyna, Eqs. (2.3.15).

Using Eqs. (2.4.1) to model the behavior of polycarbonate at different strain rates, Brinson observed that the viscosity coefficient had to vary with strain rate in order to accurately represent the experimental results. Brinson and DasGupta [24] in 1973 reported the same phenomenon using a series of Bingham elements.

It could not be ascertained directly from Eqs. (2.4.1) that μ (the coefficient of the over-stress term) was rate dependent. However, the analogous form of these equations, Eqs. (2.3.15), indicated that this coefficient may be rate dependent. Thus, insight into rate dependency not readily seen using mechanical models can be observed from incremental theory as derived for an elastic/viscoplastic material.

This rate dependency in μ is later shown (Chapter 5) to be an inherent property of rate-sensitive plastic materials.

2.4.1.1 Constant Strain Rate Solution

For constant strain rate ($\dot{\varepsilon} = R = \text{constant}$), Eqs. (2.4.1) are solved according to the initial condition,

$$\varepsilon(t = t_0) = \varepsilon_0 \tag{2.4.2}$$

where ε_0 and t_0 are strain and time, respectively, at which the elastic limit is reached. The solution is,

$$\begin{aligned} \sigma(\varepsilon) &= \varepsilon E && \sigma \leq \theta \\ \sigma(\varepsilon) &= \theta + \mu R\{1 - e^{-E(\varepsilon - \varepsilon_0)/\mu R}\} && \theta < \sigma < Y \end{aligned} \tag{2.4.3}$$

2.4.1.2 Creep and Relaxation Solutions

The constitutive equations reviewed have been concerned with modeling the effects of strain rate on material behavior. It would be ideal if these equations modeled material behavior for other loading conditions.

Equations derived from deformation theory would not be suited to this task since in deformation theory the plastic strains are a function of the current state of stress and are independent of the loading history. Equations derived from the incremental and mechanical model approaches are written in incremental form and thus can take into account the loading history. Therefore, the modified Bingham model was considered further for other than monotonically increasing loads.

For creep loading using the modified Bingham model,

$$\sigma(t) = \bar{\sigma}_0 H(t) > \theta \tag{2.4.4}$$

where H(t) represents the unit step function and $\bar{\sigma}_0$ is the level of constant stress. Eqs. (2.4.1) then become,

$$\dot{\varepsilon} = \frac{\bar{\sigma}_0 - \theta}{\mu} \qquad \sigma > \theta \tag{2.4.5}$$

The initial condition is given as,

$$\varepsilon(t = 0) = \frac{\bar{\sigma}_0}{E} \tag{2.4.6}$$

That is, the initial response is assumed to be instantaneous and elastic, and the solution to Eq. (2.4.6) is written as,

$$\varepsilon(t) = \frac{\bar{\sigma}_0 - \theta}{\mu} t + \frac{\bar{\sigma}_0}{E} \tag{2.4.7}$$

For relaxation loading,

$$\varepsilon(t) = \bar{\varepsilon}_0 H(t) > \varepsilon_0 \tag{2.4.8}$$

where $\bar{\varepsilon}_0$ is the level of constant strain and ε_0 is the elastic limit strain. Eqs. (2.4.1) then becomes

$$\frac{\dot{\sigma}}{E} + \frac{1}{\mu}(\sigma - \theta) = 0 \qquad \sigma > \theta \tag{2.4.9}$$

subject to the initial condition,

$$\sigma(t = 0) = \bar{\varepsilon}_0 E \tag{2.4.10}$$

That is, the initial response is assumed to be instantaneous and

elastic. The solution to Eq. (2.4.9) is written as,

$$\sigma(t) = \theta + (\bar{\varepsilon}_0 E - \theta)e^{-Et/\mu} \tag{2.4.11}$$

Chapter 3

PROPOSED CONSTITUTIVE EQUATIONS

3.1 Modified Ramberg-Osgood Models

The plastic strain term, $K\sigma^n$, in Eq. (2.2.7) is a function of the current state of stress. It is proposed that the plastic strain be a function of the over-stress $(\sigma - \theta)$. The proposed form is,

$$\begin{aligned} \varepsilon &= \frac{\sigma}{E} && \sigma < \theta \\ \varepsilon &= \frac{\sigma}{E} + K(\sigma - \theta)^n && \sigma > \theta \end{aligned} \tag{3.1.1}$$

where K and n are material constants.

Following a procedure similar to that of McLellan [10], section 2.1.2, Eqs. (3.1.1) were modified for rate effects. The final form is,

$$\begin{aligned} \varepsilon &= \frac{\sigma}{c\dot{\varepsilon}^d} && \sigma < \theta \\ \varepsilon &= \frac{\sigma}{c\dot{\varepsilon}^d} + a\dot{\varepsilon}^b(\sigma - \theta)^n && \sigma > \theta \end{aligned} \tag{3.1.2}$$

where a, b, c, and d are material constants. Variations in K and n with strain rate again denote work-hardening characteristics.

3.2 Nonlinear Model

The following section is a review of a nonlinear perturbation technique used in conjunction with the modified Bingham model in an attempt to describe the rate effect observed in the viscosity coefficient.

The basic hypothesis in mechanical models of linear viscoelasticity is that the elastic and viscous coefficients--parameters representing the spring and dashpot, respectively--are independent of the strain and strain rate. In this section this requirement is relaxed by assuming a small term depending on the elastic strain is added to the elastic coefficient and a small term depending on the strain rate in the viscous element is added to the viscous coefficient.

Using an hypothesis proposed by Davis [4] in 1964 for first order nonlinearity, the nonlinear modulus and viscosity coefficient can be written as,

$$E = E_0 + \gamma_E E_0 \epsilon_E$$
$$\mu = \mu_0 + \gamma_\mu \frac{E_0}{\lambda^2} \dot{\epsilon}_\mu \quad \text{1/} \tag{3.2.1}$$

where E_0 and μ_0 represent the linear modulus and viscosity coefficient of the spring and dashpot, respectively, and $\lambda = E_0/\mu_0$ represents the inverse of the linear relaxation time, τ. The parameters ϵ_E and ϵ_μ are the strains in the spring and dashpot, respectively. The coefficients γ_E and γ_μ are dimensionless constants which are a measure of the nonlinearity. The conditions of first-order nonlinearity are,

$$|\gamma_E \epsilon_E| << 1$$
$$\tau|\gamma_\mu \dot{\epsilon}_\mu| << 1 \tag{3.2.2}$$

1/ For elastic/viscoplastic materials the term $\dot{\epsilon}_\mu$ could be represented by the viscoplastic component $\dot{\epsilon}_p$. However, the above terminology is used in this development in order to distinguish between the elastic and viscous elements.

and higher order terms in $\gamma_E \dot{\varepsilon}_E$ and $\gamma_\mu \dot{\varepsilon}_\mu$ are neglected.

The nonlinear constitutive equations for the modified Bingham model using the relationships in Eqs. (3.2.1) are,

$$\dot{\varepsilon} = \frac{\dot{\sigma}}{E_0} - \gamma_E \frac{2}{E_0^2} \dot{\sigma}\sigma \qquad \sigma \leq \theta$$

$$\dot{\varepsilon} = \frac{\dot{\sigma}}{E_0} + \frac{1}{\mu_0}(\sigma - \theta) - \gamma_E \frac{2}{E_0^2} \dot{\sigma}\sigma - \gamma_\mu \frac{(\sigma - \theta)^2}{\mu_0 E_0} \qquad \theta < \sigma < Y \tag{3.2.3}$$

Eqs. (3.2.3) are derived in Appendix A. It can also be seen that when $\gamma_E = \gamma_\mu = 0$ the linear form Eqs. (2.4.1) is obtained.

The perturbation technique proposed by Davis can now be used to solve Eqs. (3.2.3) for the condition of constant strain rate. Expanding σ in a power series in terms of γ_E and γ_μ of the form,

$$\sigma = \sigma_0 + \sum_{n=1}^{\infty} \gamma_E^n \sigma_n + \sum_{n=1}^{\infty} \gamma_\mu^n S_n \tag{3.2.4}$$

and limiting this expression to first-order nonlinearities gives,

$$\sigma = \sigma_0 + \gamma_E \sigma_1 + \gamma_\mu S_1 \tag{3.2.5}$$

Eq. (3.2.5) is substituted into Eqs. (3.2.3) and the expressions for σ_0, σ_1, and S_1 determined (see Appendix A). Postulating that nonlinear effects are present in the dashpot only (i.e., $\gamma_E \equiv 0$) the following nonlinear constitutive equation is realized for the modified Bingham model,

$$\sigma(\varepsilon) = E_0\varepsilon \qquad \sigma \leq \theta$$

$$\sigma(\varepsilon,\gamma_\mu) = \theta + \mu_0 R(1 - e^{-E(\varepsilon - \varepsilon_0)/\mu_0 R}) + \gamma_\mu(2E_0 R\tau(\varepsilon - \varepsilon_0) \qquad (3.2.6)$$

$$+ E_0 R^2\tau^2(1 - e^{-2E(\varepsilon - \varepsilon_0)/\mu_0 R}) \qquad \theta < \sigma < Y$$

Eqs. (3.2.6) are also derived in Appendix A.

As stated earlier, the linear coefficient μ_0 was found to be dependent on the total strain rate $\dot{\varepsilon}$. The nonlinear hypothesis, Eqs. (3.2.1), indicates that this linear value may vary with respect to the strain rate in the viscous element. Thus, the nonlinear model does not mathematically indicate that μ_0 may be dependent on $\dot{\varepsilon}$, but rather that it may change with respect to $\dot{\varepsilon}_\mu$. However, it is shown (Chapter 5) that the nonlinear solution indicates a change in the behavior of the adhesives above and below the stress-whitening point.

3.3 Loading-Unloading Considerations

The work-hardening characteristics of the adhesives were found to be rate dependent. That is, the maximum stress and plastic flow behavior varied with strain rate. However, the elastic limit stress, the point of initiation of viscous and plastic effects, remained constant during loading and unloading cycles at a given strain rate. The adhesives were also observed to unload elastically.

For the considerations above, the function $\Phi(F)$ in Eq. (2.3.9) can be modified as,

$$\Phi(F) = \begin{cases} 0 & \text{for } F \leq 0 \\ & \text{or } \dot{F} < 0 \\ F & \text{for } F > 0 \\ & \text{and } \dot{F} > 0 \end{cases} \tag{3.3.1}$$

For one-dimensional loading and von Mises yield criteria, these conditions become,

$$\Phi(F) = \begin{cases} 0 & \text{for } \sigma \leq \theta \\ & \text{or } \dot{\sigma} < 0 \\ \frac{1}{\theta}(\sigma - \theta) & \text{for } \sigma > \theta \\ & \text{and } \dot{\sigma} > 0 \end{cases} \tag{3.3.2}$$

The conditions given by Eq. (3.3.2) can be incorporated into the modified Bingham model as,

$$\begin{aligned} \dot{\varepsilon} &= \frac{\dot{\sigma}}{E} && \text{for } \sigma \leq \theta \\ & && \text{or } \dot{\sigma} < 0 \\ \dot{\varepsilon} &= \frac{\dot{\sigma}}{E} + \frac{\sigma - \theta}{\mu} && \text{for } \theta < \sigma < Y \\ & && \text{and } \dot{\sigma} > 0 \end{aligned} \tag{3.3.3}$$

Eqs. (3.3.3) constitute the proposed form of the modified Bingham model for loading-unloading considerations.

Chapter 4

EXPERIMENTAL CONSIDERATIONS

4.1 Materials and Specimen Features

The two adhesives investigated in this study were Narmco Whittaker's Metlbond 1113 and 1113-2. Metlbond 1113 is a 100% solids, modified epoxy film with a synthetic carrier cloth. Metlbond 1113-2 is the identical film without the carrier cloth. Tests were run on both materials to ascertain the behavior of the modified epoxy in both supported and unsupported form, that is, to establish the effect of the carrier cloth by comparison.

All tests were conducted on bulk specimens such as that shown in Fig. 2. Load was introduced through steel plates bolted to the specimen and aligned using a special alignment fixture. The specimens were cut from $\sim$ 0.140 in. ($\sim$ 0.355 cm.) thick sheets which were laid up using fourteen plies of film and cured according to manufacturer's specifications [28] in a platen press at NASA-Langley Research Center. These sheets were $\sim$ 12 in. ($\sim$ 30.5 cm.) square. The width of each specimen was $\sim$ 0.5 in. ($\sim$ 1.27 cm.) and the gauge length was $\sim$ 3.25 in. ($\sim$ 8.26 cm.). Initially six sheets of each adhesive were fabricated and either six or seven specimens were cut from each sheet. These specimens were used to conduct constant strain rate, creep (constant stress), and relaxation (constant strain) tests. Six more sheets of each adhesive were then fabricated from a second batch of material. The majority of specimens from these sheets were used for the loading-

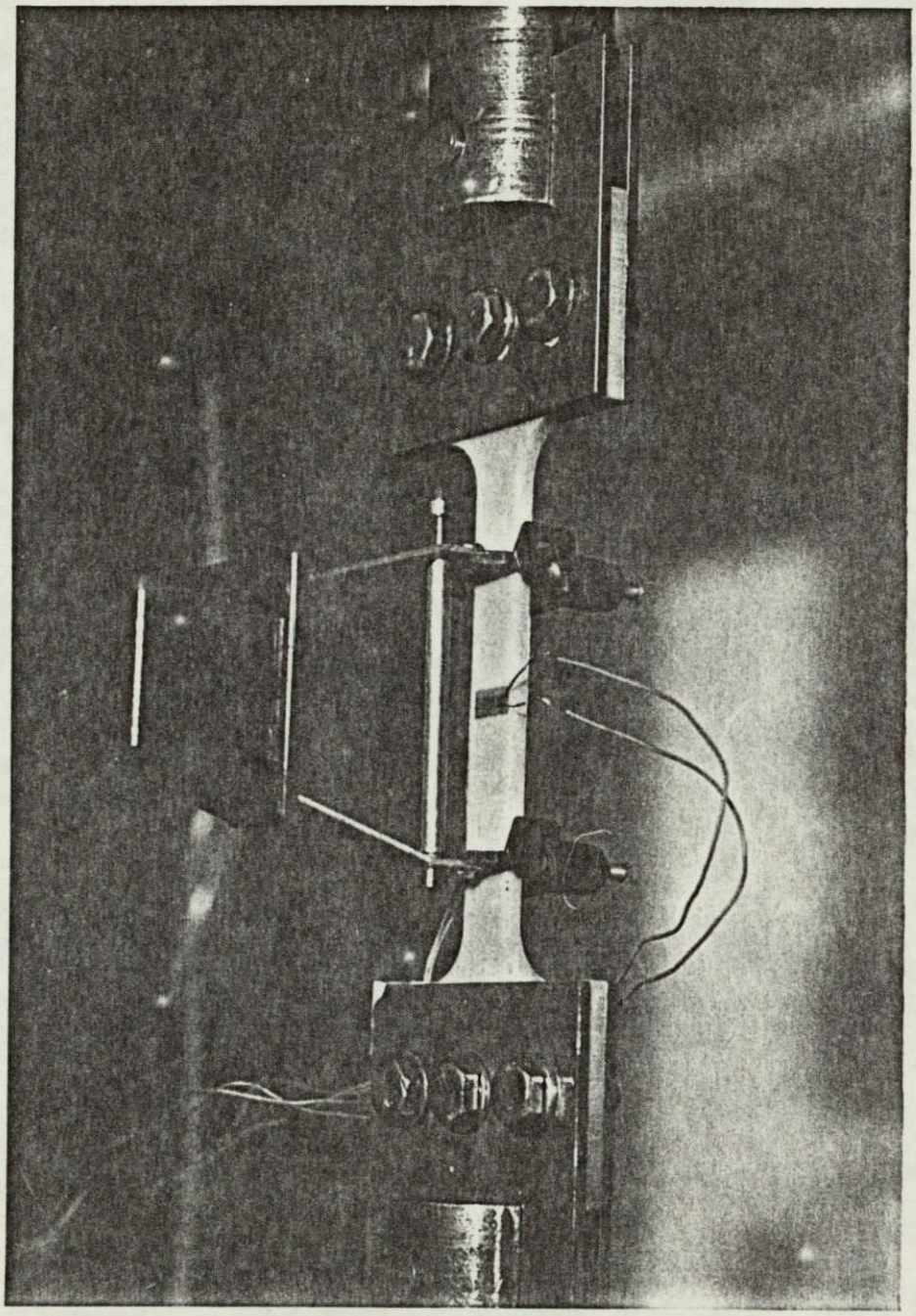

Figure 2. Specimen Mounted for Testing

unloading tests and for the high temperature testing. Over 90 specimens were tested in all. Controlled environmental conditions of approximately 72° F and 75% relative humidity were used in all tests.

4.2 Experimental Procedure

4.2.1 Constant Strain Rate Tests

Constant strain rate tests were performed on an Instron testing machine using constant head rates ranging from 0.002 in./min. (0.00508 cm./min.) to 2 in./min. (5.08 cm./min.). The experimental apparatus for these experiments is shown in Fig. 3. Each specimen was instrumented with an Instron model G-51-13 extensometer (Fig. 2) and both longitudinal and transverse electrical resistance foil type strain gauges (M.M. EP-08-125BB-120 LE). The extensometer was used to ascertain if heating or reinforcement of the electrical gauges affected strain gauge results. There was good agreement between both methods for nearly the full range of strain. A small difference in strain values was observed after local yielding (i.e., the formation of crazing or microcracks), with the electrical gauges giving slightly lower results. This behavior has been attributed to the slight reinforcing effect of the strain gauge. The signals from the extensometer and the foil gauges were amplified using Vishay (Model BAM-1) bridge amplifiers and were recorded on a Hewlett Packard (7100 B) dual channel strip chart recorder. The bridge amplifiers were operated at a reduced voltage which allowed recording of strains up to 10% (0.10 m/m). The reduced voltage also lowered strain gauge heating effects.

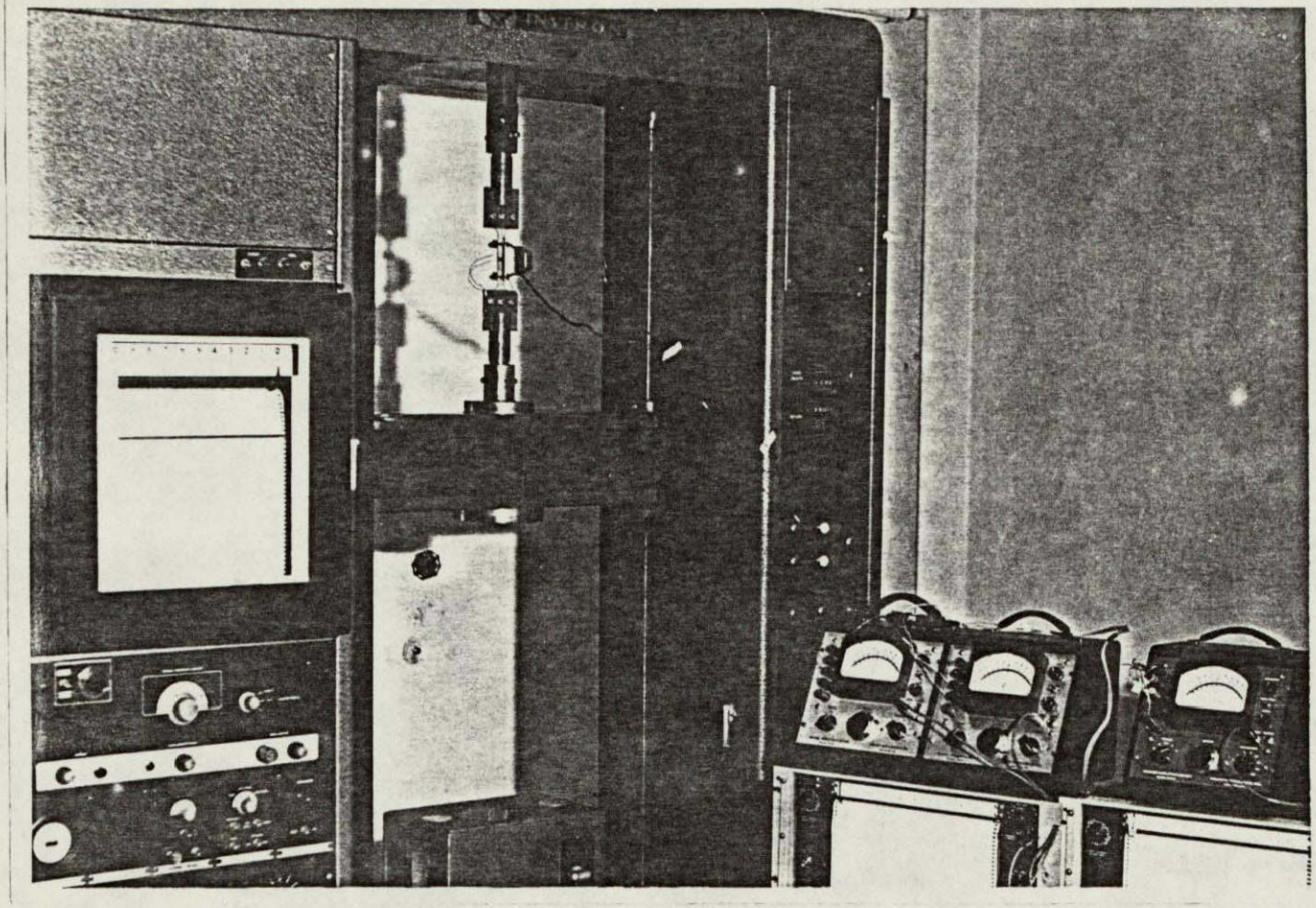

Figure 3. Constant Strain Rate Testing Apparatus

To establish the repeatability of results, two specimens from one sheet and one specimen from a second sheet of each adhesive were tested at the same strain rate. In all cases, differences of less than 2% were found in the stress-strain behavior below failure. The variation in the failure stresses varied similarly, but failure strains were more random. As a general rule, results were obtained on the bases of a single test. However, a second specimen was tested whenever a specimen failed prematurely due to defects in the specimen. Such defects were occasionally present in the form of internal bubbles which formed during the curing process.

4.2.2 Creep Tests

Creep tests were performed using a pneumatic testing machine (manufactured by Allied Research Associates) which was capable of loading at a rate of approximately 20 in./min. (50.8 cm./min.) and then maintaining a constant load. This apparatus is shown in Fig. 4. The load level was monitored using a Baldwin SR-4 (Type U-1) load cell with a Baldwin (Type L) strain indicator. The load was constant throughout the duration of each test. Since the reduction in cross-sectional area of the specimens was found to be small during these tests, stress calculations were based upon the initial area. Both longitudinal and transverse strains were recorded using the electrical strain gauges and instrumentation described previously.

4.2.3 Relaxation Tests

Relaxation tests were conducted using a Twing-Albert test machine with initial strain applied at a head rate of 20 in./min.

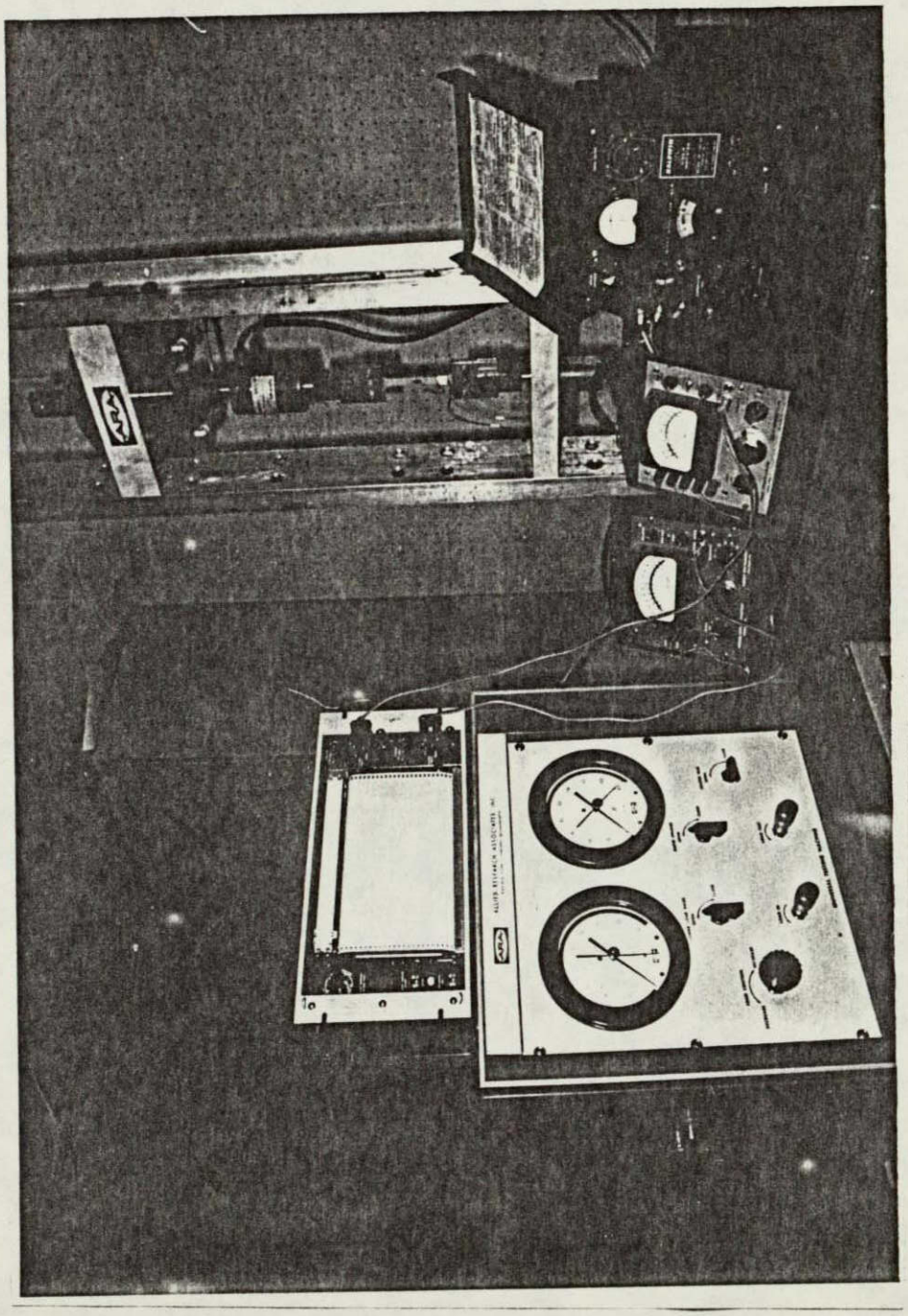

Figure 4. Creep Testing Apparatus

(50.8 cm./min.). This apparatus is shown in Fig. 5. The strain level was found to remain constant for the complete duration of each test. The same load cell and strain gauge instrumentation as described for the creep tests was used. However, the signal from the load cell was amplified and recorded continuously on a Hewlett Packard (7100 B) dual channel strip chart.

4.2.4 Loading-Unloading Tests

The loading-unloading tests employed essentially the same equipment as the constant strain rate tests. However, a considerable amount of this data was recorded on cassette tape and transmitted to the IBM/370 facility at VPI&SU for processing using the CB^2 data acquisition system [26] which was under development at the time. The system utilized the signals from the Instron load cell and Vishay amplifiers. Thus the essential components of the experimental apparatus were identical to those used in the constant strain rate tests.

4.2.5 Elevated Temperature Tests

Relaxation tests at various temperatures above and below the glass transition temperature of the adhesives were conducted on the Instron Machine in combination with an Instron environmental chamber. The apparatus used is shown in Fig. 6. Special test fixtures were fabricated to position the specimen inside the chamber. A copper cooling coil was affixed to the top fixture to dissipate heat away from the load cell. The axial strain was recorded using an Instron high temperature extensometer (Model G51-14A) which was capable of 50% (0.5 m/m) strain. It is shown mounted on a specimen, in the

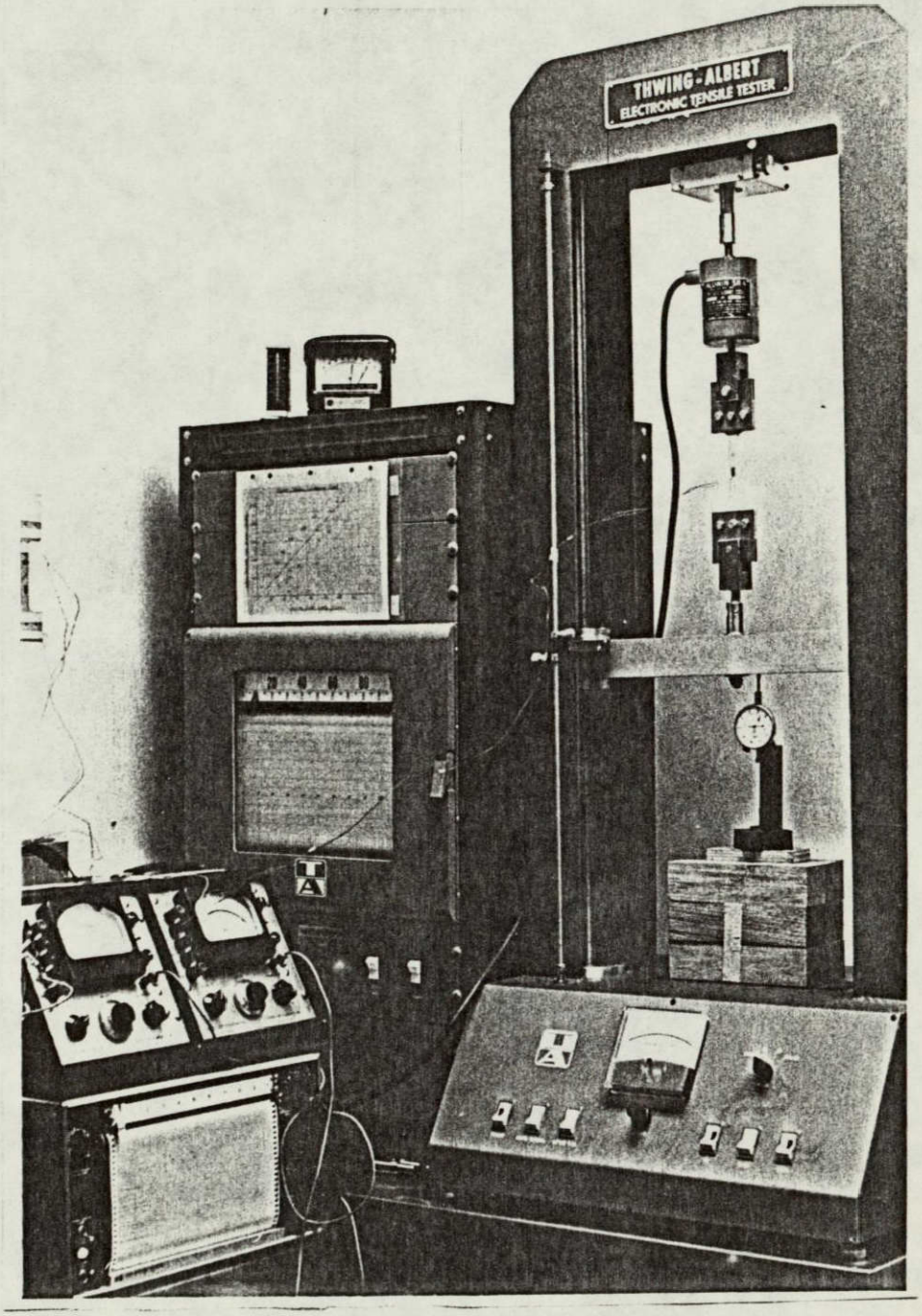

Figure 5. Relaxation Testing Apparatus

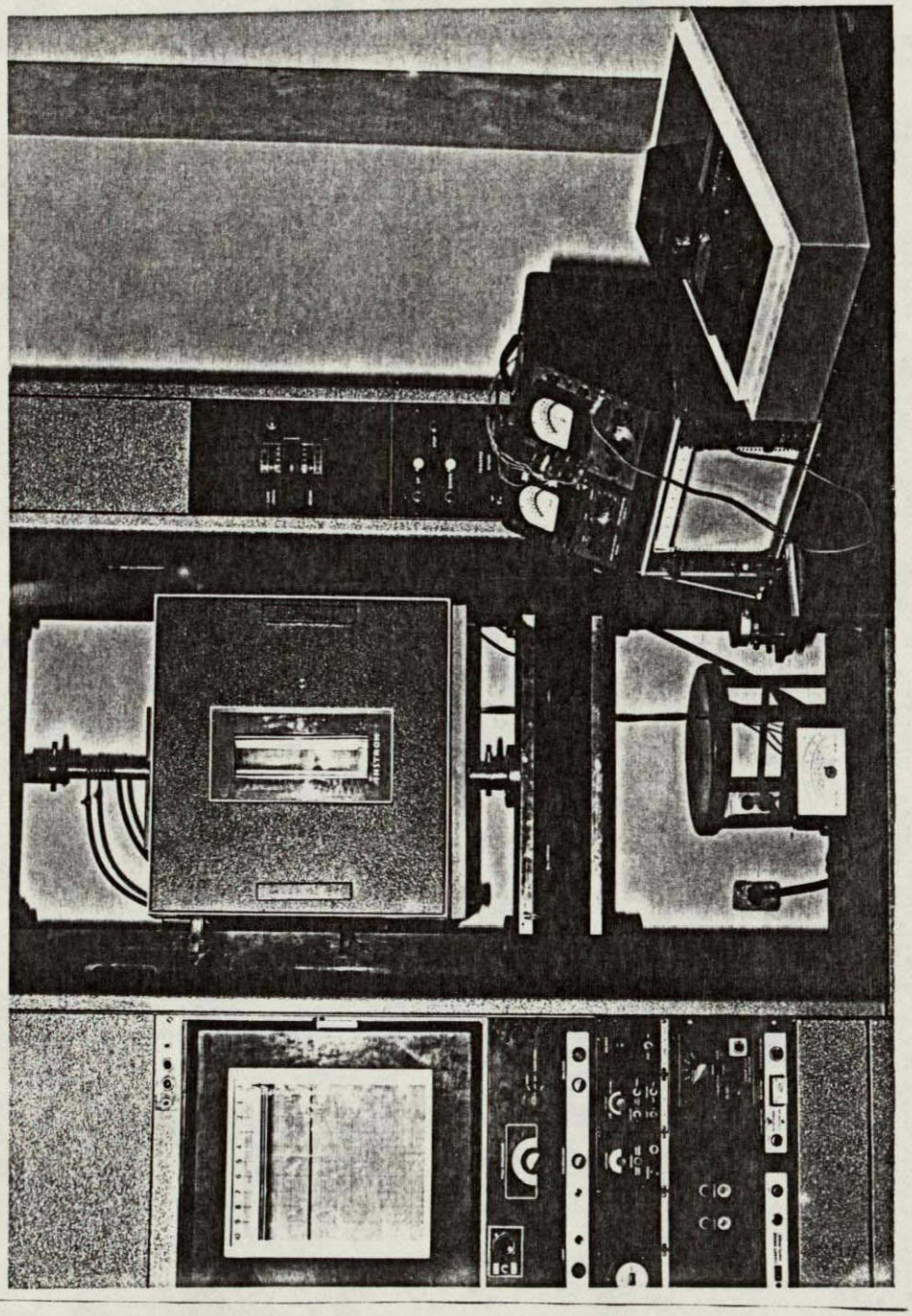

Figure 6. Elevated Temperature Testing Apparatus

environmental chamber, in Fig. 7. The signals from the extensometer and the load cell were amplified and recorded as in the relaxation tests described above.

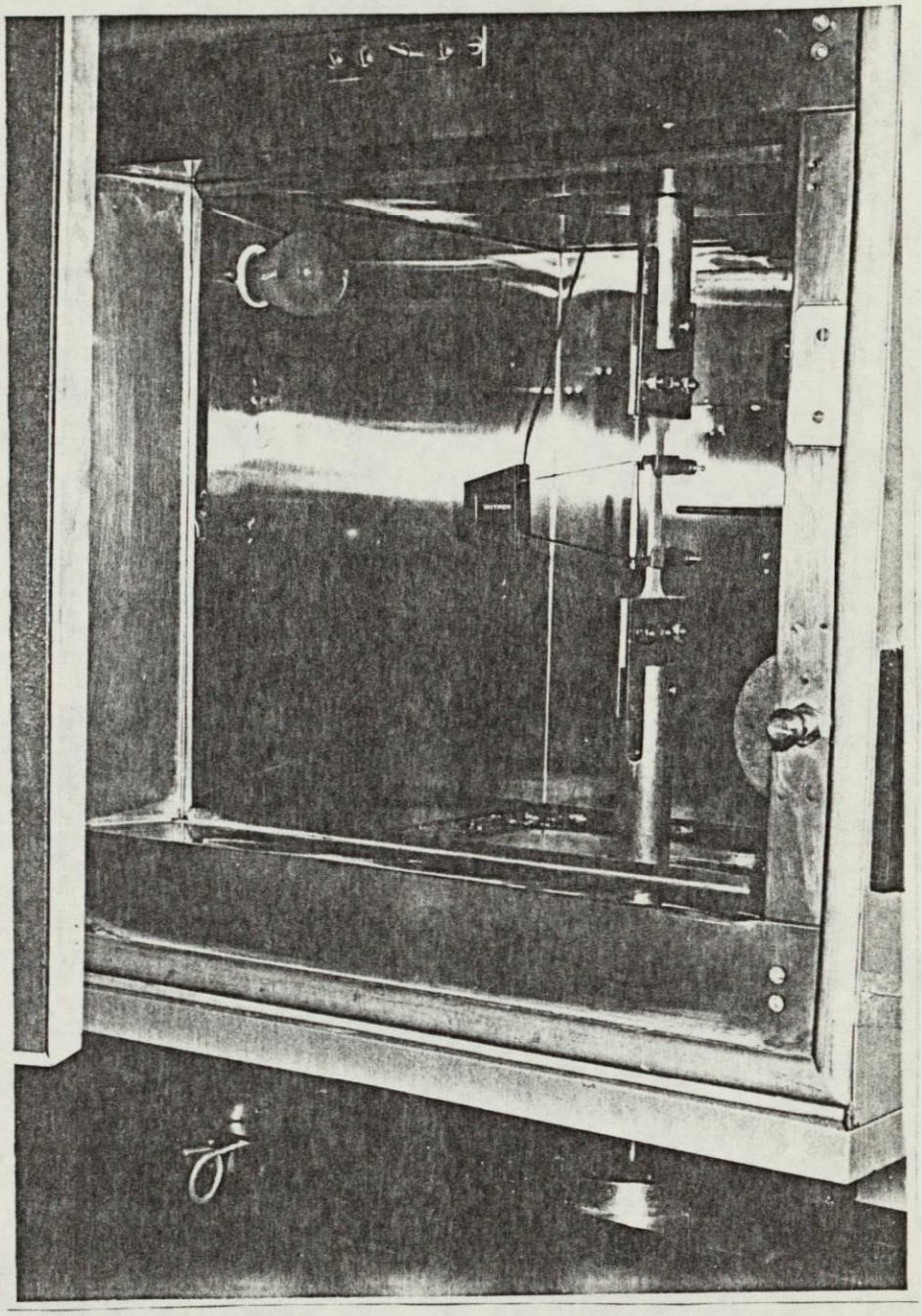

Figure 7. Specimen Mounted in Environmental Chamber

Chapter 5

CONSTANT STRAIN RATE BEHAVIOR

This chapter is concerned with the experimental results from the constant strain rate tests and the ability of the constitutive equations reviewed in Chapters 2 and 3 to predict this behavior. The first two equations considered are the Ramberg-Osgood models, Eqs. (2.2.7) and (3.3.1), and their respective rate forms, Eqs. (2.2.10) and (3.1.2). The effect of the stress-whitening phenomenon on these equations is also presented. The modified Bingham model, Eqs. (2.4.3), is considered next; and the effect of the stress-whitening phenomenon on this model is observed through the use of the nonlinear model, Eqs. (3.4.6).

5.1 Constant Strain Rate Results

The stress-strain behavior of Metlbond 1113 is shown in Fig. 8 for four different strain (head) rates. Linear elastic behavior with little rate effect was found for low stress levels. However, the elastic limit was found to be rate dependent. Above the elastic limit, significant rate effects were observed which can be attributed to viscoplastic behavior. The maximum stress was also found to be significantly rate dependent. The failure strains, while rate dependent, did not follow a consistent pattern. Similar results were observed for Metlbond 1113-2 (Fig. 9). It can be observed, by comparison, that the modulus, elastic limit stress, and maximum stress are lower for

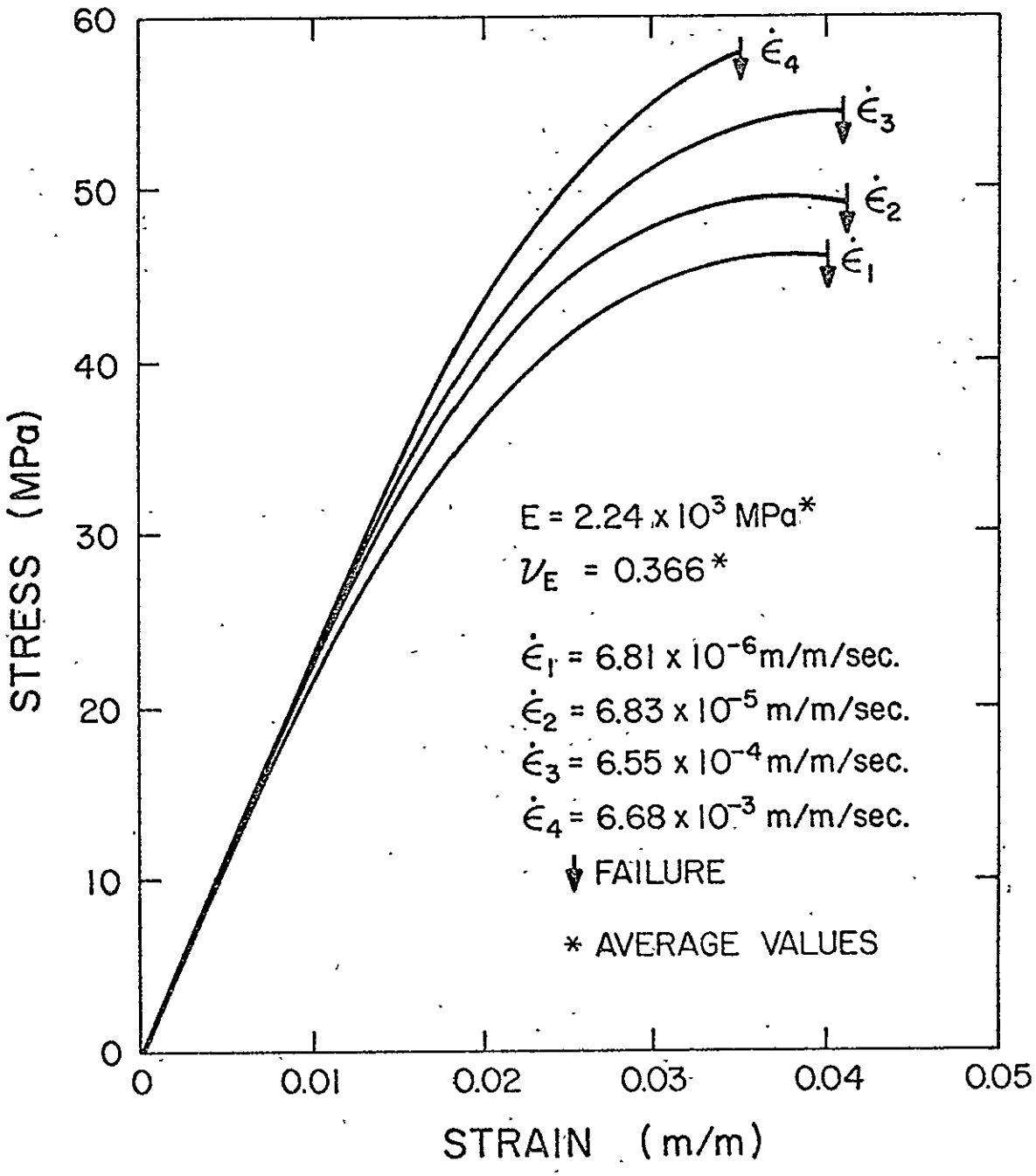

Figure 8. Stress-Strain-Strain Rate Response of Metlbond 1113

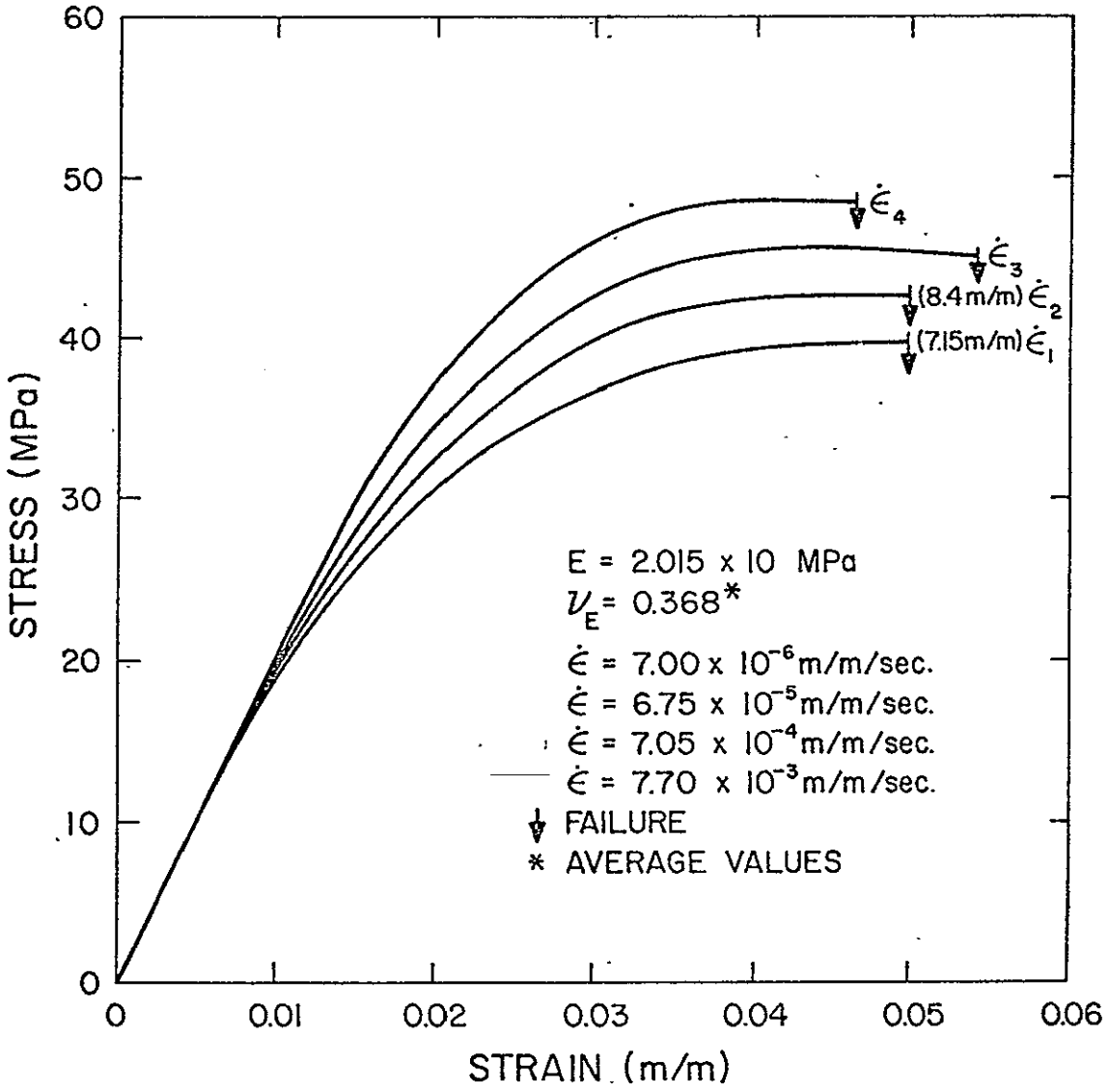

Figure 9. Stress-Strain-Strain Rate Response of Metlbond 1113-2

Metlbond 1113-2. This is attributed to the reinforcing effect of the synthetic carrier cloth present in Metlbond 1113. The strain rates recorded in Figs. 8 and 9 were calculated from the slope of the strain-time data and were found to be constant up to local yield (i.e., the initiation of crazing or microcracks), after which the strain rate decreased slightly due to a small reinforcing effect of the strain gauge.

Figs. 10(a) and (b) are photographs of specimen surfaces before and after testing, respectively. The failed specimen is typical of all failures observed during this investigation. The failure surface is perpendicular to the loading axis and has the general appearance of a brittle tensile failure. Essentially no permanent necking was observed.

5.1.1 Stress-Whitening Phenomenon

In the rate tests, a stress-whitening phenomenon was observed to occur at stresses and strains well below the maximum stress levels. This phenomenon was similar to that observed by Shouldberg and Lang [30] during their investigation of polymeric materials. It is believed that the stress-whitening observed was a crazing phenomenon which is frequently observed in polymers [31]. Crazing in a material may be defined as the occurance of localized highly elongated regions (crazes) whose density may vary from zero (true crack) to that of the virgin material depending upon conditions during their formation [32]. Hull [31] states that crazes formed in a uniaxial tensile stress field have a shape similar to a crack, and the plane of the craze is at right

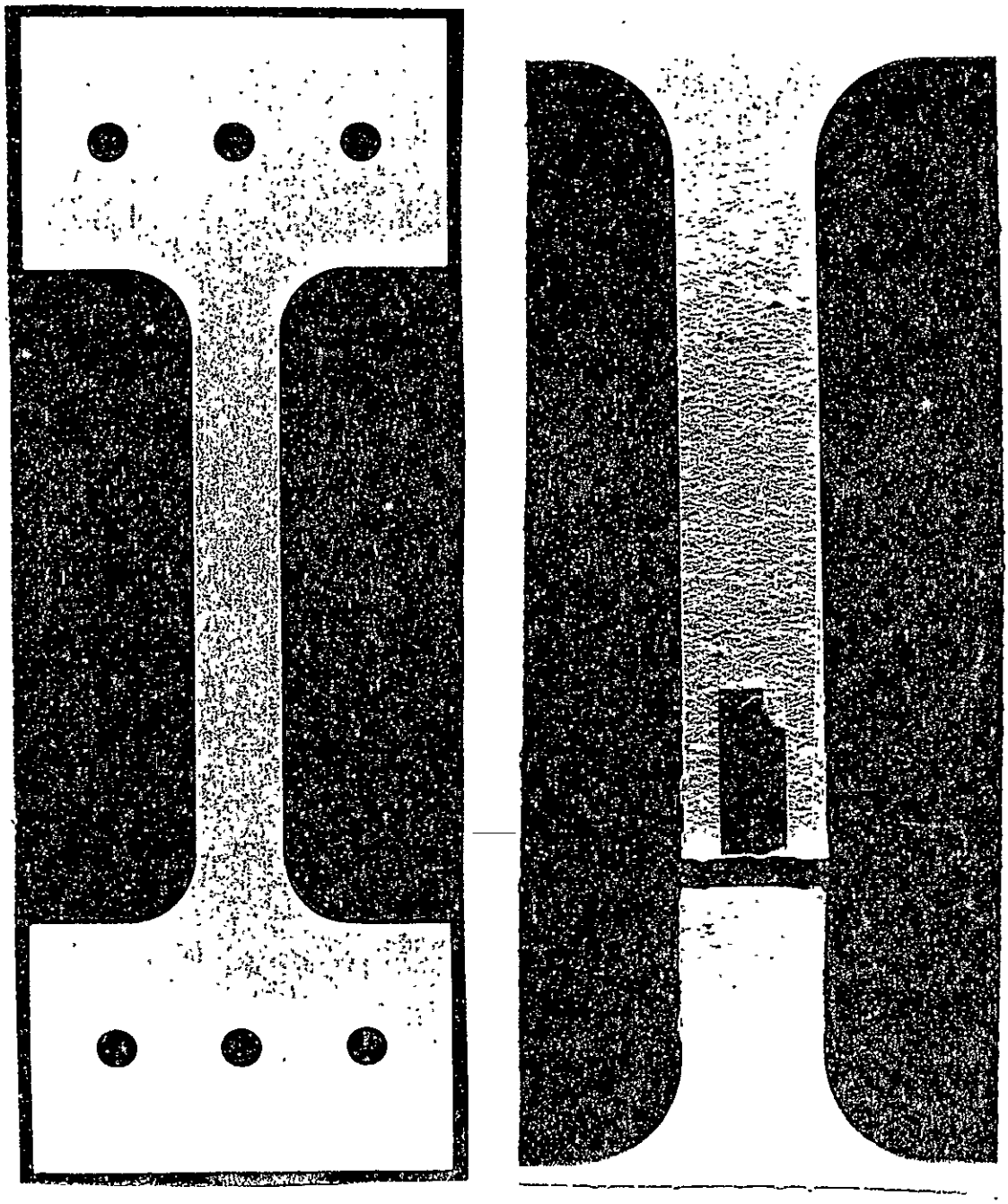

a. Untested Specimen

b. Failed Specimen

Figure 10. Specimen Surfaces of Metlbond 1113-2

angles to the stress axis. Hull also states that in a complex stress field, the plane of the craze is normal to the maximum principal tensile stress. Since complex stress fields often exist in areas of local yield, it would then be possible for a specimen in which areas of localized yield occur during a uniaxial tension test to have crazes both normal and at various angles to the loading direction.

The stress-whitening may be seen in the photograph shown in Fig. 10(b) for a specimen of Metlbond 1113-2. An untested specimen was shown in Fig. 10(a) for comparison. The stress-whitening pattern observed in Fig. 10(b) is very similar to a photograph presented by Hull [31] showing the crazes which formed prior to the maximum stress during a tensile test on polystyrene. Fig. 11 is a photograph of a failed specimen surface at approximately 30X. It can be observed that the crazes appear both normal and at various angles (vertical markings are from sanding) to the loading direction. These angles range from approximately ± 45° to ± 90° with respect to the loading axis. It is interesting to note that a considerable amount of these angles are similar to the angle (± 54.1° to the loading axis) at which slip bands occur in many metals in uniaxial tension [8].

The time, stress and strain levels where the whitening occured in the rate tests can be found in Table 1. The stress level at the occurence of stress-whitening was rate dependent, but the strain level was nearly constant. It is believed that the observed stress-whitening effects can be attributed to crazing and that this process is evidence that a local damage or failure mechanism occurs well in

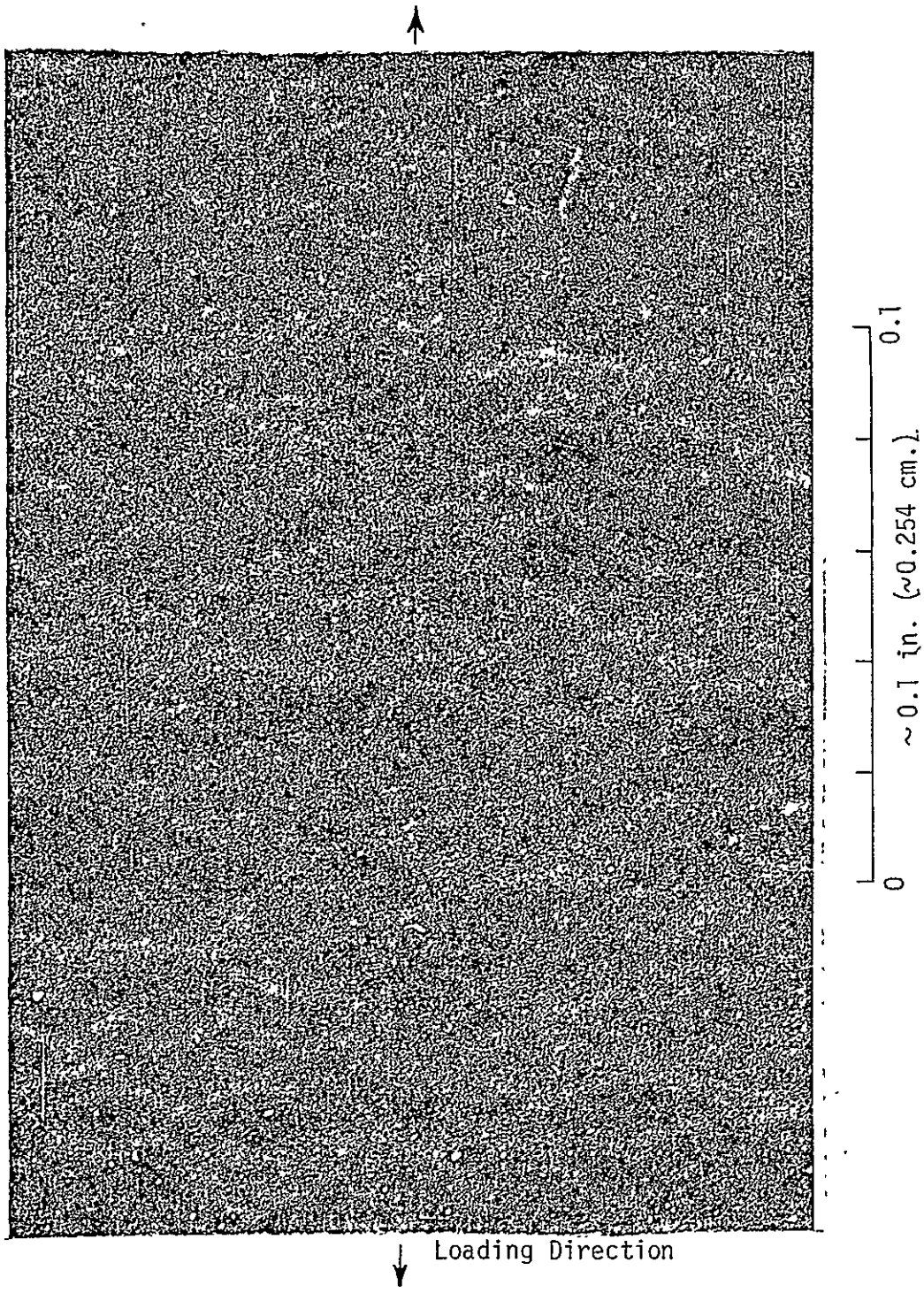

Figure 11. Failed Specimen Surface at 30X

Table 1. CONSTANT STRAIN RATE PROPERTIES.

Adhesive	Specimen	Symbols for Figure 13	Strain Rate $\dot{\varepsilon}$ (m/m/sec)	Elastic Modulus E (MPa)	Elastic Limit Stress θ (MPa)	Elastic Limit Strain ε_0 (m/m)
Metlbond 1113	B-4-3	13(a),○	6.81×10^{-6}	2161	22.48	0.0104
	B-3-2	13(a),●	6.83×10^{-5}	2241	26.89	0.0120
	B-3-4	13(a),△	6.55×10^{-4}	2265	31.72	0.0140
	B-4-4	13(a),▽	6.68×10^{-3}	2284	37.92	0.0166
Metlbond 1113-2	A-3-5	13(b),○	7.00×10^{-6}	1970	16.55	0.0084
	A-4-3	13(b),●	6.75×10^{-5}	2010	18.89	0.0094
	A-3-4	13(b),△	7.05×10^{-4}	1982	23.79	0.0120
	A-8-1	13(b),▽	7.70×10^{-3}	2042	29.00	0.0142

Elastic Poisson's Ratio ν	Maximum Stress Y (MPa)	Stress-Whitening Strain ε_{sw} (m/m)	Stress-Whitening Stress σ_{sw} (MPa)	Stress-Whitening Time t_{sw} (min)	Failure Time t* (min)
0.351	46.19	0.0330	45.57	75.0	96
0.382	49.71	0.0332	49.64	4.0	10.44
0.360	54.68	0.0348	53.37	0.769	1.105
0.370	57.77	---	---	---	0.085
0.380	40.33	0.0378	39.23	84.0	159.5
0.392	42.75	0.0377	42.47	8.8	19.5
0.343	45.92	0.0368	45.37	0.883	1.633
0.370	48.60	---	---	---	0.130

advance of gross fracture. As such, it is an important characteristic of this material.

For a material in which the density is lower in the crazed area, the material in this location has undergone a type of phase change. To determine whether the crazed areas observed in the adhesives were true cracks (zero density) or material of less density, the microscopic picture shown in Fig. 11 was taken with the light source at an angle to the specimen surface. The photograph indicates that no shaded valleys (true cracks) are visible. This would indicate that the crazed areas of the adhesives are not true cracks, but areas of lower density. Although subsurface studies were not conducted, it is believed that this condition exists throughout the specimen since the primary stress field (uniaxial stress) responsible for this phenomenon is constant across the thickness. This change of density (or phase) is shown to influence the adhesives' constitutive equations.

Table 1 also gives further information regarding the properties found for the adhesives in the rate tests. The elastic moduli, Poisson's ratios for the initial elastic region, elastic limit stresses and strains, and maximum stresses may be found therein.

Variations in Poisson's ratio with strain rate and with time are shown in Fig. 12. The results are shown in terms of a nondimensional time which is based upon the time required for failure in each test. The values for the failure times are given in Table 1. The region at which stress-whitening occured during the rate tests is also shown. It is believed that the occurence of stress-whitening is the reason

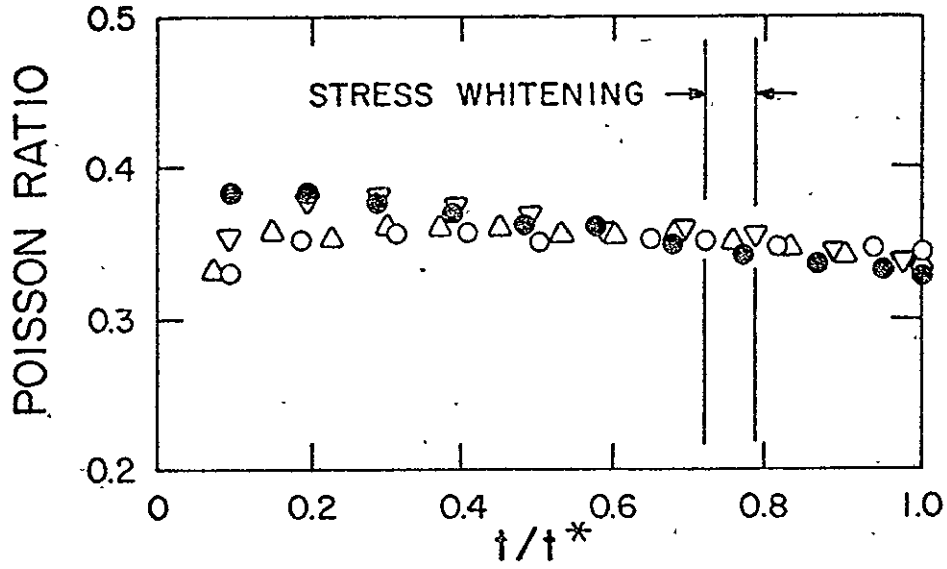

a. METLBOND 1113

(SEE TABLE I FOR SYMBOL IDENTIFICATION)

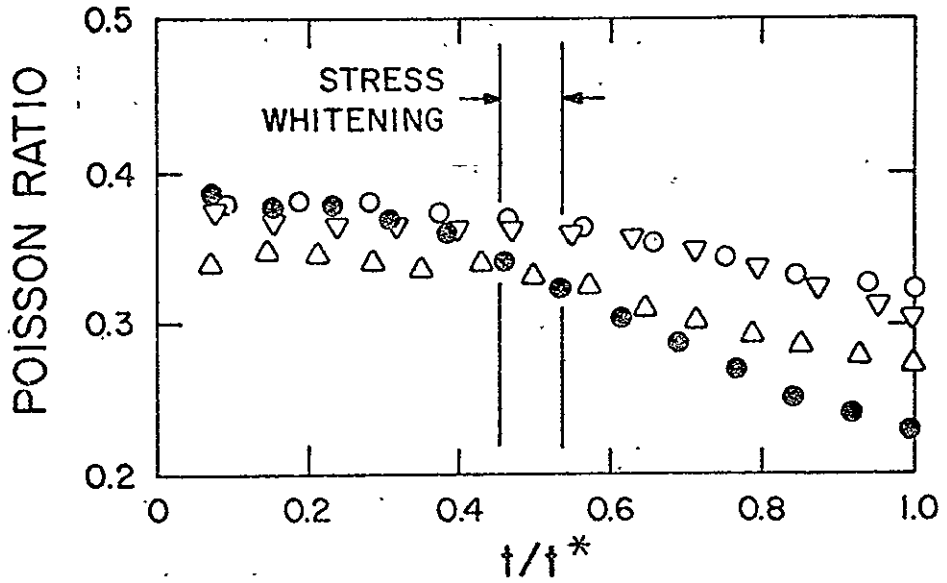

b. METLBOND 1113-2

Figure 12. Poisson's Ratio During Constant Strain Rate Tests

for the general decrease in Poisson's ratios with time. This decrease is Poisson's ratio is much less pronounced in Metlbond 1113 as compared to Metlbond 1113-2. This is attributed to the stabilizing effect of the carrier cloth present in the former adhesive.

5.2 Ludwik's Equation

Before investigating the ability of the constitutive equations to model the constant strain rate behavior, certain essential empirical relationships describing the rate behavior of the elastic limit stress and strain and maximum stress observed in the adhesives need to be discussed.

The elastic limit stress, θ, and elastic limit strain, ε_o, have been defined as the value of stress and strain separating the elastic region from the viscoplastic region. These values were taken from data such as that shown in Figs. 8 and 9 to be the upper limit of linearity for a given rate. Values for θ and ε_o are recorded in Table 1. The maximum stress, Y, has been defined to be value of stress at the initiation of perfectly plastic flow. While these definitions are to some extent arbitrary, they do provide for consistent comparison of experimental results with an empirical relationship proposed strictly for yield behavior by Ludwik [27].

As proposed by Ludwik, the variation in yield stress, σ_y, with strain rate may be written as,

$$\sigma_y = \sigma_y' + \sigma_y'' \log \frac{\dot{\varepsilon}}{\dot{\varepsilon}'} \tag{5.2.1}$$

where σ_y', σ_y'', and $\dot{\varepsilon}'$ are material constants.

The elastic limit stress and yield stress are identical. It is proposed, therefore, that the variation of elastic limit stress and strain, and maximum stress with strain rate follow similar expressions. These can be written as,

$$\theta = \theta' + \theta'' \log \frac{\dot{\varepsilon}}{\dot{\varepsilon}_1} \tag{5.2.2}$$

$$\varepsilon_0 = \varepsilon_0' + \varepsilon_0'' \log \frac{\dot{\varepsilon}}{\dot{\varepsilon}_1} \tag{5.2.3}$$

$$Y = Y' + Y'' \log \frac{\dot{\varepsilon}}{\dot{\varepsilon}_1} \tag{5.2.4}$$

where additional material constants are defined accordingly.

Fig. 13 shows a comparison of experimental results for θ and ε_0 as a function of $\dot{\varepsilon}$ compared with Eqs. (5.2.2) and (5.2.3), respectively. It may be observed that the equations fit the experimental data quite well and could be used to interpolate the data to other strain rates within the range of data. The variation of the maximum stress with strain rate is shown in Fig. 14. These results compare very well with Eq. (5.2.4).

5.3 Modified Ramberg-Osgood Models

5.3.1 RAMOD-1

The first Ramberg-Osgood model studied is Eq. (2.2.7) which is repeated below as,

$$\varepsilon = \varepsilon_E + \varepsilon_p = \frac{\sigma}{E} + K\sigma^n \tag{5.3.1}$$

and is called RAMOD-1 (Ramberg-Osgood Model - 1). The modulus, E, is

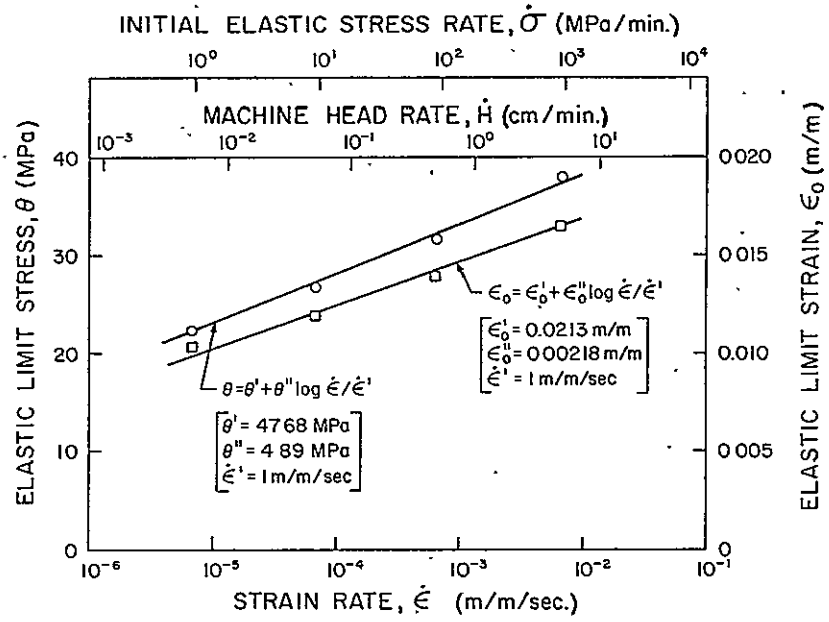

a METLBOND 1113

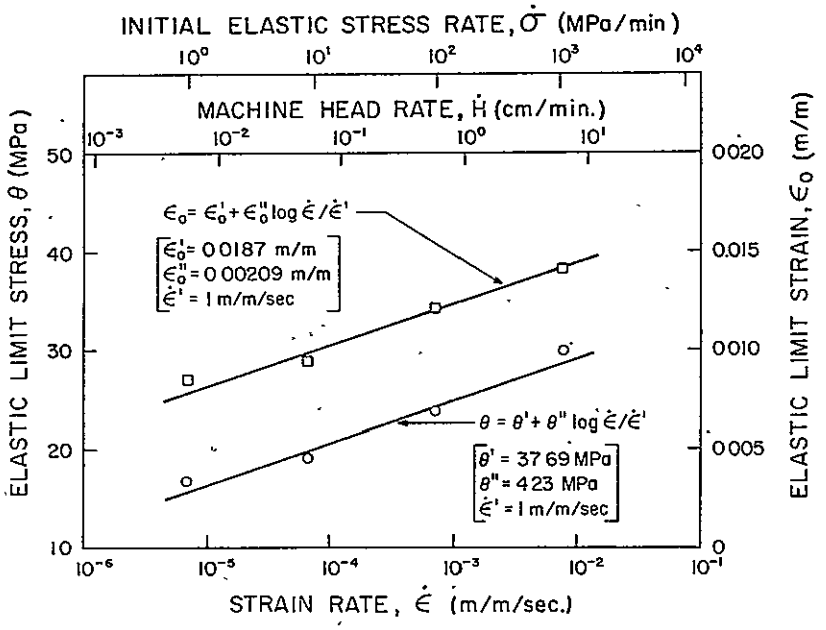

b METLBOND 1113-2

Figure 13. Variation of Elastic Limit Stress and Strain and Comparison with Ludwik's Equation

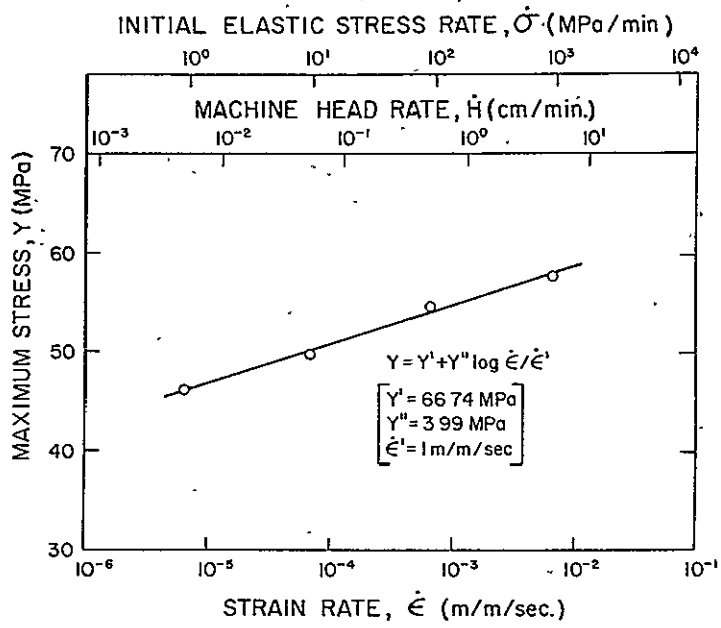

a. METLBOND 1113

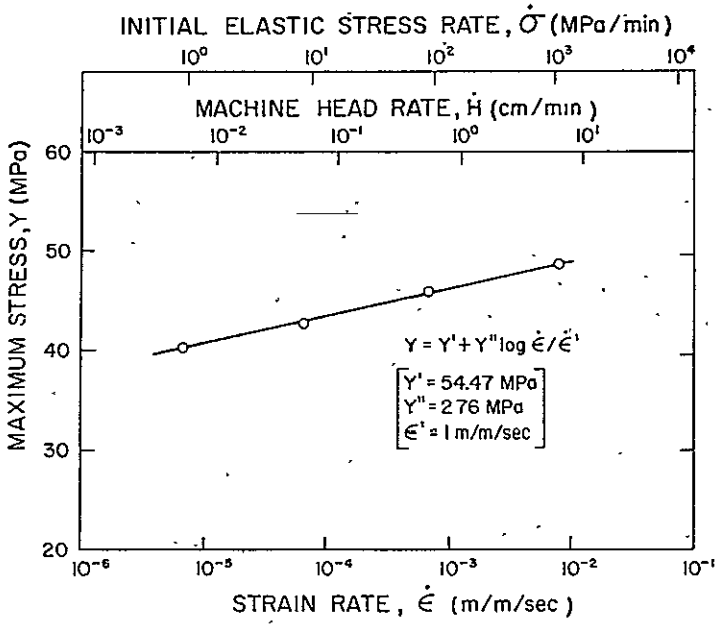

b METLBOND 1113-2

Figure 14. Variation of Maximum Stress and Comparison with Ludwik's Equation

taken directly from the stress-strain curve. Values for K and n are determined from a log-log plot of σ versus ε_p for each strain rate.

Using values of E, K, and n from each rate test, RAMOD-1 was used to describe the behavior of Metlbond 1113 and 1113-2. This model is called RAMOD-1-A. From the data presented in Figs. 8 and 9 log-log plots of σ versus ε_p were determined and fitted with a least squares approximation. These curves are presented in Figs. 15. It can be noted that these curves deviate from the linear approximation at higher values of stress and plastic strain.

Values for E, K, and n for each strain rate were determined as described earlier and are recorded in Table 2. Figs. 16 and 17 are comparisons of RAMOD-1-A to experimental data for Metlbond 1113 and 1113-2, respectively. Ludwik's equation (Eq. 5.2.4) was used to determine the maximum stress. It can be observed that the data for both adhesives is approximated reasonably well up to the maximum stress with this model.

In the rate form of RAMOD-1, Eq. (2.2.10), the coefficient n was considered to be invariant with strain rate. Using an average value of n, $\bar{n}$, from the rate data, Eq. (2.1.14) can be written as,

$$\varepsilon = \frac{\sigma}{c\dot{\varepsilon}^d} + a\dot{\varepsilon}^b\sigma^{\bar{n}} \qquad (5.3.2)$$

and is called RAMOD-1-B. The coefficients a and b were determined from a log-log plot of K versus $\dot{\varepsilon}$; coefficients c and d were determined from a log-log plot of E versus $\dot{\varepsilon}$. Values for these coefficients and $\bar{n}$ are recorded in Table 2.

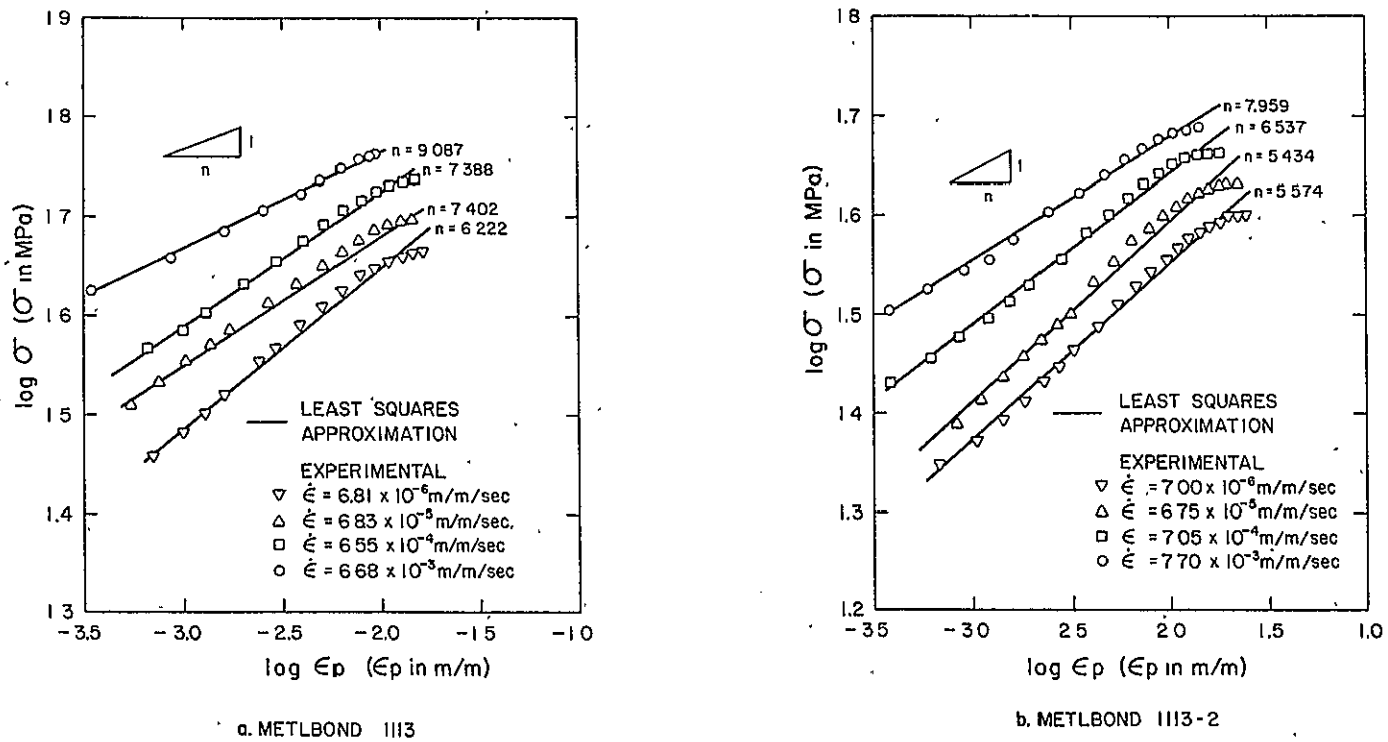

Figure 15. Log σ Versus Log εp for RAMOD-1-A

Table 2. COEFFICIENTS FOR RAMBERG-OSGOOD MODEL - 1 (RAMOD-1) COEFFICIENT.

Strain Rate (m/m/sec)	K (MPa^{-n})	n	K_1 (MPa^{-n_1})	n_1	K_2 (MPa^{-n_2})	n_2	$a(sec^b MPa^{-n})$	3.767×10^{-22}
							b	-1.779
							$c(sec^d MPa)$	2388.1
6.81×10^{-6}	5.505×10^{-13}	6.222	3.048×10^{-12}	5.734	7.197×10^{-29}	15.816	d	0.0077
6.83×10^{-5}	3.251×10^{-15}	7.402	1.336×10^{-14}	7.011	1.829×10^{-25}	13.506	f	11.34
6.55×10^{-4}	1.787×10^{-15}	7.388	7.374×10^{-15}	7.003	6.629×10^{-22}	11.118	g	0.0496
6.68×10^{-3}	8.563×10^{-19}	9.087	1.368×10^{-18}	8.967	4.962×10^{-26}	13.261	$\bar{n}$	7.525

a. Metlbond 1113

Strain Rate (m/m/sec)	K (MPa^{-n})	n	K_1 (MPa^{-n_1})	n_1	K_2 (MPa^{-n_2})	n_2	$a(sec^b MPa^{-n})$	6.257×10^{-19}
							b	-1.606
							$c(sec^d MPa)$	2069.6
7.00×10^{-6}	2.284×10^{-11}	5.574	5.628×10^{-11}	5.300	1.000×10^{-22}	12.697	d	0.004
6.75×10^{-5}	2.188×10^{-11}	5.434	1.080×10^{-10}	4.962	7.943×10^{-29}	16.183	f	9.91
7.05×10^{-4}	1.856×10^{-13}	6.537	5.099×10^{-13}	6.245	2.264×10^{-32}	18.000	g	0.0539
7.70×10^{-3}	4.405×10^{-16}	7.959	1.033×10^{-15}	7.723	5.196×10^{-24}	12.686	$\bar{n}$	6.376

b. Metlbond 1113-2

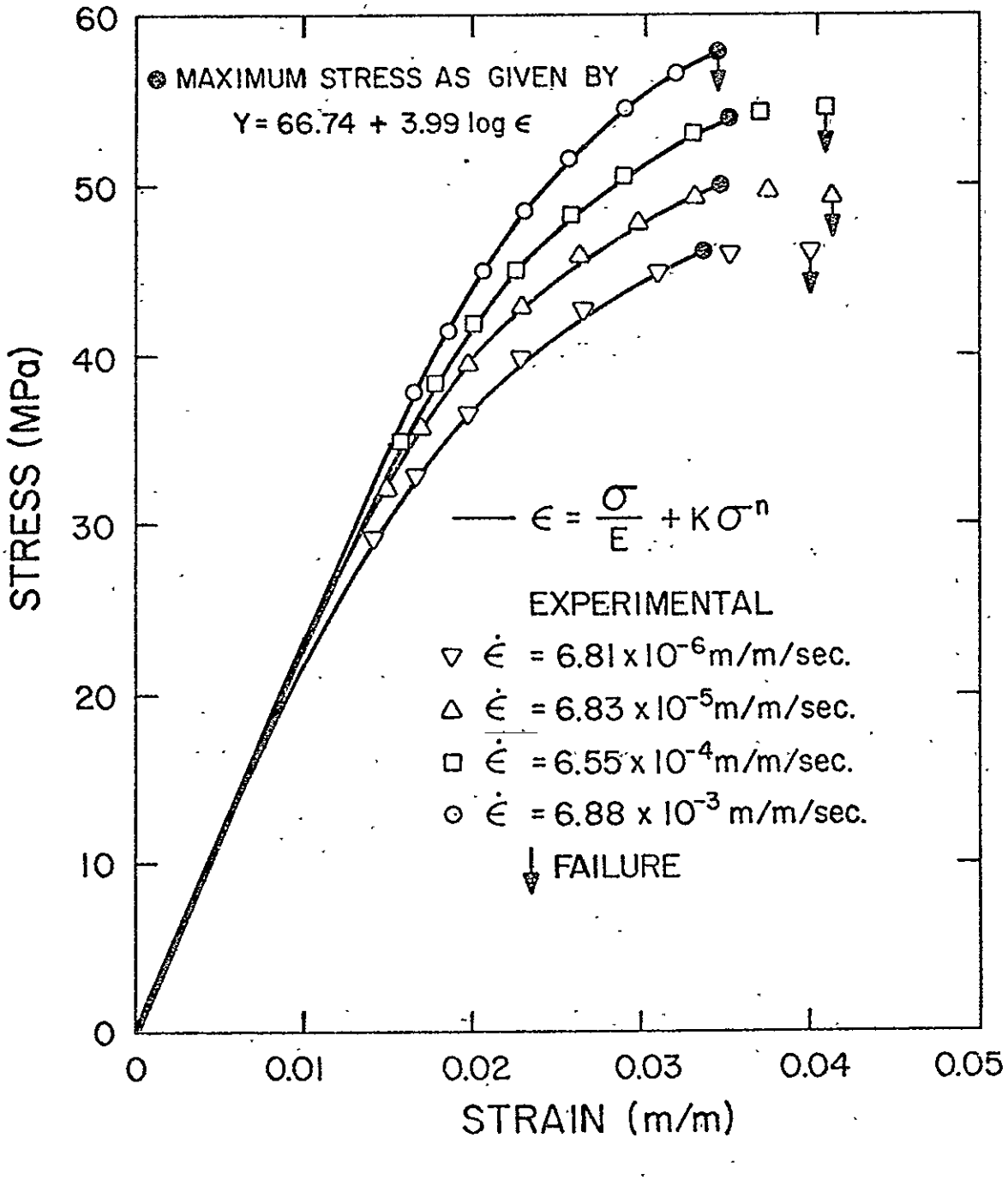

Figure 16. Stress-Strain-Strain Rate Behavior of Metlbond 1113 and Comparison to RAMOD-1-A

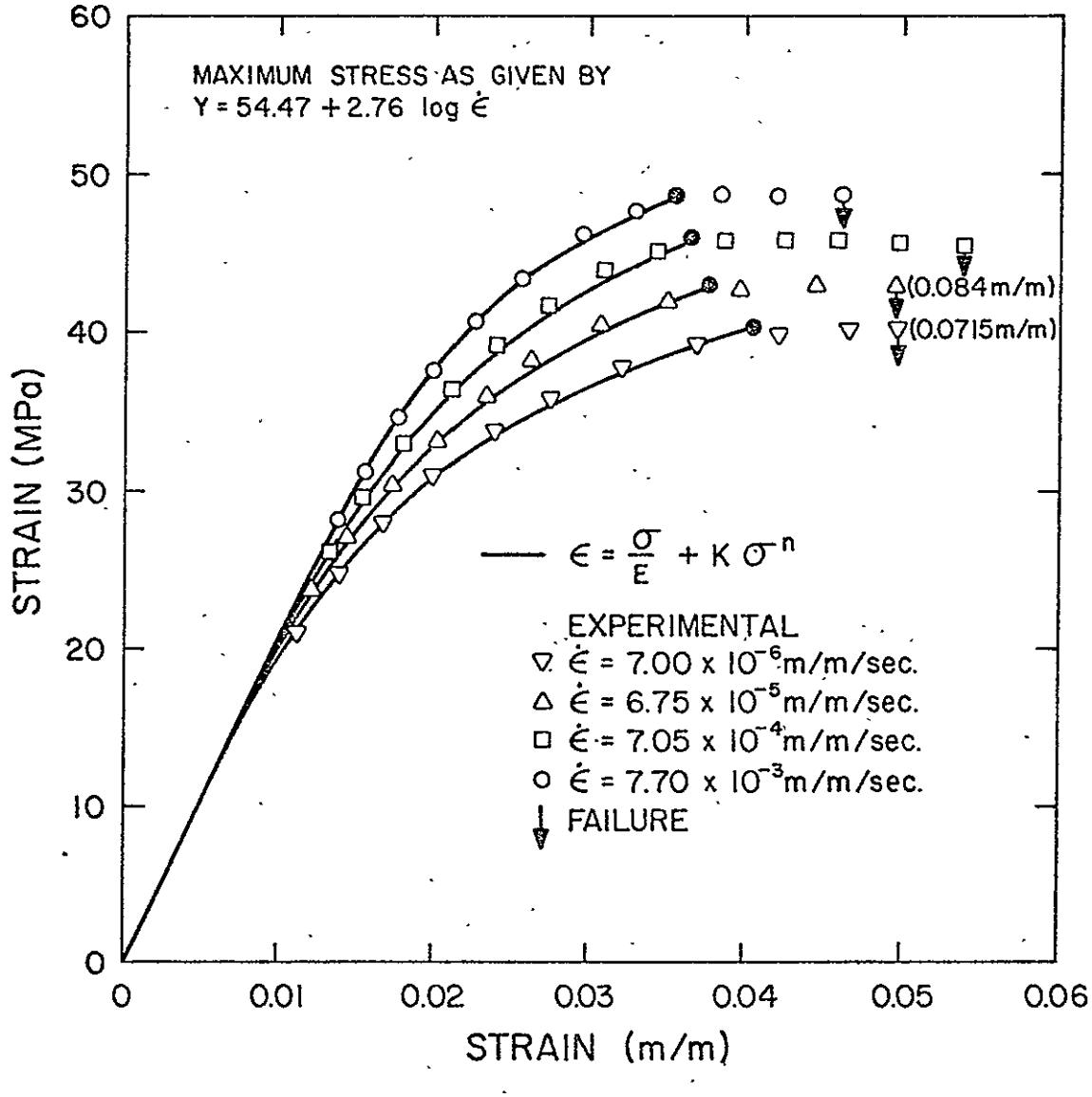

Figure 17. Stress-Strain-Strain Rate Behavior of Metlbond 1113-2 and Comparison to RAMOD-1-A

RAMOD-1-B did not model the rate behavior of the adhesives very well and the theoretical curves are not shown for this reason. The main difficulty is that n is not invariant with strain rate. Thus the average value of n predicts very large plastic strains for the lowest strain rate and small plastic strains for the highest strain rate. This, of course, does not agree with the experimental data for the range of strain rates investigated.

It is proposed to modify the form of RAMOD-1-B to allow for the rate dependency in n. The proposed form is,

$$\varepsilon = \frac{\sigma}{c\dot{\varepsilon}^{d}} + a\dot{\varepsilon}^{b}\sigma f\dot{\varepsilon}^{g} \qquad (5.3.3)$$

and is called RAMOD-1-C. The coefficients a, b, c, and d are identical to the previous model; the coefficients f and g (also recorded in Table 2) were determined from a log-log plot of n versus $\dot{\varepsilon}$ using a least squares approximation. Although this model was a definite improvement over RAMOD-1-B, it did not adequately model the behavior of the adhesives for the complete range of strain rates. The main deterent here is that the proposed form for the rate dependency in n,

$$n(\dot{\varepsilon}) = f\dot{\varepsilon}^{g} \qquad (5.3.4)$$

does not adequately model the experimental data.

5.3.2 Bilinear Form of RAMOD-1

Re-examination of Figs. 15(a) and (b) indicates that the results presented in these figures may be better represented by two straight lines for each strain rate. Figs. 18(a) and (b) are the bilinear

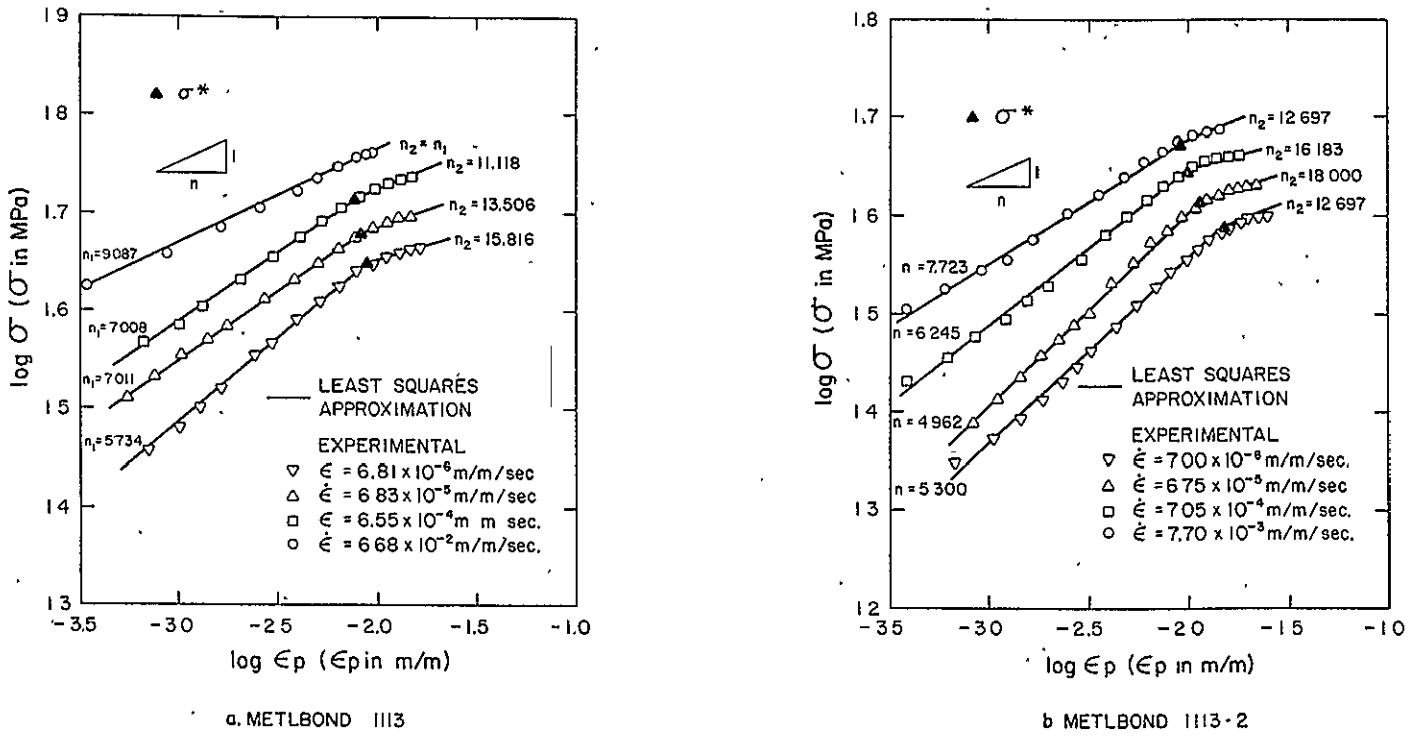

Figure 18. Bilinear Approximation of Log σ Versus Log ε_p for RAMOD-1-BL

approximations. The stress value at which these lines intersect has been defined as σ^*. Thus, RAMOD-1 has the form,

$$\begin{aligned} \varepsilon &= \frac{\sigma}{E} + K_1\sigma^{n_1} \qquad 0 < \sigma < \sigma^* \\ \varepsilon &= \frac{\sigma}{E} + K_2\sigma^{n_2} \qquad \sigma^* < \sigma < Y \end{aligned} \tag{5.3.5}$$

and appropriately called RAMOD-1-BL. Values for the bilinear coefficients for K and n (K_1, K_2, n_1, and n_2) are recorded in Table 2. Results using RAMOD-1-BL are compared to the experimental data in Figs. 19 and 20 for Metlbond 1113 and 1113-2, respectively. This model is an improvement over RAMOD-1-A in which values of K and n were used. These improvements are a better representation of the slope throughout and the prediction of larger strains corresponding to the values of stress prior to the maximum stress.

5.3.3 RAMOD-2

A Ramberg-Osgood type model was proposed, Eq. (3.1.1), in which the plastic strain, ε_p, is a function of the over-stress above the elastic limit stress. This equation has the form,

$$\begin{aligned} \varepsilon &= \frac{\sigma}{E} \qquad 0 < \sigma < \theta \\ \varepsilon &= \frac{\sigma}{E} + K(\sigma - \theta)^n \qquad \theta < \sigma < Y \end{aligned} \tag{5.3.6}$$

and is called RAMOD-2. Values for K and n are determined from a log-log plot of $(\sigma - \theta)$ versus ε_p for each strain rate. As in the previous model, variations in E with strain rate denote viscoelastic effects,

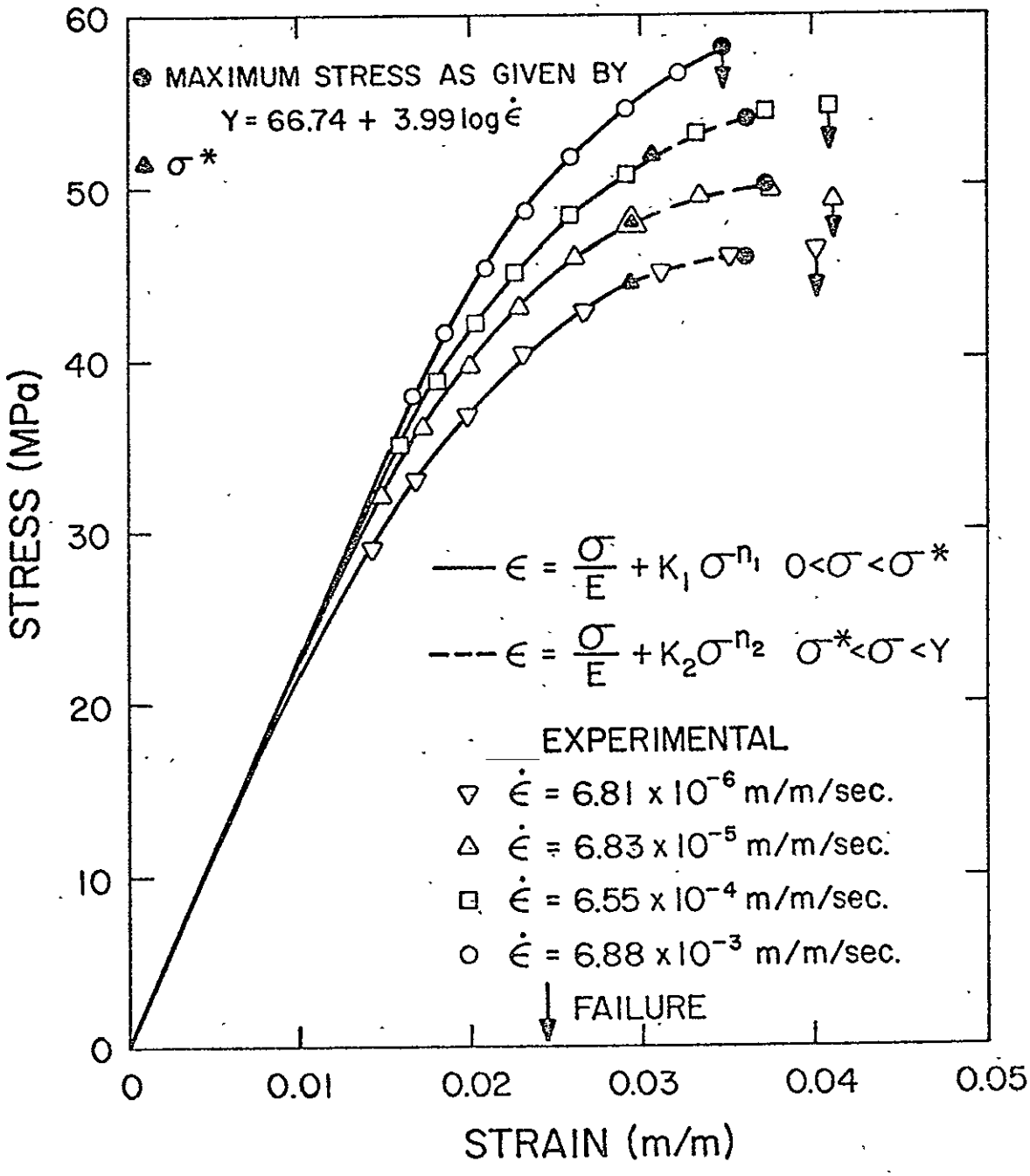

Figure 19. Stress-Strain-Strain Rate Behavior of Metlbond 1113 and Comparison to RAMOD-1-BL

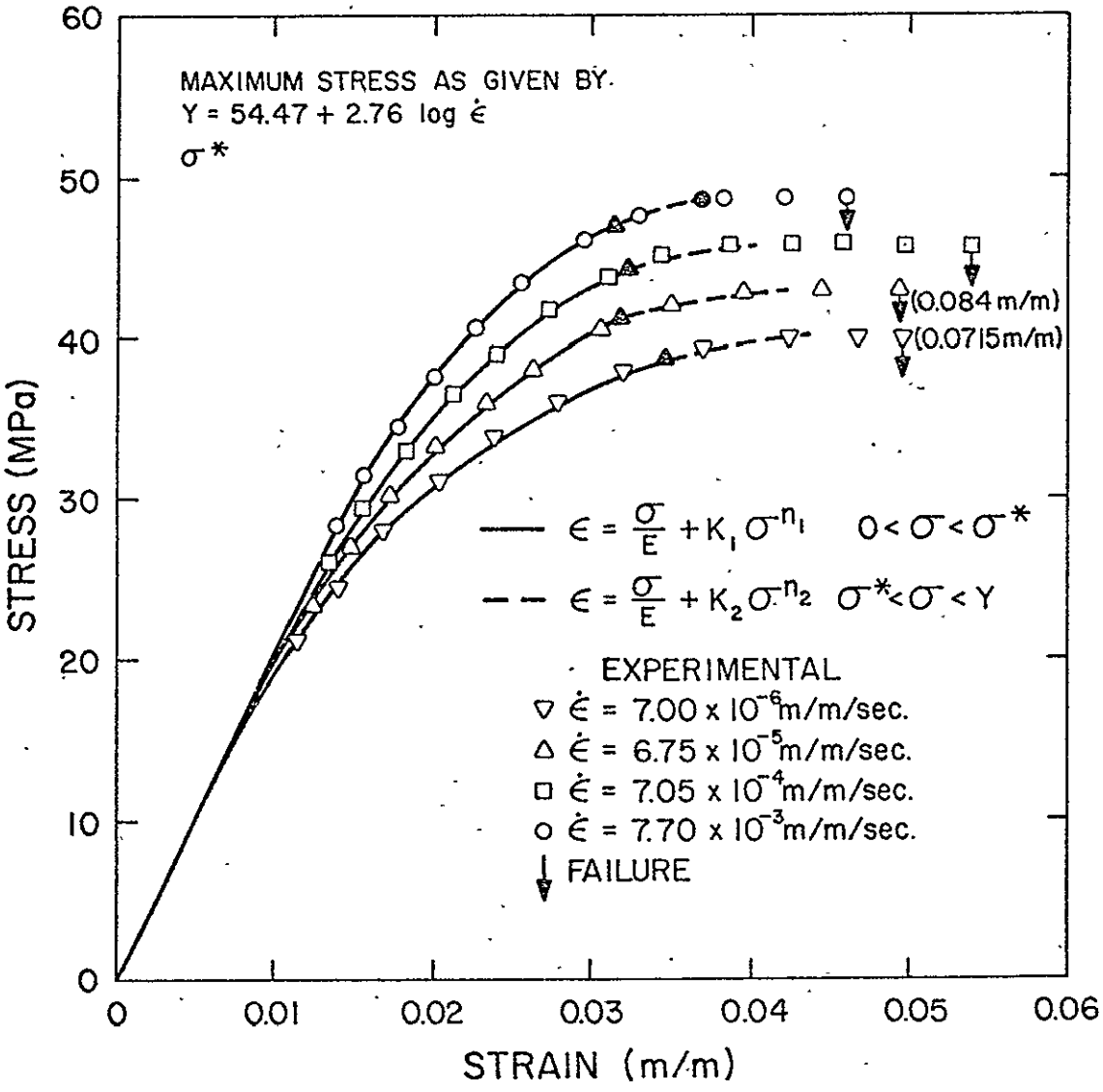

Figure 20. Stress-Strain-Strain Rate Behavior of Metlbond 1113-2 and Comparison to RAMOD-1-BL

while the parameters K and n represent variations in work-hardening characteristics with strain rate.

Proceeding in the same manner as RAMOD-1, the first model investigated was RAMOD-2-A which is actually written in the form of Eq. (5.3.6) and employs the values of E, K, and n for a given strain rate. Log-log plots of $(\sigma - \theta)$ versus ε_p are shown in Fig. 21. A least squares approximation for these results yielded the values for K and n for each strain rate which are recorded in Table 3. It can also be observed in Fig. 21 that these results may be represented by a bilinear approximation.

Results using RAMOD-2-A are compared to the experimental data in Figs. 22 and 23. Ludwik's equations, Eqs. (5.2.2) and (5.2.4), were used to determine the theoretical values for the elastic limit and maximum stresses, respectively. The results presented in Figs. 22 and 23 indicate that this model predicts the behavior of both adhesives reasonably well up to the maximum stress. However, it would be desirable to have a better representation of the slope throughout and the prediction of more plastic flow at the higher stresses.

In the derivation of the rate form of RAMOD-2, Eqs. (3.1.2), the coefficient n was also considered to be invariant with strain rate. Using an average value of n, $\bar{n}$, Eqs. (3.1.2) can be written as,

$$\varepsilon = \frac{\sigma}{c\dot{\varepsilon}^d} \qquad 0 < \sigma < \theta$$

$$\varepsilon = \frac{\sigma}{c\dot{\varepsilon}^d} + a\dot{\varepsilon}^b(\sigma - \theta)^{\bar{n}} \qquad \theta < \sigma < Y \tag{5.3.7}$$

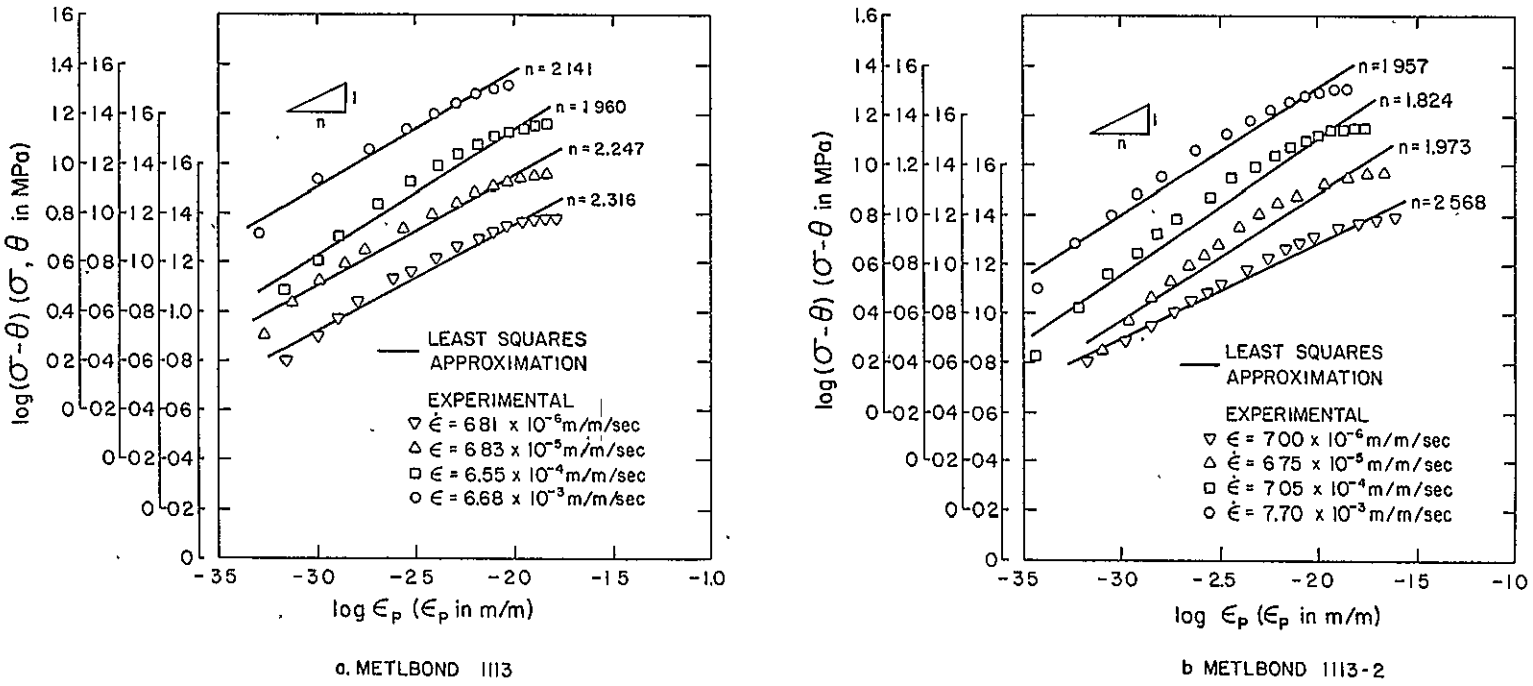

Figure 21. Log (σ - θ) Versus Log εp for RAMOD-2-A

Table 3. COEFFICIENTS FOR RAMBERG-OSGOOD MODEL - 2 (RAMOD-2) COEFFICIENT.

Strain Rate (m/m/sec)	K (MPa^{-n})	n	K_1 (MPa^{-n_1})	n_1	K_2 (MPa^{-n_2})	n_2	$a(sec^b MPa^{-n})$	2.778×10^{-5}
							b	0.102
							$c(sec^d MPa)$	2388.1
6.81×10^{-6}	7.318×10^{-6}	2.316	1.370×10^{-5}	2.045	1.715×10^{-13}	7.958	d	0.0077
6.83×10^{-5}	9.428×10^{-6}	2.247	1.437×10^{-5}	2.053	2.457×10^{-12}	7.210	f	1.885
6.55×10^{-4}	2.370×10^{-5}	1.960	3.818×10^{-5}	1.733	3.114×10^{-9}	4.912	g	-0.0162
6.68×10^{-3}	1.175×10^{-5}	2.141	1.689×10^{-5}	1.972	8.647×10^{-9}	4.574	$\bar{n}$	2.166

a. Metlbond 1113

Strain Rate (m/m/sec)	K (MPa^{-n})	n	K_1 (MPa^{-n_1})	n_1	K_2 (MPa^{-n_2})	n_2	$a(sec^b MPa^{-n})$	1.430×10^{-4}
							b	0.233
							$c(sec^d MPa)$	2069.6
7.00×10^{-6}	4.961×10^{-6}	2.568	7.365×10^{-6}	2.400	1.073×10^{-14}	8.969	d	0.004
6.75×10^{-5}	2.968×10^{-5}	1.973	4.544×10^{-5}	1.772	1.505×10^{-16}	10.419	f	1.500
7.05×10^{-4}	4.115×10^{-5}	1.824	5.260×10^{-5}	1.689	4.062×10^{-18}	12.478	g	-0.0379
7.70×10^{-3}	2.779×10^{-5}	1.957	3.397×10^{-5}	1.848	2.971×10^{-13}	8.227	$\bar{n}$	2.081

b. Metlbond 1113-2

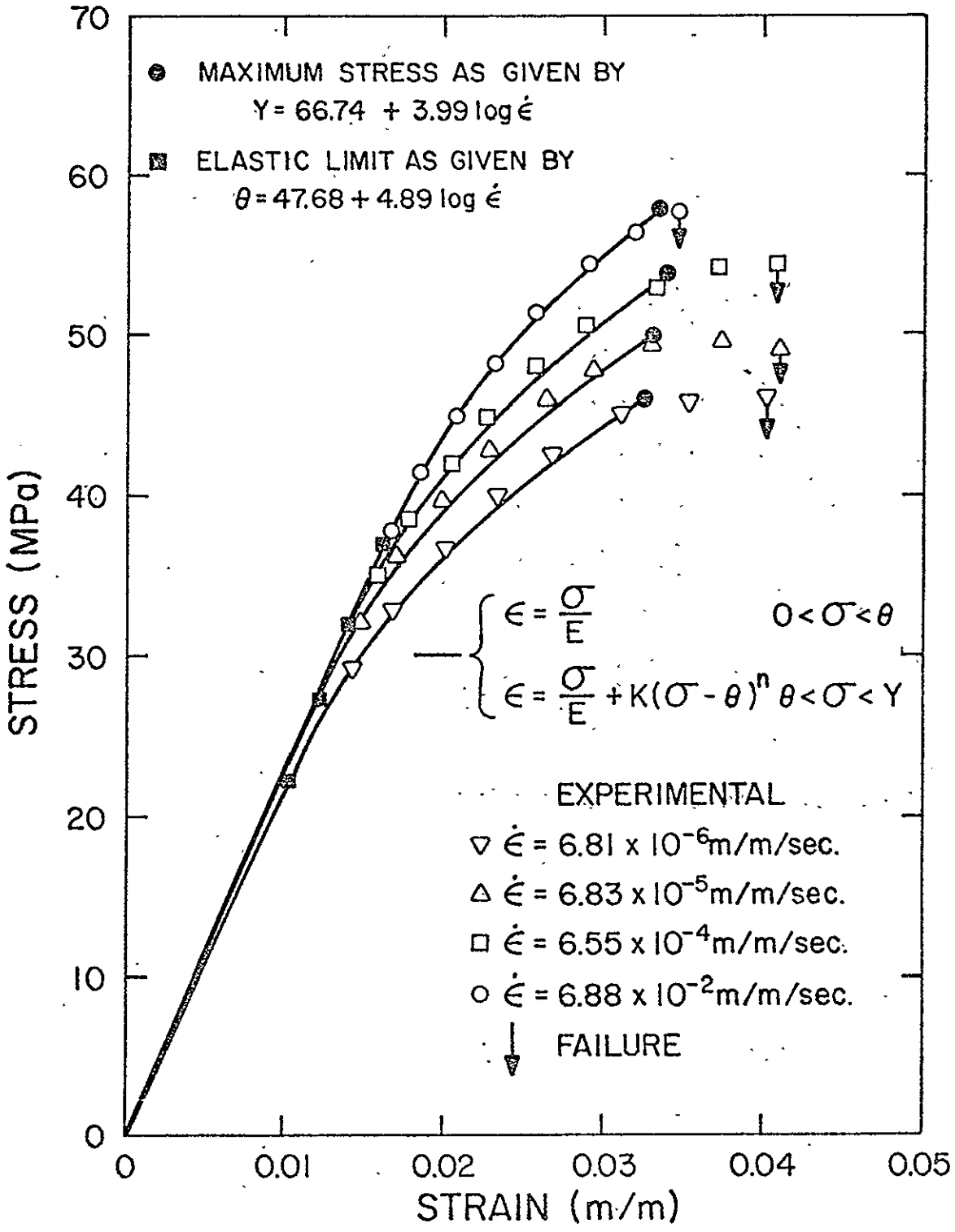

Figure 22. Stress-Strain-Strain Rate Behavior of Metlbond 1113 and Comparison to RAMOD-2-A

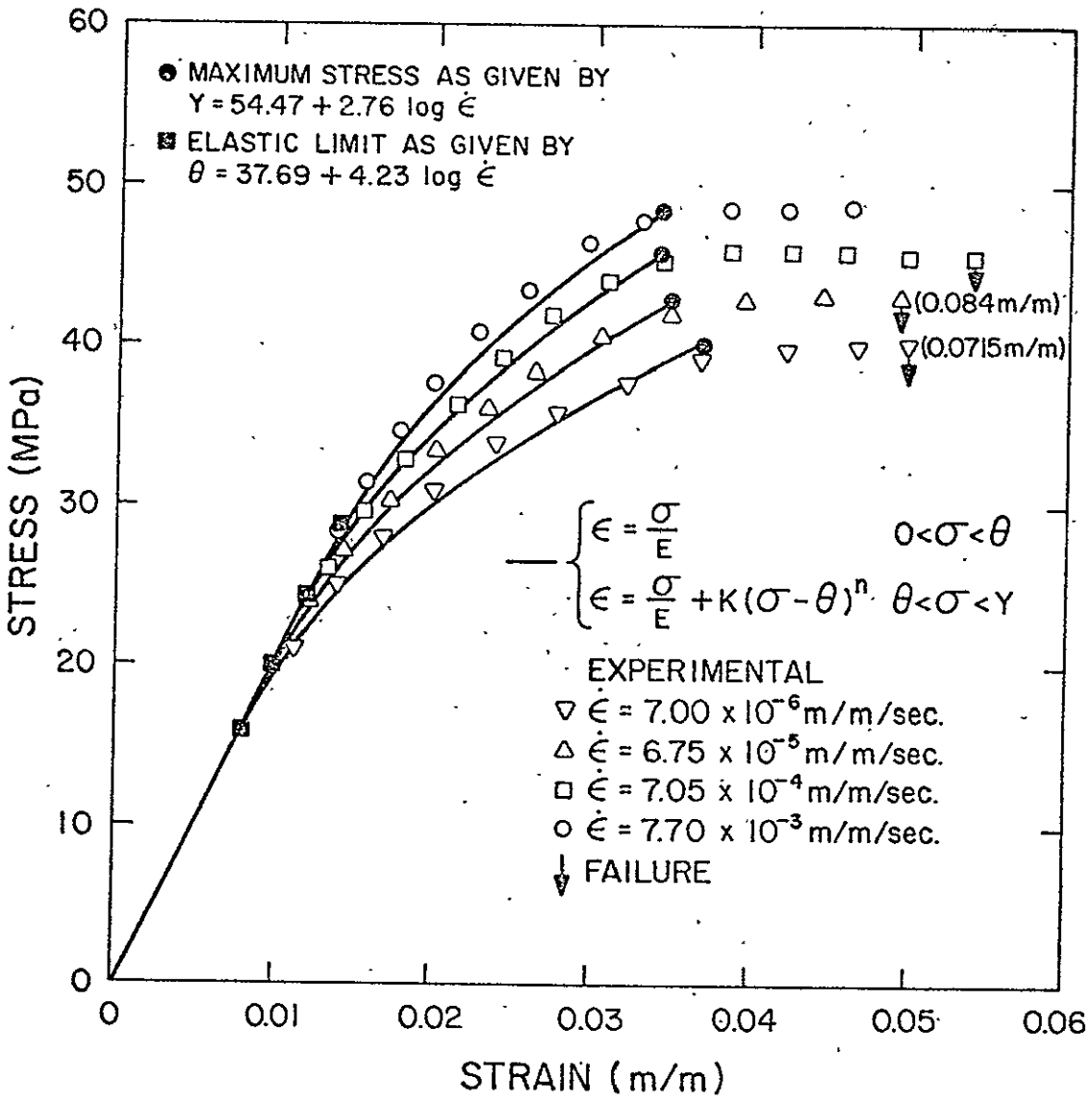

Figure 23. Stress-Strain-Strain Rate Behavior of Metlbond 1113-2 and Comparison to RAMOD-2-A

and termed RAMOD-2-B. The coefficients a and b were determined from a log-log plot of K versus $\dot{\varepsilon}$ as shown in Fig. 24. The coefficients c and d were determined from a log-log plot of E versus $\dot{\varepsilon}$ (Fig. 24). Values for these coefficients and $\bar{n}$ are recorded in Table 3.

The theoretical results using RAMOD-1-B did not adequately represent the rate behavior for either adhesive. This is attributed to the fact that although n is nearly a constant, RAMOD-2 is very sensitive to the small variations in n with strain rate.

It is proposed to modify RAMOD-2-B to account for the rate dependency in n. The proposed form is,

$$\begin{aligned} \varepsilon &= \frac{\sigma}{c\dot{\varepsilon}^{d}} && 0 < \sigma, < \theta \\ \varepsilon &= \frac{\sigma}{c\dot{\varepsilon}^{d}} + a\dot{\varepsilon}^{b}(\sigma - \theta)^{f\dot{\varepsilon}^{g}} && \theta < \sigma < Y \end{aligned} \tag{5.3.8}$$

and titled RAMOD-2-C. The coefficients f and g were calculated from log-log plots of n versus $\dot{\varepsilon}$ in Fig. 25 and are recorded in Table 3. Figs. 26 and 27 are comparisons of RAMOD-2-C with the experimental data for Metlbond 1113 and 1113-2, respectively. This model was a definite improvement over the previous rate form, RAMOD-2-B, and actually predicts the rate behavior better over all than RAMOD-2-A. From a programming aspect RAMOD-2-C is ideal in that only one parameter, $\dot{\varepsilon}$, needs to vary in the input data in order to study rate effects.

Models RAMOD-2-A and RAMOD-2-C are adequate in predicting the strain rate response of the adhesives. However, there is still a need

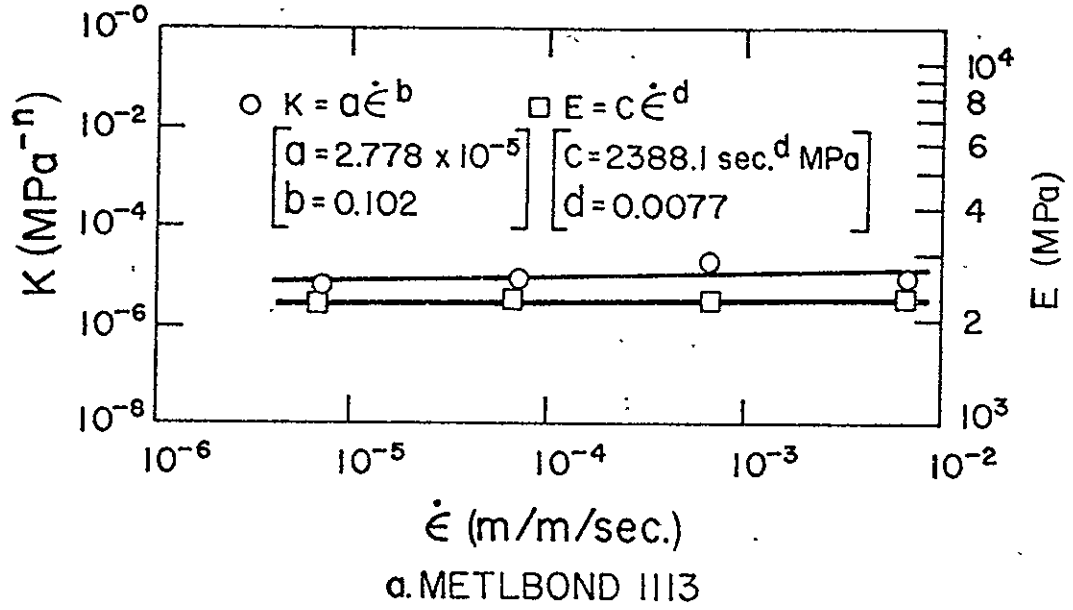

a. METLBOND 1113

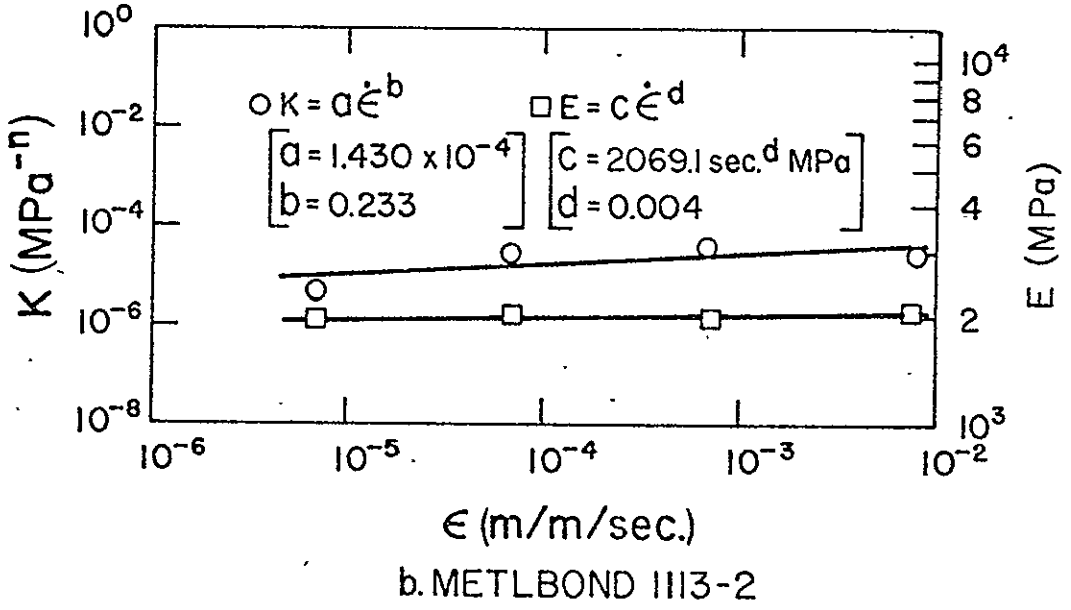

b. METLBOND 1113-2

Figure 24. Log K and Log E Versus Log $\dot{\epsilon}$ for RAMOD-2-B and RAMOD-2-C

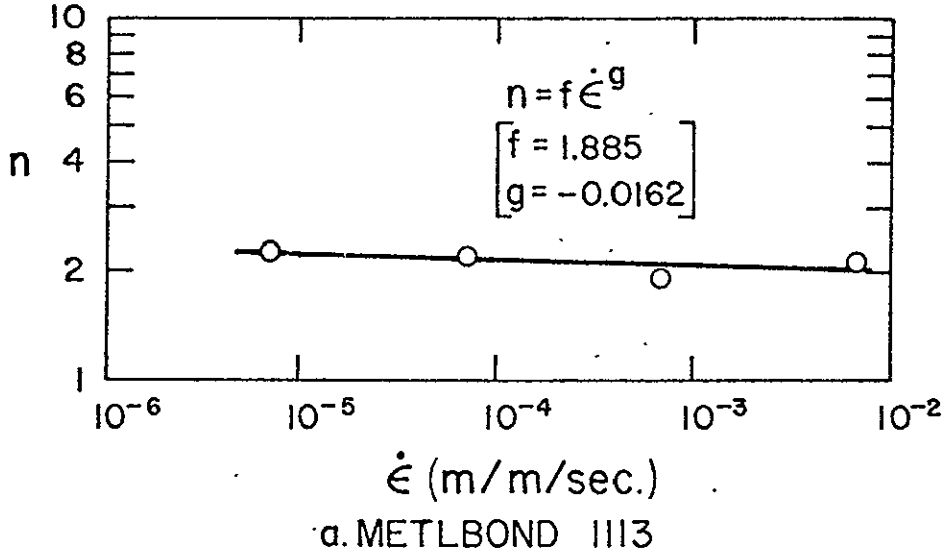

a. METLBOND 1113

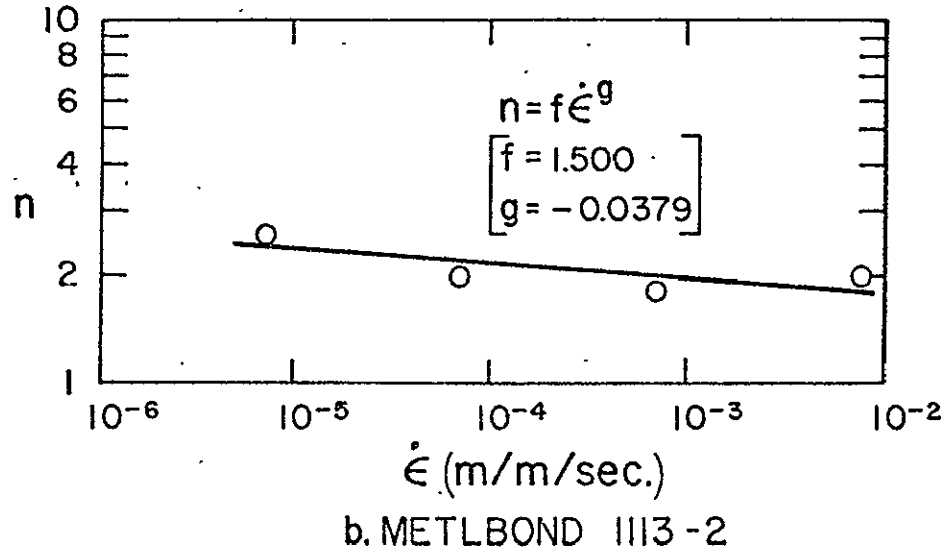

b. METLBOND 1113-2

Figure 25. Log n Versus Log $\dot{\epsilon}$ for RAMOD-2-C

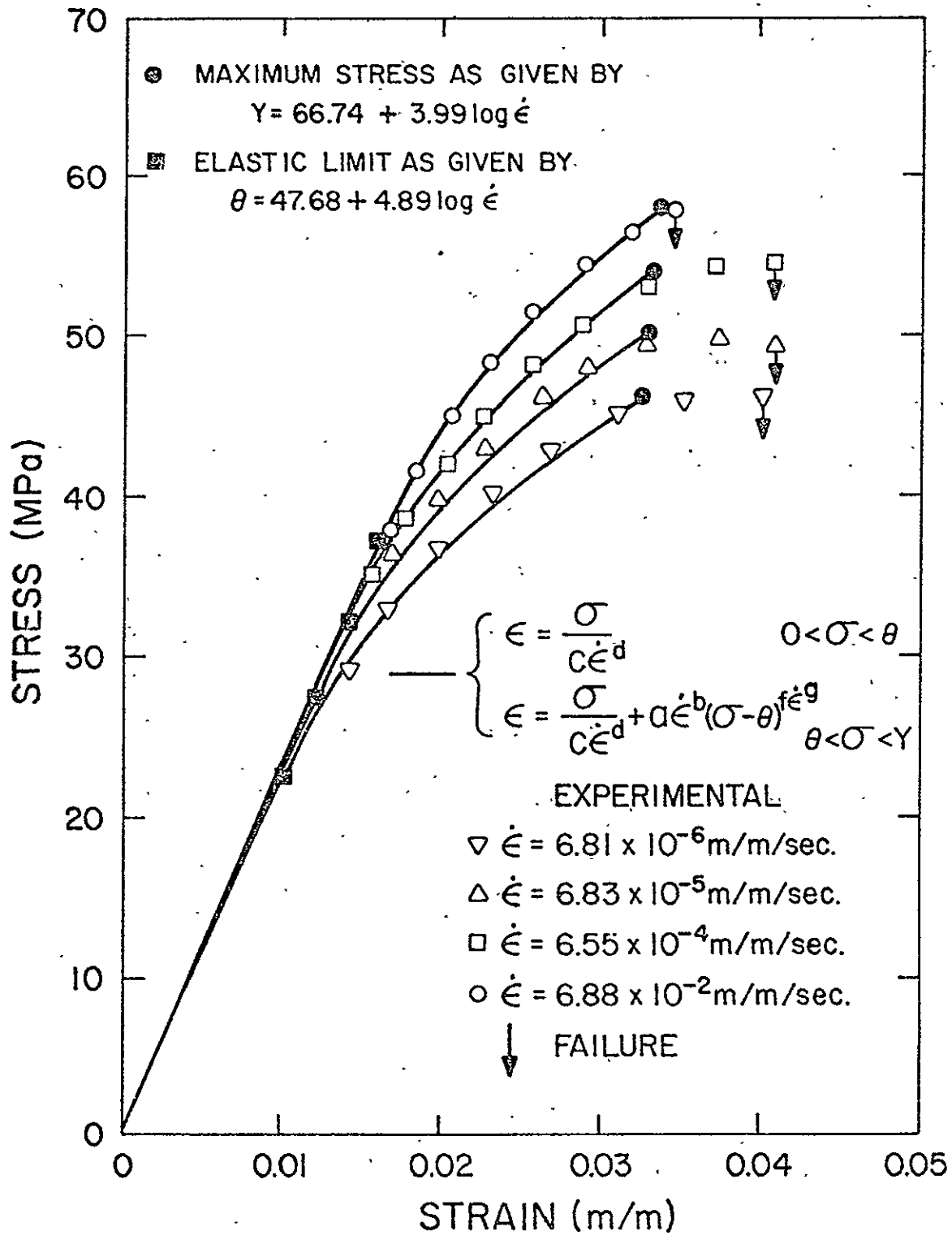

Figure 26. Stress-Strain-Strain Rate Behavior of Metlbond 1113 and Comparison to RAMOD-2-C

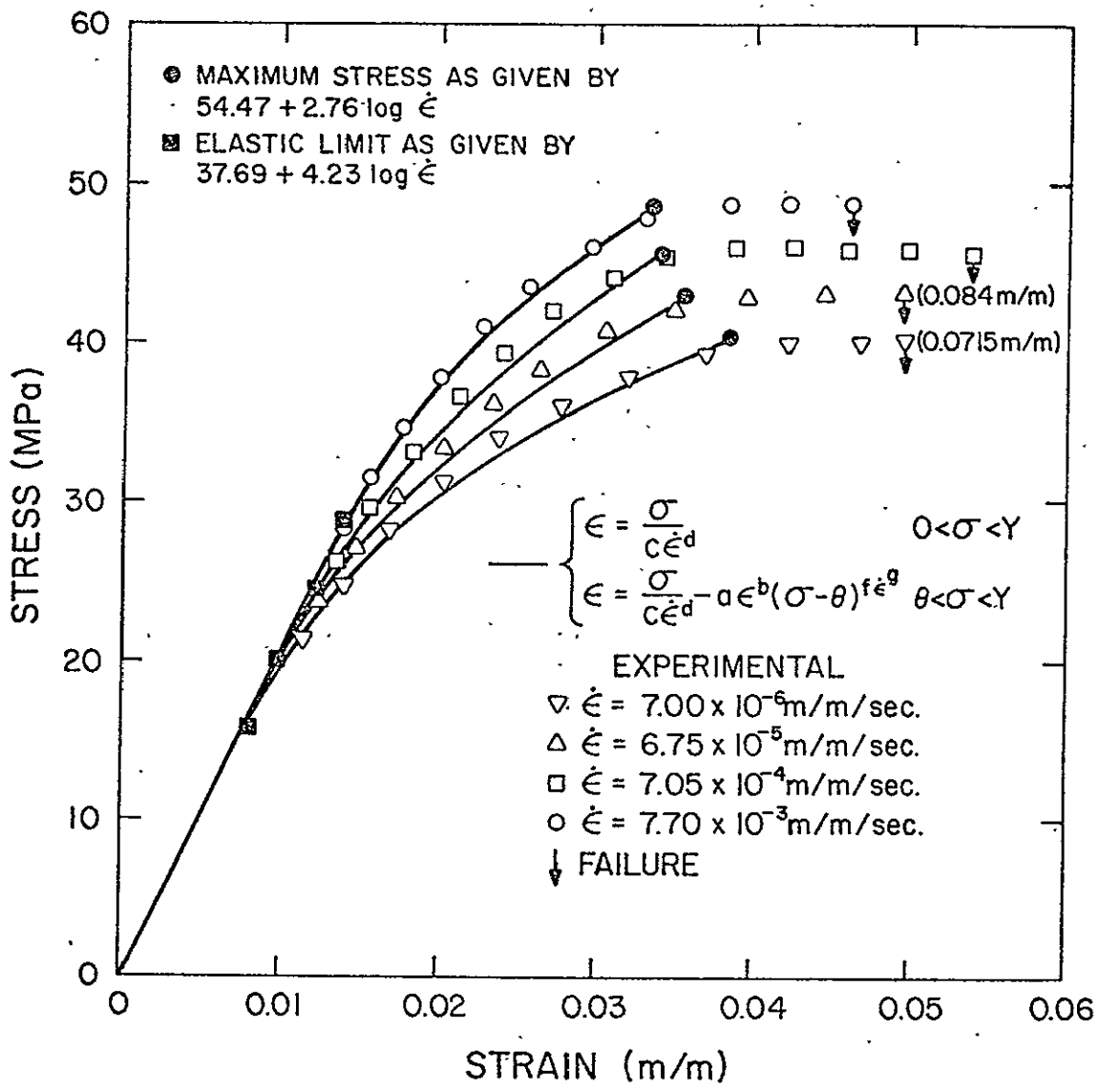

Figure 27. Stress-Strain-Strain Rate Behavior of Metlbond 1113-2 and Comparison to RAMOD-2-C

for an improvement both the representation of slope and the prediction of larger plastic strains correspond to stresses near the maximum stress. This suggests the bilinear approach used in RAMOD-1.

5.3.4 Bilinear Form of RAMOD-2

Fig. 28 is the bilinear approximations of log $(\sigma - \theta)$ versus log ε_p. The stress magnitude at the intersection of the two straight lines for each strain rate has again been defined as σ^*. The bilinear values of K and n generated for each strain rate are given in Table 3. Thus RAMOD-2-BL has the form,

$$\begin{aligned} \varepsilon &= \frac{\sigma}{E} && 0 < \sigma < \theta \\ \varepsilon &= \frac{\sigma}{E} + K_1(\sigma - \theta)^{n_1} && \theta < \sigma < \sigma^* \\ \varepsilon &= \frac{\sigma}{E} + K_2(\sigma - \theta)^{n_2} && \sigma^* < \sigma < Y \end{aligned} \qquad (5.3.9)$$

Results using RAMOD-2-BL are compared to the experimental data in Figs. 29 and 30 for Metlbond 1113 and 1113-2, respectively. Observation of these results indicate that a better representation of slope throughout and the prediction of larger plastic strains corresponding to stresses just prior to the maximum stress are realized.

5.3.5 Stress-Whitening-Stress and σ^*

In the bilinear models of both RAMOD-1 and RAMOD-2, σ^* has been defined as the stress at the intersection of the bilinear curves. It is interesting to compare these values to each other, and also to the value of the stress-whitening stress observed experimentally. These

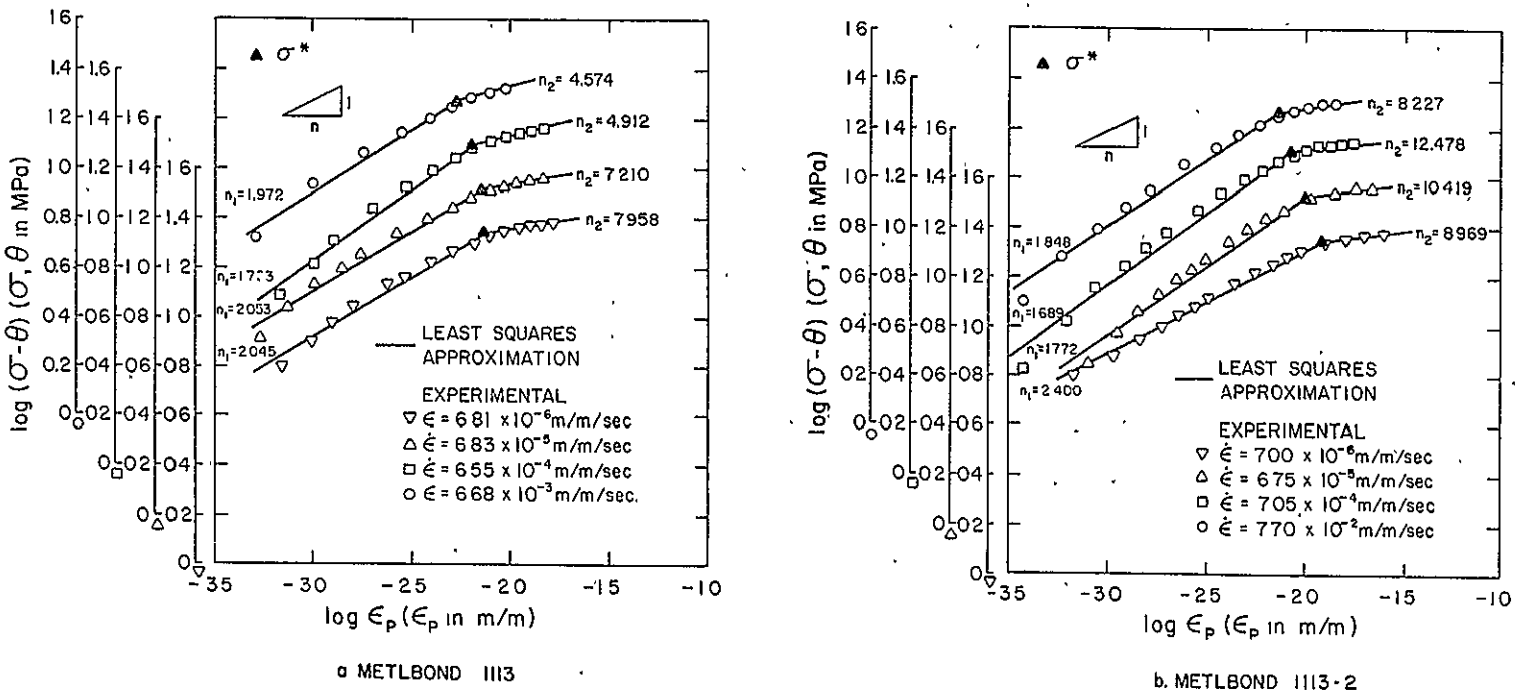

Figure 28. Bilinear Approximation of Log ($\sigma - \theta$) Versus Log ϵ_p for RAMOD-2-BL

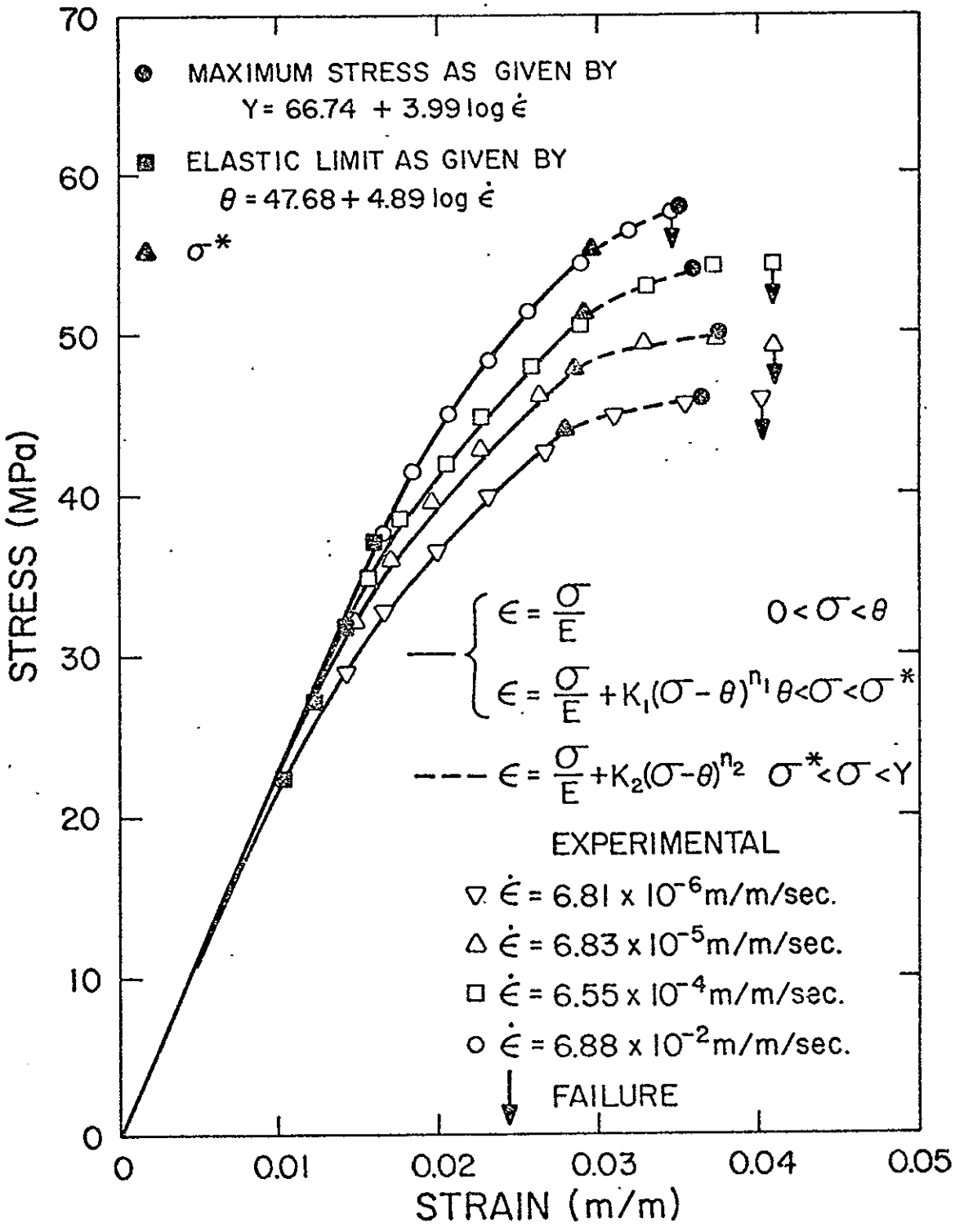

Figure 29. Stress-Strain-Strain Rate Behavior of Metlbond 1113 and Comparison to RAMOD-2-BL

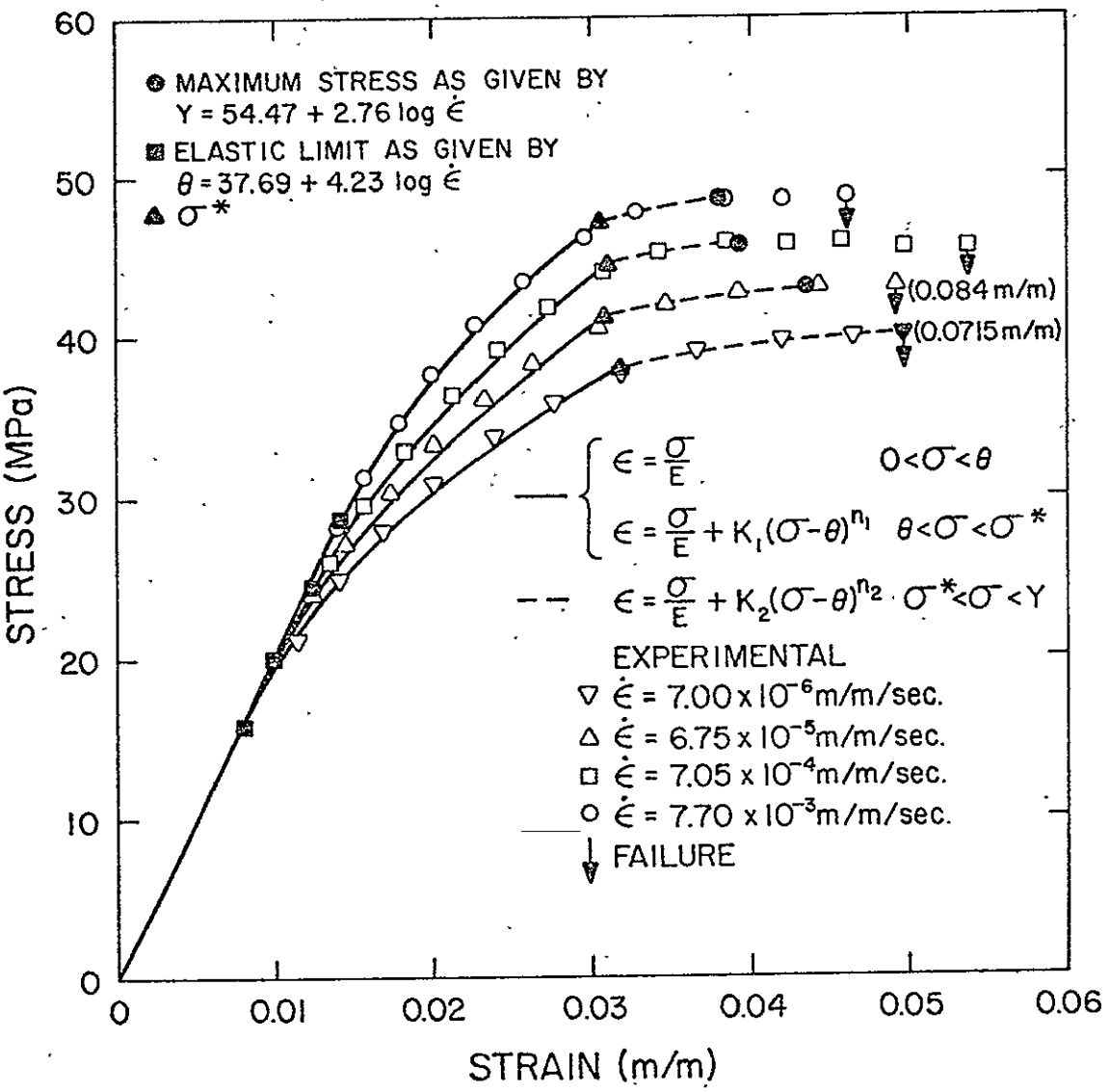

Figure 30. Stress-Strain-Strain Rate Behavior of Metlbond 1113-2 and Comparison to RAMOD-2-BL

results are presented in Table 4. It can be observed that the σ^* values for both stress and strain are very close for the two models. These values are also slightly lower than the stress-whitening values. It should be noted that the point at which stress-whitening occured during the rate tests was recorded by visual observation. Thus, the true point of initiation of the whitening may have occured earlier and was not readily visible. The strain values corresponding to σ^* were relatively constant for all rates. It is apparent that in the region of stress-whitening, a change of phase occurs both physically in the material and analytically in the bilinear models.

5.4 Modified Bingham Model

The constitutive equations for the modified Bingham model (Eqs. 2.4.1), which is shown in Fig. 1(a), are

$$\begin{aligned} \dot{\varepsilon} &= \frac{\dot{\sigma}}{E} && \sigma \leq \theta \\ \dot{\varepsilon} &= \frac{\dot{\sigma}}{E} + \frac{\sigma - \theta}{\mu} && \theta < \sigma < Y \end{aligned} \tag{5.4.1}$$

A stress such that $\sigma > Y$ is not allowed. For a constant strain-rate test, the solution of Eqs. (5.4.1) is Eqs. (2.4.3). This solution can be written as,

$$\begin{aligned} \sigma(\varepsilon) &= E\varepsilon && \sigma \leq \theta \\ \sigma(\varepsilon) &= \theta + ER\tau(1 - e^{-(\varepsilon - \varepsilon_0)/R\tau}) && \theta < \sigma < Y \end{aligned} \tag{5.4.2}$$

where $\tau = \mu/E$ is the relaxation time.

Table 4. σ^* AND STRESS-WHITENING STRESS.

Strain Rate (m/m/sec)	Stress Whitening Stress (MPa)	Strain (m/m)	RAMOD-1-BL σ^* (MPa)	Strain (m/m)	RAMOD-2-BL σ^* (MPa)	Strain (m/m)
6.81×10^{-6}	45.57	0.0330	44.58	0.0293	44.11	0.0278
6.83×10^{-5}	49.64	0.0332	47.91	0.0295	47.83	0.0284
6.55×10^{-4}	53.37	0.0348	51.84	0.0305	51.44	0.0292
6.68×10^{-3}	---	---	---	---	55.44	0.0295

a. Metlbond 1113

Strain Rate (m/m/sec)	Stress Whitening Stress (MPa)	Strain (m/m)	RAMOD-1-BL σ^* (MPa)	Strain (m/m)	RAMOD-2-BL σ^* (MPa)	Strain (m/m)
7.00×10^{-6}	39.23	0.0378	38.77	0.0345	38.03	0.0318
6.75×10^{-5}	42.47	0.0377	41.30	0.0318	41.31	0.0308
7.05×10^{-4}	45.37	0.0368	44.29	0.0321	44.68	0.0310
7.70×10^{-3}	---	---	46.97	0.0314	47.08	0.0304

b. Metlbond 1113-2

Eqs. (5.4.2) were fitted to the rate dependent stress-strain behavior presented in Figs. 8 and 9. These results are shown in Figs. 31 and 32 for Metlbond 1113 and 1113-2, respectively. Ludwik's equations for the θ and ε_0 (Eqs. (5.2.2) and (5.2.3)) and Y (Eq. (5.2.4)) were used to determine the theoretical values for the elastic limit and maximum stress, respectively. With this procedure it was possible to accurately represent the rate dependent behavior with the modified Bingham model. An accurate representation of slope is observed throughout. This model also allows perfectly plastic behavior after the maximum stress is reached which is in agreement with the experimental results.

5.4.1 Rate Dependent Viscosity Coefficient

It was found that a single relaxation time for each adhesive was inadequate to fit full range of the strain rate results. Therefore, a relaxation time (or viscosity coefficient, since $\mu = \tau E$) was determined to give the best fit at a given rate. The relaxation times necessary to achieve the close approximations obtained in Figs. 31 and Figs. 32 are plotted in Fig. 33. It is interesting to note that a single linear curve can approximate the data for both adhesives when plotted on log-log scales. The values for the relaxation times as well as the viscosity coefficients for each strain rate are presented in Table 5. It can be observed that as the strain rate increases an order of magnitude the viscosity coefficient decreases by an order of magnitude.

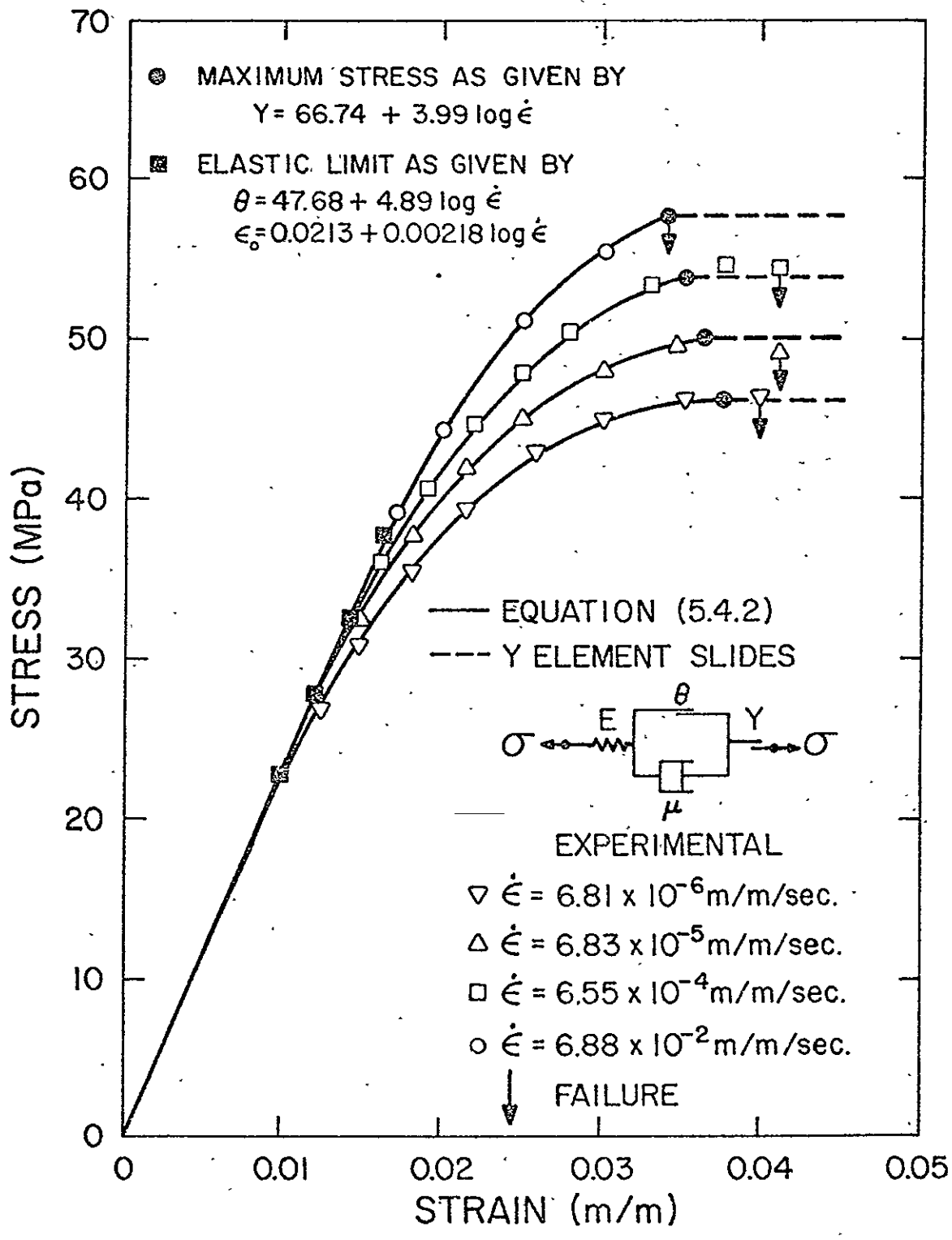

Figure 31. Stress-Strain-Strain Rate Behavior of Metlbond 1113 and Comparison to Modified Bingham Model

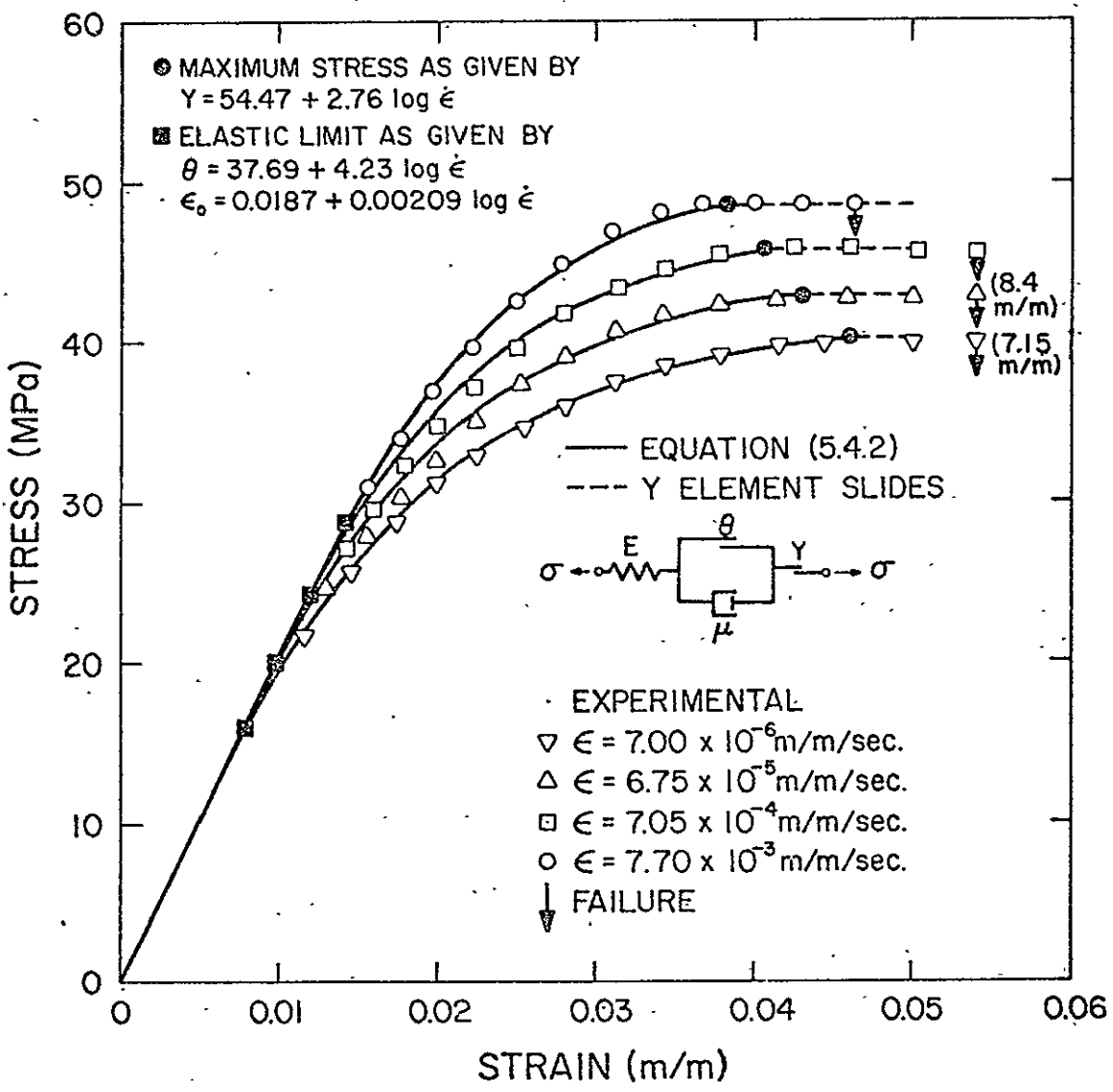

Figure 32. Stress-Strain-Strain Rate Behavior of Metlbond 1113-2 and Comparison to Modified Bingham Model

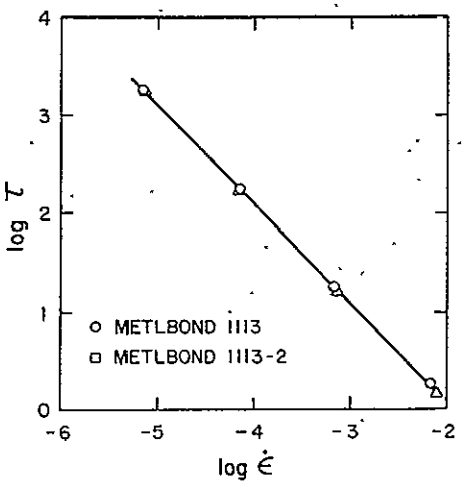

Figure 33. Relaxation Time Versus Strain Rate for Modified Bingham Model

Table 5. RATE DEPENDENT RELAXATION TIMES AND VISCOSITY COEFFICIENTS.

$\dot{\epsilon}$ (m/m/sec)	τ (sec)	μ (MPa - sec)
6.81×10^{-6}	1800.00	4.03×10^{6}
6.83×10^{-5}	173.85	3.89×10^{5}
6.55×10^{-4}	18.15	4.07×10^{4}
6.68×10^{-3}	1.85	4.14×10^{3}

a. Metlbond 1113

$\dot{\epsilon}$ (m/m/sec)	τ (sec)	μ (MPa - sec)
7.00×10^{-6}	1816.80	3.67×10^{6}
6.75×10^{-5}	180.20	3.64×10^{5}
7.05×10^{-4}	16.49	3.33×10^{4}
7.70×10^{-3}	1.45	2.93×10^{3}

b. Metlbond 1113-2

The constitutive form of the modified Bingham model, Eqs. (2.4.3), does not specifically indicate that μ may be rate dependent. However, the analogous form of these equations, Eqs. (2.3.15), derived from incremental theory indicated this possibility. Other investigators, such as Chase and Goldsmith [22], using mechanical models to predict the behavior of rate-sensitive plastic materials observed this same phenomenon. The rate dependency in μ is therefore considered to be an inherent property of rate-sensitive materials.

5.4.2 Nonlinear Model

In an attempt to mathematically describe the rate effect observed in the viscosity coefficient for the modified Bingham model, the nonlinear perturbation technique proposed by Davis [4] (Section 3.2) was investigated. This technique did not show the viscosity coefficient to be dependent on the total strain rate $\dot{\varepsilon}$, since the nonlinear hypothesis, Eqs. (3.2.1), states that variations in μ are dependent on the strain rate in the dashpot, $\dot{\varepsilon}_\mu$. However, the nonlinear model did yield some interesting information relative to the viscosity coefficient of the adhesives above and below the stress-whitening point.

Postulating that the nonlinear effects were present in the dashpot only, the nonlinear constitutive equations for the modified Bingham model (Eqs. (3.4.6)) can be written as,

$$\sigma(\varepsilon) = E_0\varepsilon \qquad \sigma \leq \theta$$

$$\sigma(\varepsilon,\gamma_\mu) = \theta + E_0R\tau(1 - e^{-(\varepsilon - \varepsilon_0)/R\tau}) + \gamma_\mu(2E_0R\tau(\varepsilon - \varepsilon_0) \qquad (5.4.3)$$

$$+ E_0R^2\tau^2(1 - e^{-2(\varepsilon - \varepsilon_0)/R\tau}) \qquad \theta < \sigma < Y$$

where $\tau = \mu_0/E_0$ is the linear relaxation time as before. For $\theta < \sigma < Y$ the second of Eqs. (5.4.3) can be written as

$$\sigma(\varepsilon,\gamma_\mu) = \sigma_0 + \gamma_\mu S_1 \qquad \theta < \sigma < Y \qquad (5.4.4)$$

where

$$\sigma_0 = \theta + E_0R\tau(1 - e^{-(\varepsilon - \varepsilon_0)/R\tau}) \qquad (5.4.5)$$

is the linear solution as before and

$$S_1 = 2E_0R\tau(\varepsilon - \varepsilon_0) + E_0R^2\tau^2(1 - e^{-2(\varepsilon - \varepsilon_0)/R\tau}) \qquad (5.4.6)$$

The term $\sigma(\varepsilon,\gamma_\mu)$ is considered to be the experimental data, and the coefficient γ_μ is allowed to vary to fit the experimental data exactly. Then Eq. (5.4.4) can be written as,

$$\frac{(\sigma_{exp} - \sigma_{theo})}{S_1} = \gamma_\mu \qquad (5.4.7)$$

where $\sigma_{theo} = \sigma_0$ represents the theoretical curve from the linear solution. As an example of the implications of Eq. (5.4.7), the parameters in this equation were calculated using the data for Metlbond 1113-2 at a constant strain rate of $\dot{\varepsilon} = 7.05 \times 10^{-4}$ m/m/sec (Fig. 9). These results are presented in Fig. 34.

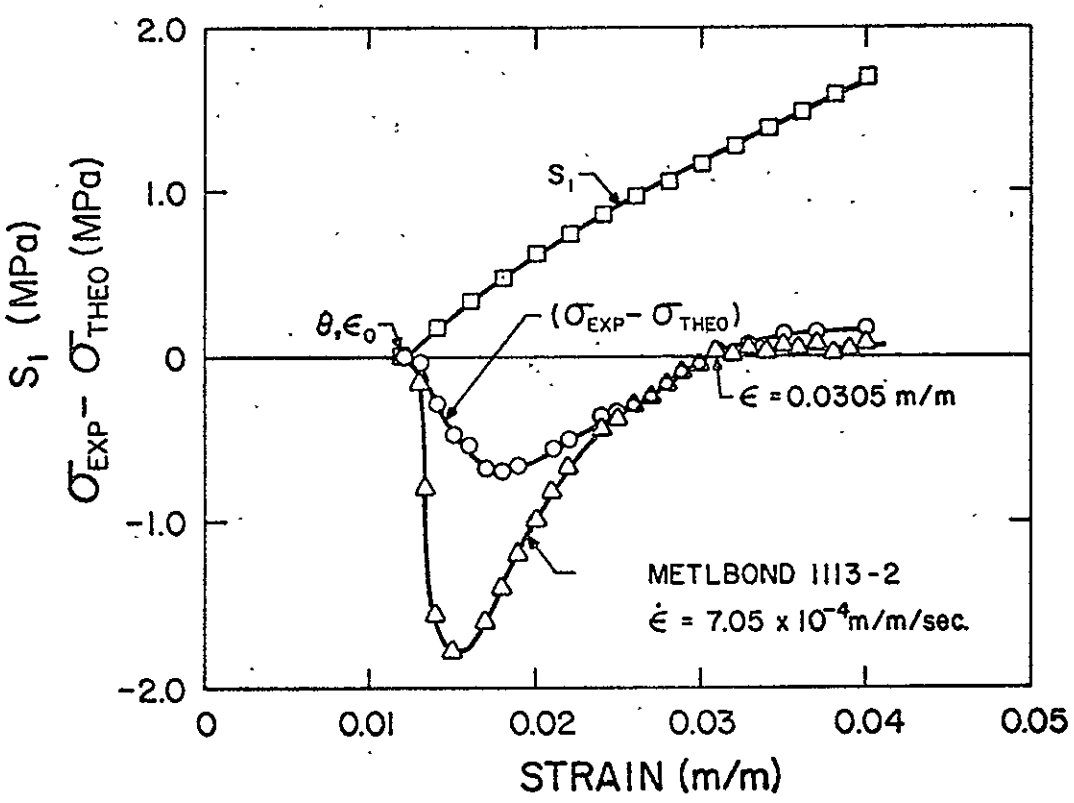

Figure 34. Parameters in Nonlinear Model

5.4.3 Significance of Stress-Whitening Stress

It is interesting to note the point (in Fig. 33) at which the linear solution and the experimental results agree exactly (i.e., $\gamma_\mu = 0$). The stress and strain values, 43.0 MPa and 0.305 m/m, respectively, are slightly lower but very close to the stress-whitening values for this rate (i.e., 45.37 MPa and 0.0368 m/m, respectively). Similar results can be obtained for the other strain rates. It can also be observed that the value of γ_μ changes sign in this transition (stress-whitening) region. Therefore, the perturbation analysis shows that the value of the viscosity coefficient prior to the stress-whitening region is lower than that predicted by the linear solution and higher above this region. This indicates that coefficients present in the modified Bingham could vary above and below the stress-whitening region in order to obtain a more accurate representation of the experimental results. This same phenomenon was observed in the modified Ramberg-Osgood models.

Although this nonlinear analysis yielded interesting information relative to the linear solution above and below the stress-whitening region, it has not been considered further in this study since the nonlinear effects present are very small. That is, the linear solution of the modified Bingham model adequately predicts the rate behavior.

5.5 Models in Advanced Laminate Analysis

A goal of this study has been to develop analytical models capable of predicting the strain rate behavior of Metlbond 1113 and 1113-2. These models should also be easily adaptable for use in

advanced analysis of material systems. Recent investigators [28, 29, 30] have used various modified Ramberg-Osgood equations in advanced analysis of composite laminates. Hashin, et al. [28] use a modified form of RAMOD-1, written as,

$$\varepsilon = \frac{\sigma}{E}\left(1 + \left(\frac{\sigma}{\bar{\sigma}_y}\right)^{n-1}\right) \tag{5.5.1}$$

where $\bar{\sigma}_y$ is a curve fitting parameter, to describe the behavior of the matrix material in boron/epoxy laminates. Kibler [29] also used the form of Eq. (5.5.1) to model the nonlinear behavior of the transverse extensional and inplane shear stress-strain relationships for unidirectional, fiber reinforced laminae. In an effort to describe these same latter two relationships, G. Renieri [30] is currently using a model in the form of RAMOD-1. The model is being used in an incremental loading scheme in conjunction with the finite element method in order to predict the stress distributions in composite laminates. RAMOD-1 was considered since it gave an accurate representation of the slope which is essential in the incremental analysis. For example, using RAMOD-1, the slope would be,

$$\frac{d\sigma}{d\varepsilon} = \frac{E}{1 + En K\sigma^{n-1}} \tag{5.5.2}$$

and similar equations would prevail for the various forms of RAMOD-1 and RAMOD-2. For stresses below the elastic limit, the slope, $d\sigma/d\varepsilon$, given by Eq. (5.5.2) is essentially the modulus E. Above the elastic limit the slope begins to decay exponentially from a value of E.

Although the literature has not produced such evidence, the modified Bingham model could also be used in advanced laminate analysis. This model would be ideally suited for the analysis of material systems using Metlbond 1113 or 1113-2. For incremental formulations the slope using the modified Bingham model would be,

$$\frac{d\sigma}{d\varepsilon} = Ee^{-(\varepsilon - \varepsilon_0)/R\tau} \tag{5.5.3}$$

which shows that the slope is E at the elastic limit ($\varepsilon = \varepsilon_0$) and the n decays exponentially, as expected, for higher strains.

The modified Bingham model could also be used to model a single nonlinear stress-strain curve (i.e., rate data not available). For example, Eqs. (5.4.2) can be written as,

$$\begin{aligned} \sigma &= E\varepsilon && \sigma \leq \theta \\ \sigma &= \theta + EK_0(1 - e^{-(\varepsilon - \varepsilon_0)/K_0}) && \theta < \sigma < Y \end{aligned} \tag{5.5.4}$$

where K_0 is a material constant determined empirically to give the best fit to the experimental data. Equations of this form may be useful in modeling the nonlinear behavior of composite laminate in future investigations.

Chapter 6

CREEP, RELAXATION, AND UNLOADING BEHAVIOR

This chapter is concerned with the ability of the modified Bingham model to predict the behavior of Metlbond 1113 and 1113-2 for loading conditions other than constant strain rate. Creep results are presented initially. The relaxation results are then reviewed. The final section of this chapter presents the experimental and theoretical results for two, more complex strain histories.

6.1 Creep Results

Creep results are shown in Figs. 35 and 36 for Metlbond 1113 and 1113-2, respectively. For these tests the levels of stress were purposely larger than the elastic limit values found in the rate tests as little time effects were expected below these levels.

It may be seen from Figs. 35 and 36 that the adhesives exhibit a delayed failure phenomenon. That is, in the creep tests, failure was observed to occur after a period of time at a particular stress level. The time to failure decreased with increasing stress level; these times are recorded in Table 6. These results are similar to the delayed failure phenomenon found for polycarbonate by Brinson [23]. Delayed stress-whitening was also found to occur and is evidence that both local and gross failure are time dependent.

Variations in Poisson's ratio with stress level and time during the tests for both materials are shown in Fig. 37. These results are

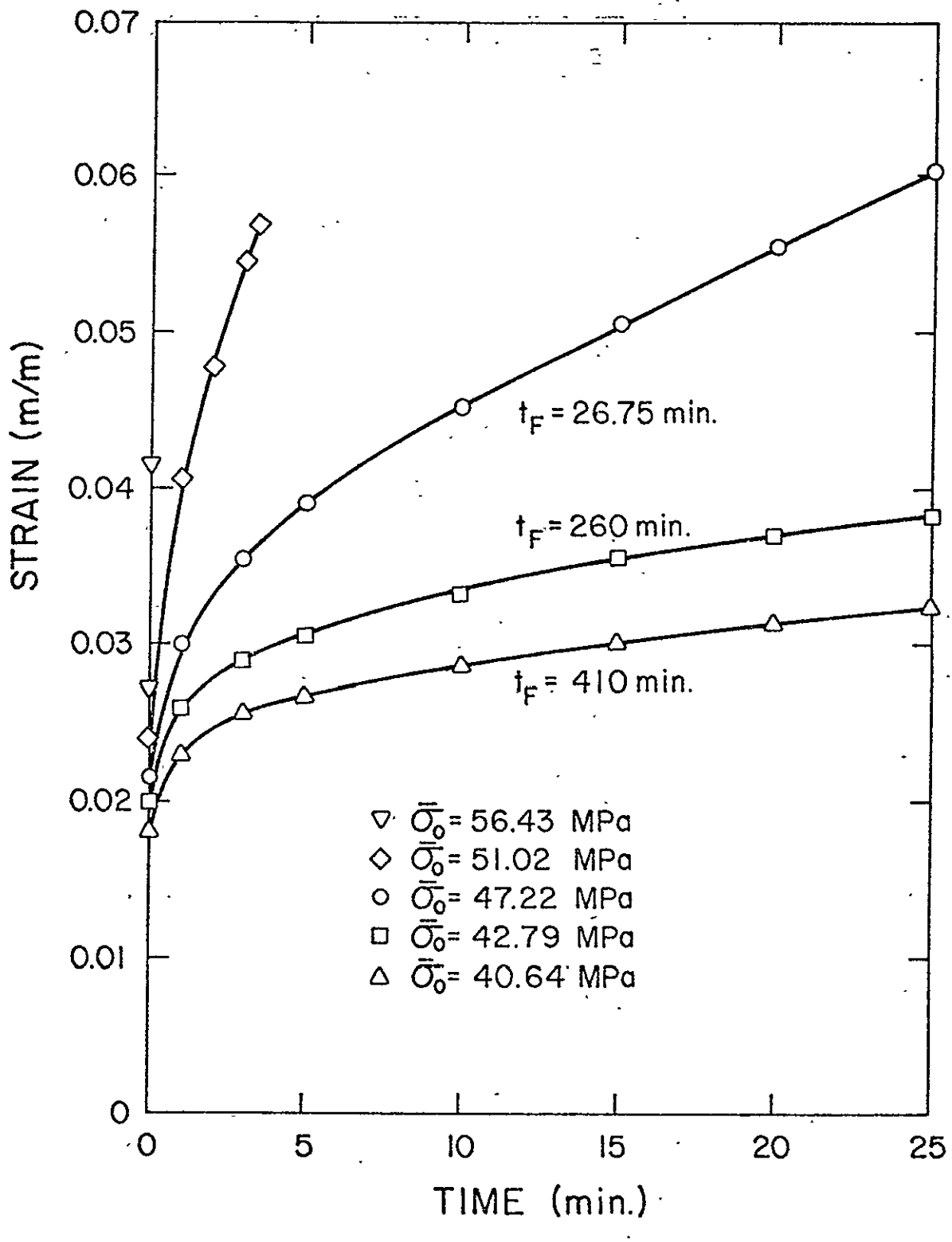

Figure 35. Creep Behavior of Metlbond 1113

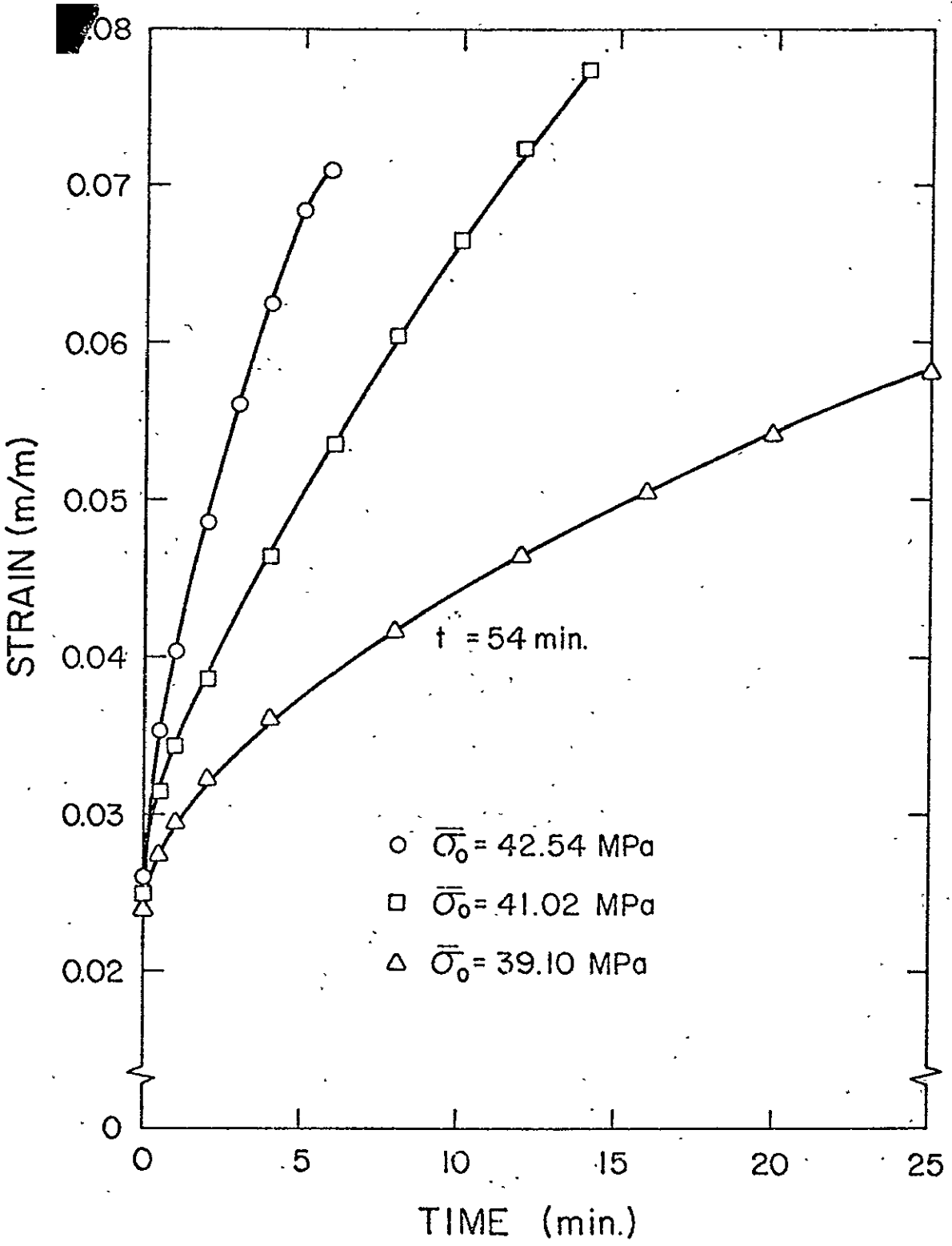

Figure 36. Creep Behavior of Metlbond 1113-2

Table 6. CREEP PROPERTIES.

Adhesive	Specimen	Symbols for Figure 37	Stress $\bar{\sigma}_o$ (MPa)	Creep to Failure Time, t_F (min)
Metlbond 1113	B-6-2	37(a), ■	40.64	410
	B-6-5	37(a), □	42.79	260
	B-5-3	37(a), ●	47.22	26.75
	B-5-4	37(a), ○	51.02	3.35
	B-5-5	--	56.43	0.046
Metlbond 1113-2	A-6-3	37(b), □	39.09	54
	A-6-1	37(b), ●	41.02	14
	A-6-2	37(b), ○	42.54	5.9

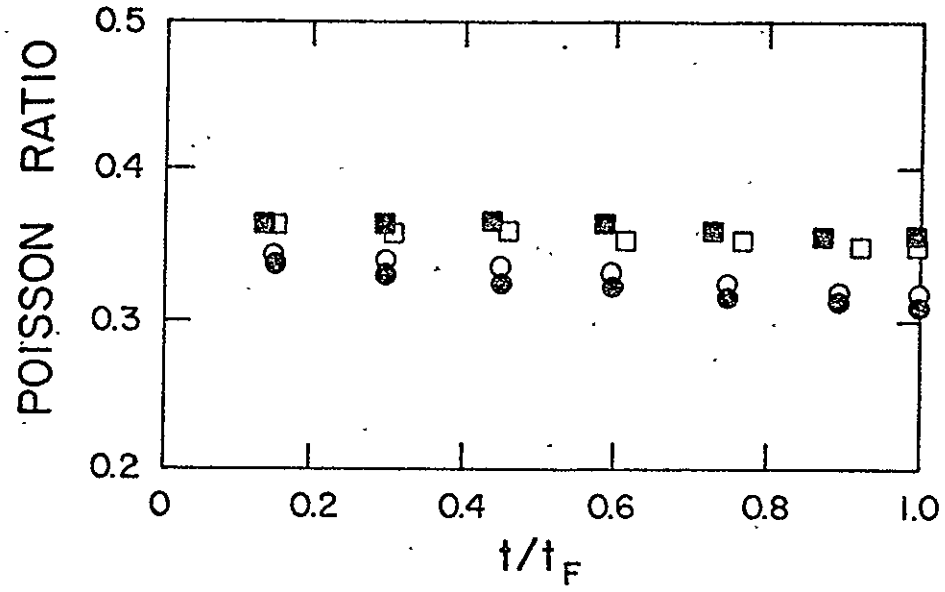

a. METLBOND 1113

(SEE TABLE 6 FOR SYMBOL IDENTIFICATION)

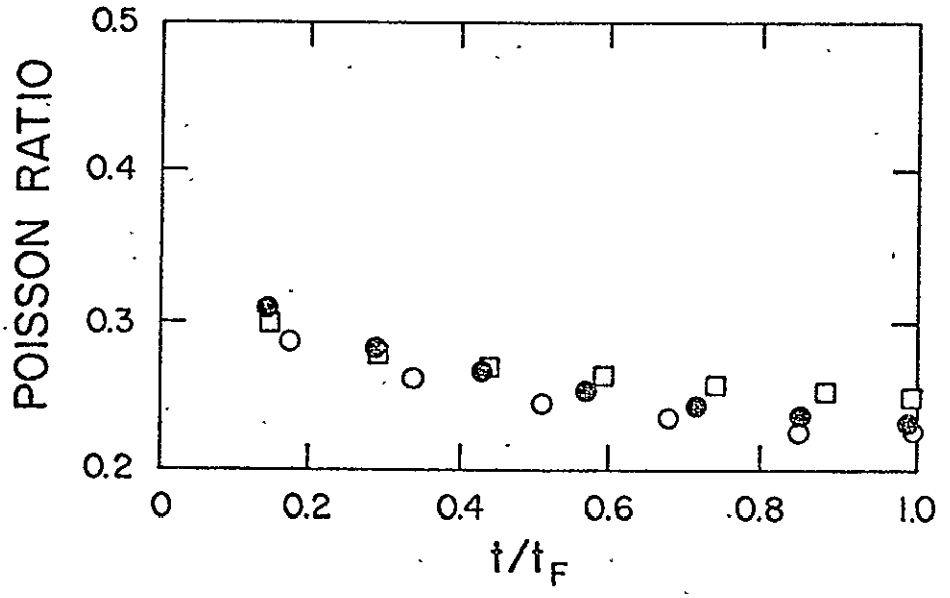

b. METLBOND 1113-2

Figure 37. Poisson's Ratio During Creep Tests

shown in terms of nondimensional time which is based upon the time required for failure in each test. As in the rate tests, Poisson's ratios generally decreased with time with Metlbond 1113 being more stable due to the presence of the carrier cloth. After stress-whitening occurred in the rate tests, Poisson's ratio was observed to decrease more rapidly. In the creep tests stress-whitening occurred either during loading (that is, nearly instantaneously) or very early in time with respect to the failure time. Therefore, it is felt that this phenomenon is responsible for the lower initial values of Poisson's ratio in the creep tests as compared to the rate tests.

The creep response of the modified Bingham model is given by Eq. (2.4.7),

$$\varepsilon(t) = \frac{\bar{\sigma}_0 - \theta}{\mu} t + \frac{\bar{\sigma}_0}{E} \qquad \sigma > \theta \tag{6.1.1}$$

Equation (6.1.1) did not adequately model the creep behavior of the adhesives. The discrepancy here is that the modified Bingham model predicts a linear response for creep which obviously does not correspond to the experimental data. However, the modified Bingham model was found to accurately predict the delayed failure phenomenon when used in conjunction with an equation for maximum stress proposed by Crochet [31].

6.1.1 Creep to Failure Behavior

A possible rational mathematical characterization of delayed failure phenomenon has been proposed by Crochet. He assumed that the maximum stress would increase for increasing strain rate and proposed

the equation,

$$Y(t) = A + B \exp(-C\chi) \tag{6.1.2}$$

where A, B, and C are material constants and χ is a time dependent material property given by,

$$\chi = [(\varepsilon_{ij}^{V} - \varepsilon_{ij}^{E})(\varepsilon_{ij}^{V} - \varepsilon_{ij}^{E})]^{1/2} \tag{6.1.3}$$

In Eq. (6.1.3) ε_{ij}^{V} and ε_{ij}^{E} refer to viscoelastic and elastic strains, respectively.

In the work of Crochet, the material behavior was considered as viscoelastic/plastic. That is, below the maximum stress, material behavior was considered to be viscoelastic. Stresses above the maximum stress were not allowed and perfectly plastic flow was postulated once the maximum stress was reached.

For creep in uniaxial tension, Eq. (6.1.3) can be written as,

$$\chi = [(\varepsilon_{11}^{V} - \varepsilon_{11}^{E})^2 + (\varepsilon_{22}^{V} - \varepsilon_{22}^{E})^2 + (\varepsilon_{33}^{V} - \varepsilon_{33}^{E})^2]^{1/2} \tag{6.1.4}$$

The second term in Eq. (6.1.1) represents the elastic behavior. Thus the term $(\varepsilon_{11}^{V} - \varepsilon_{11}^{E})^2$ in Eq. (6.1.4) becomes,

$$(\varepsilon_{11}^{V} - \varepsilon_{11}^{E})^2 = \left[\frac{\bar{\sigma}_o - \theta}{\mu} t\right]^2 \tag{6.1.5}$$

If a constant Poisson's ratio is assumed, the second and third terms of Eq. (6.1.4) can be written as,

$$(\varepsilon_{22}^{V} - \varepsilon_{22}^{E})^2 = (\varepsilon_{33}^{V} - \varepsilon_{33}^{E})^2 = \nu^2\left[\frac{\bar{\sigma}_o - \theta}{\mu} t\right] \qquad (6.1.6)$$

Thus Eq. (6.1.4) becomes,

$$\chi = \frac{\bar{\sigma}_o - \theta}{\mu} t(1 + 2\nu^2)^{1/2} \qquad (6.1.7)$$

and by using this result, Eq. (6.1.2) becomes,

$$Y(t) = A + B \exp[-C'(\sigma_o - \theta)t] \qquad (6.1.8)$$

where $C' = \frac{C(1 + 2\nu^2)}{\mu}$ is a constant containing various material parameters. In a creep test with $\sigma > \theta$, $Y(t)$ and $\bar{\sigma}_o$ are identical. Hence,

$$Y(t) = A + B \exp\{C'[Y(t) - \theta]t\} \qquad (6.1.9)$$

and t represents the time for creep to failure to occur under constant stress.

The material constants A, B, and C' were determined for Metlbond 1113 and creep to failure times for different stress levels were calculated according to Eq. (6.1.9). These results are shown in Fig. 38 together with the experimental data. As may be observed, close correlation between measured and predicted values was found.

6.2 Relaxation Results

Relaxation results are shown in Figs. 39 and 40 for Metlbond 1113 and 1113-2, respectively. For these tests, the levels of strain were purposely larger than the elastic limit values found in the rate tests since little time effects were expected below these levels.

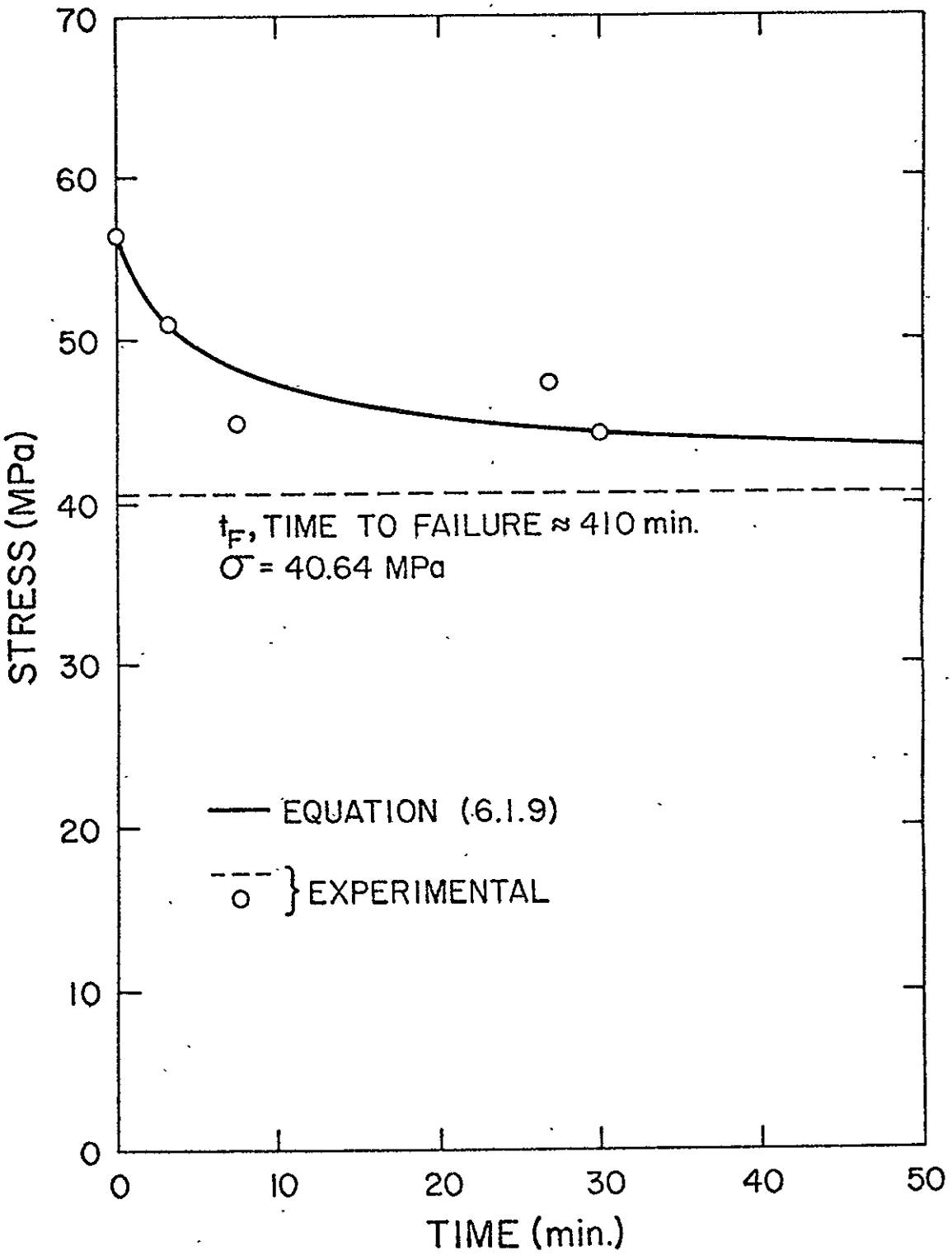

Figure 38. Comparison Between Creep to Failure Data and Theory

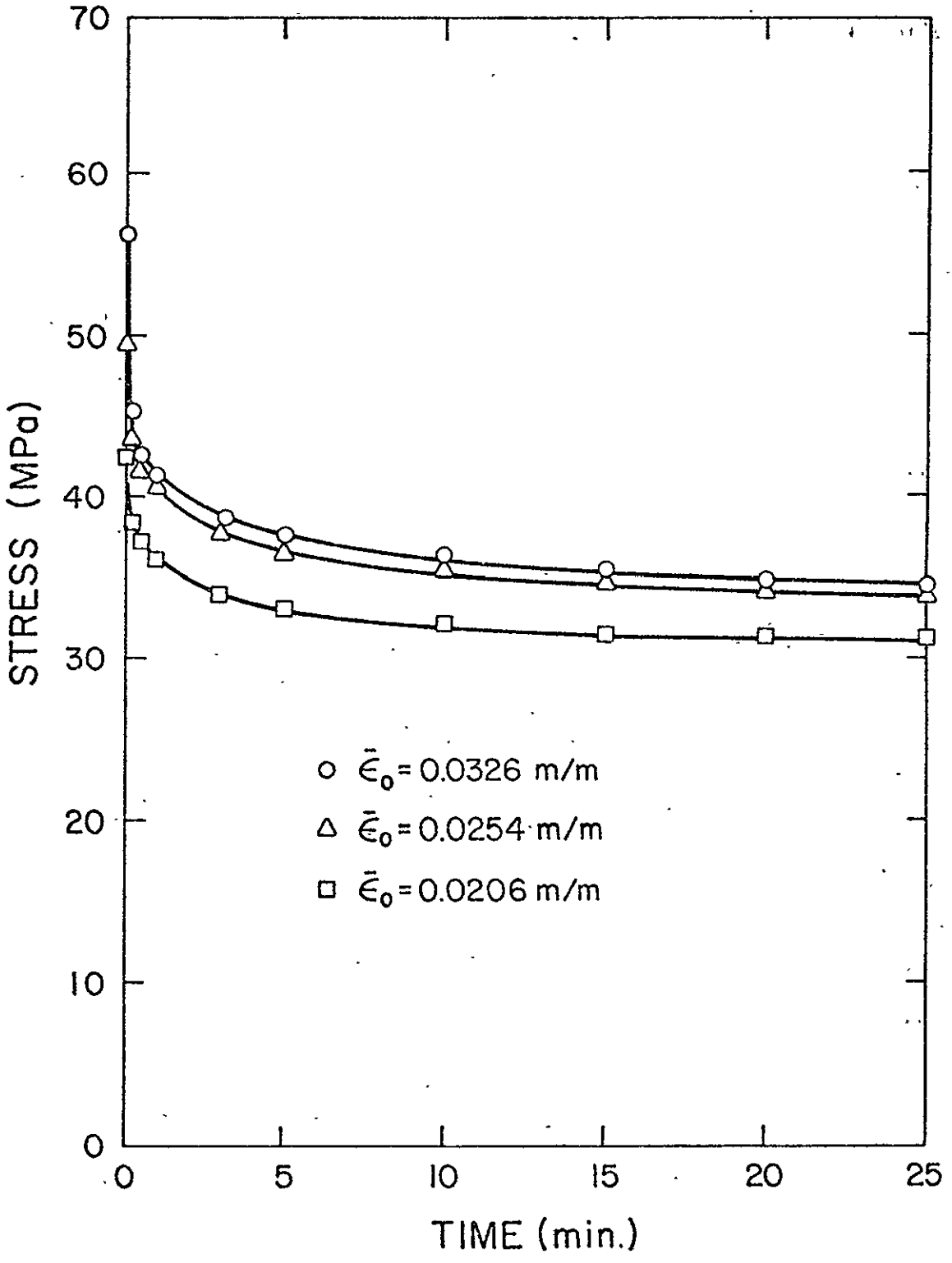

Figure 39. Relaxation Behavior of Metlbond 1113

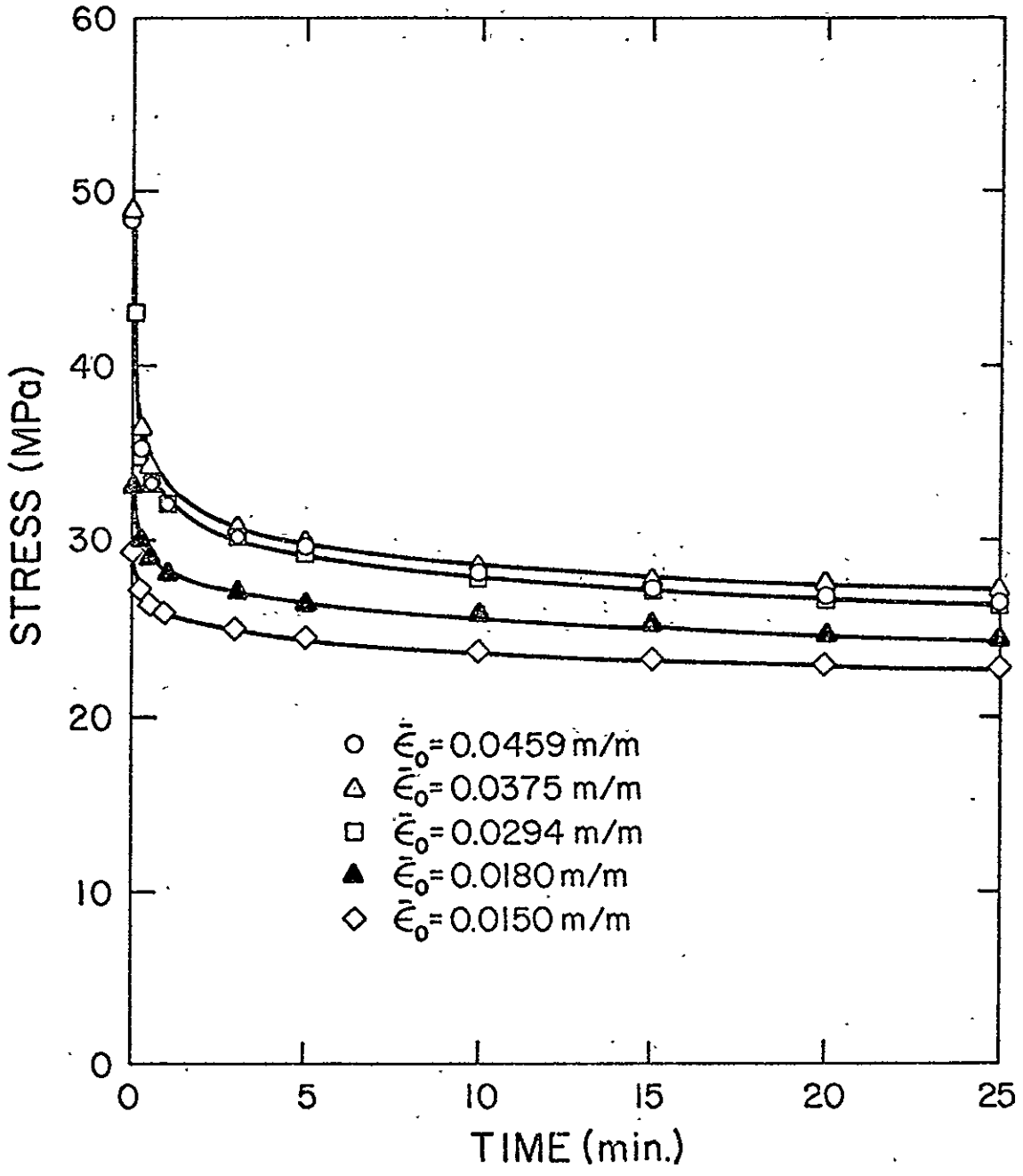

Figure 40. Relaxation Behavior of Metlbond 1113-2

The relaxation response of the modified Bingham model is given by Eq. (2.4.11),

$$\sigma(t) = \theta + (\bar{\varepsilon}_0 E - \theta)e^{-Et/\mu} \qquad \sigma > \theta \tag{6.2.1}$$

Eq. (6.2.1) states that, regardless of the strain level $\bar{\varepsilon}_0$, as t approaches infinity, $\sigma(t)$ asymtotically approaches θ. However, it can be observed that the experimental data for each strain level does not approach the same value of θ for large time. It can also be observed that the initial condition,

$$\sigma(t = 0) = \bar{\varepsilon}_0 E \tag{6.2.2}$$

does not adequately represent the data.

In an attempt to use Eq. (6.2.1) to model the relaxation behavior, the initial condition was modified as,

$$\sigma(t = 0+) = \sigma_0' \tag{6.2.3}$$

where σ_0' is the initial experimental value of stress for a given strain level. Various schemes were then tried in order to fit the data. The modified Bingham model was unable to predict the relaxation behavior for the entire time span present in the experimental data. However, reasonable results were realized for short time (t < 2 min.) by using the value of the viscosity coefficient during loading[1] and

---

[1]The loading rate was 20 in/min (50.8 cm/min) which is an order of magnitude above the highest head rate used in the rate tests. Thus, the data in Fig. 33 was extrapolated to the a strain rate of $\dot{\varepsilon} \approx 7.00 \times 10^{-2}$ m/m/sec and a value for μ determined.

adjusting the asymtotic value of θ.

6.3 Loading-Unloading Results

The loading-unloading tests were conducted on the most recent set of adhesive panels. To compare the properties of these panels to the previous panels, constant strain rate tests were conducted at 0.2 in/min (0.508 cm/min). These results are shown in Figs. 41 and 42 for Metlbond 1113A and 1113-2A where the (A) represents the second set of panels.

The properties of Metlbond 1113-2A are identical to those for Metlbond 1113-2 when tested at the same rate. Although higher values in modulus, elastic limit and maximum stresses are observed in Metlbond 1113A, these values are not as high as those for Metlbond 1113. This has been attributed to the possibility that the properties of the carrier cloth varied between these two sets of panels.

Constant strain rate properties of Metlbond 1113A and 1113-2A tested at a head rate of 0.2 in/min (0.508 cm/sec) are presented in Table 7. The values of the viscosity coefficient used to approximate the experimental results in Figs. 41 and 42 can also be found therein. The stress-whitening phenomenon was observed to occur in the same manner as in the previous panels.

6.3.1 Strain History - 1

The first strain history considered is constant strain rate loading and unloading cycles followed by constant strain rate to failure. Fig. 43 is a schematic representation of one cycle. The

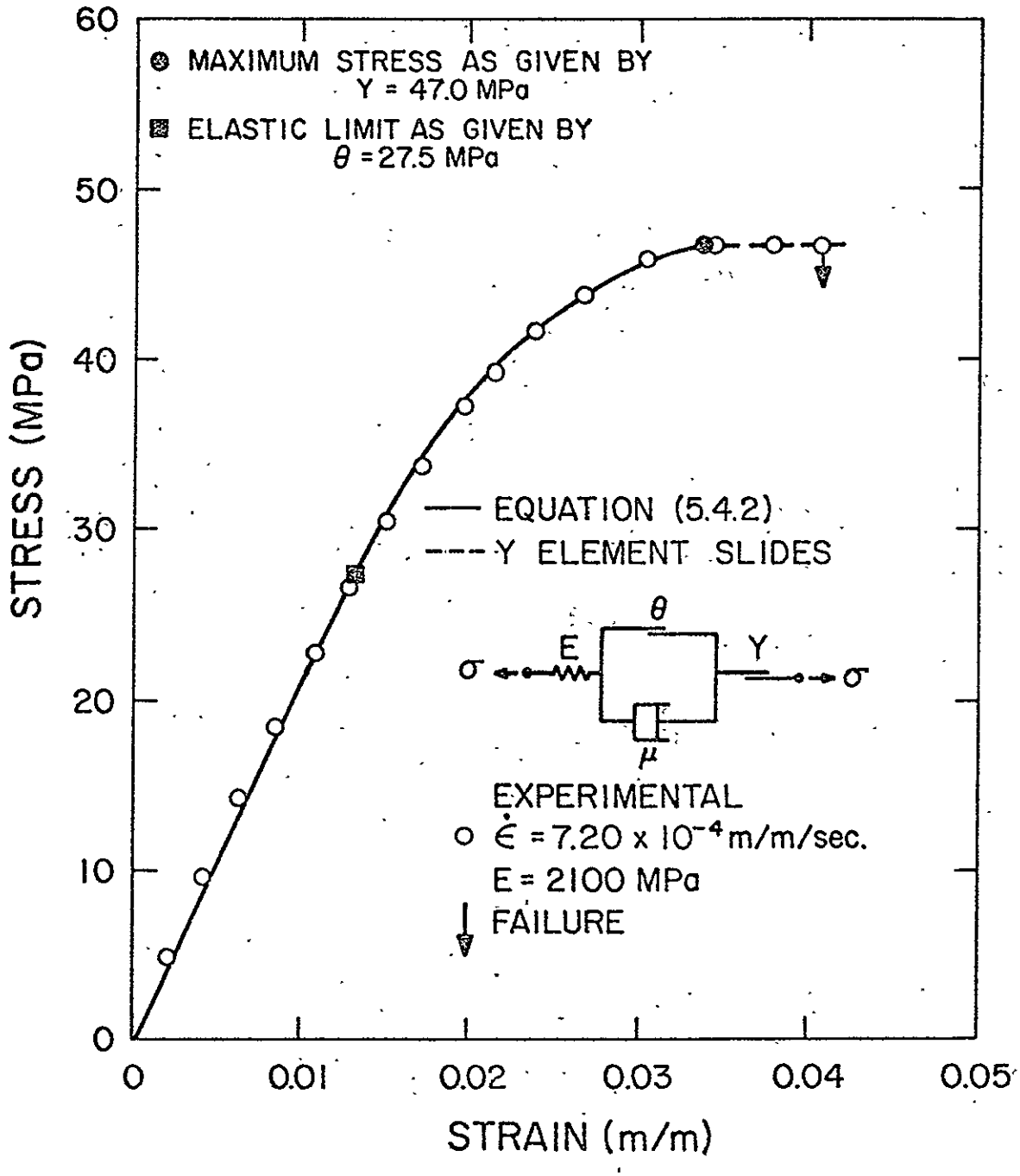

Figure 41. Stress-Strain Behavior of Metlbond 1113A and Comparison to Modified Bingham Model

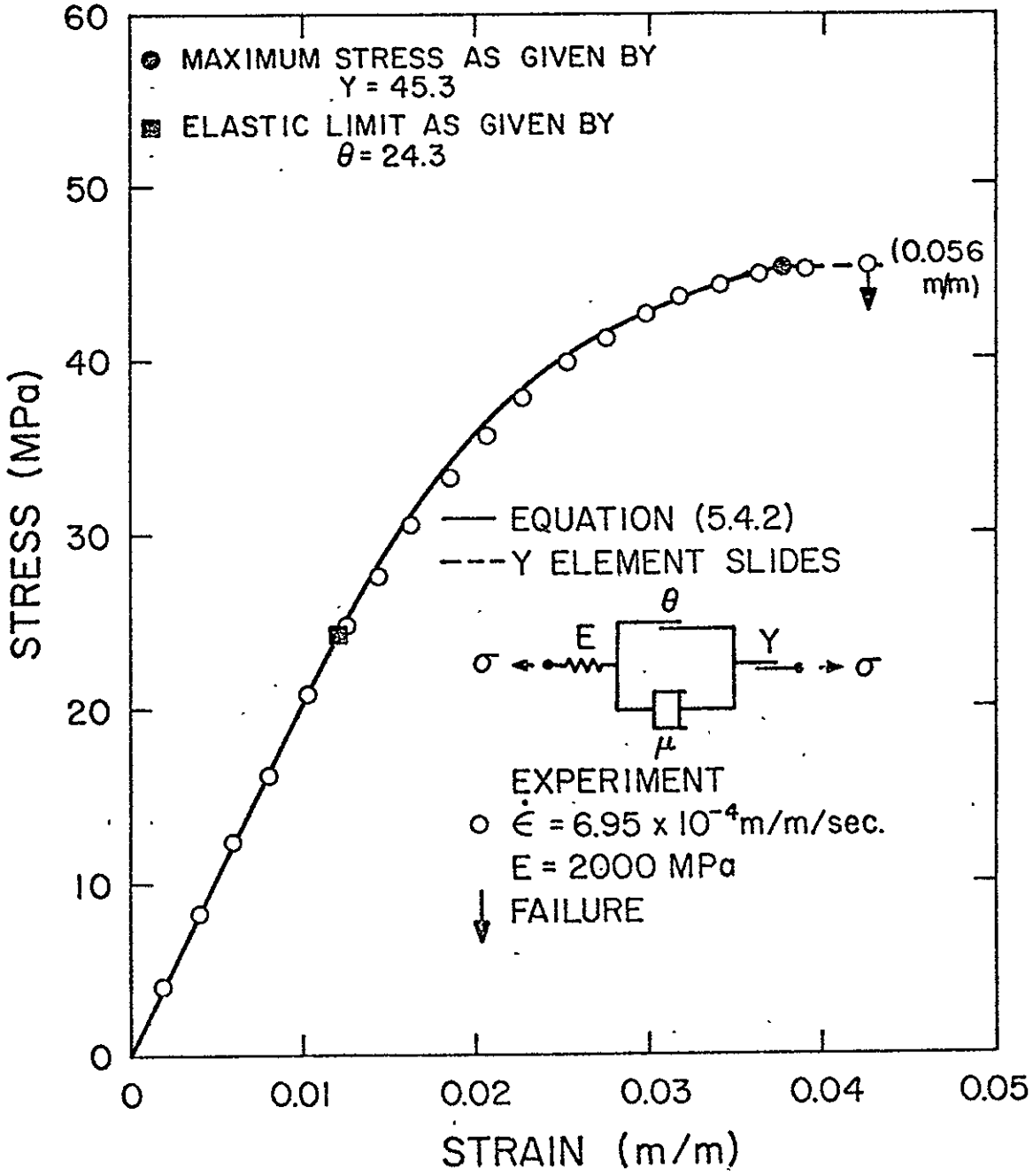

Figure 42. Stress-Strain Behavior of Metlbond 1113-2A and Comparison to Modified Bingham Model

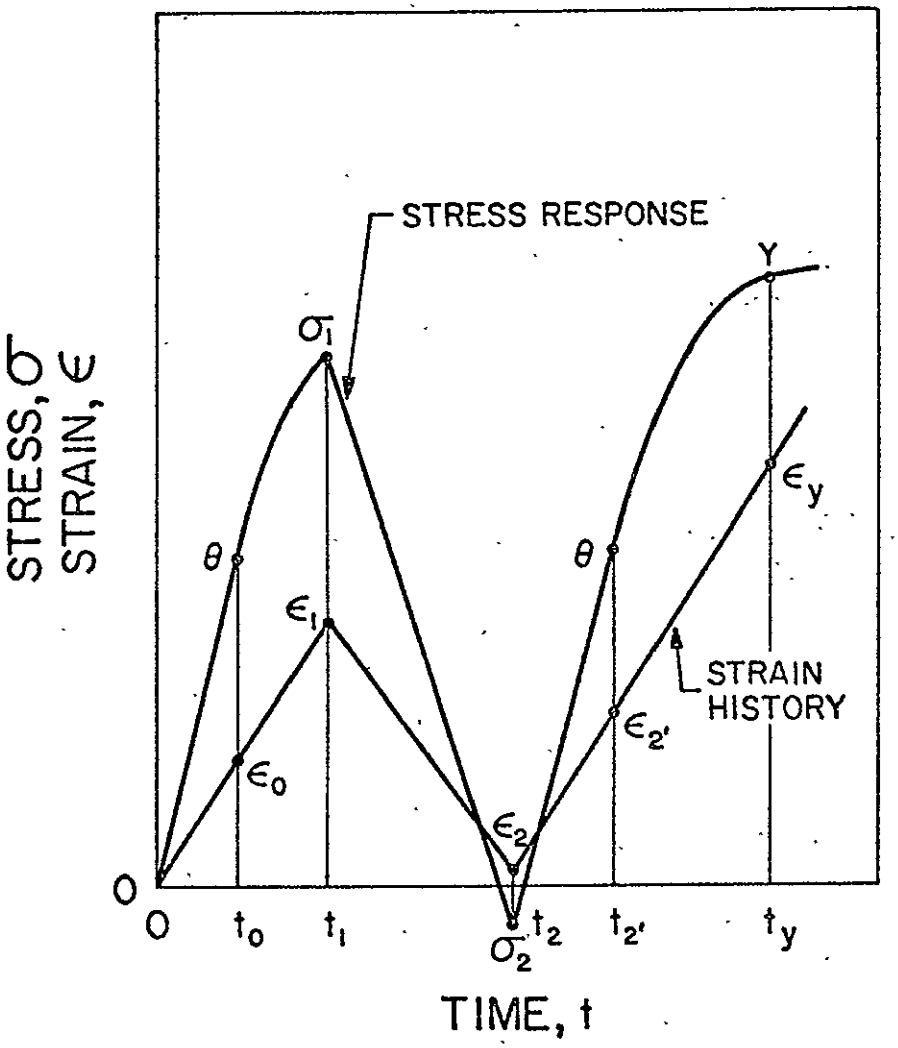

Figure 43. Strain History - 1 and Stress Response

assumed stress response is also shown.

For loading-unloading considerations, the constitutive equations for the modified Bingham model, Eqs. (3.3.3), are,

$$\dot{\varepsilon} = \frac{\dot{\sigma}}{E} \qquad \text{for } \sigma \leq \theta \text{ or } \dot{\sigma} < 0$$

$$\dot{\varepsilon} = \frac{\dot{\sigma}}{E} + \frac{\sigma - \theta}{\mu} \qquad \text{for } \sigma > \theta \text{ and } \dot{\sigma} > 0 \tag{6.3.1}$$

That is, unloading occurs elastically and the elastic limit stress is non-work-hardening as shown in Fig. 42. The various times shown in Fig. 43 indicate the points in time where changes from elastic to viscoplastic behavior or from loading to unloading behavior occur. Eqs. (6.3.1) are solved between these times for the stress response. Values of stress and strain generated at the end of a given time segment are used as initial conditions for the next segment.

For the range $0 < t < t_0$, the strain is given by,

$$\varepsilon(t) = Rt \tag{6.3.2}$$

and the stress response is,

$$\sigma(t) = ERt \tag{6.3.3}$$

The time t_0 is determined from Eq. (6.3.3) as,

$$t_0 = \frac{\theta}{ER} \tag{6.3.4}$$

and ε_0 is determined from Eq. (6.3.2) as,

$$\varepsilon_0 = Rt_0 \tag{6.3.5}$$

In the interval $t_0 < t < t_1$,

$$\varepsilon(t) = \varepsilon_0 + R(t - t_0) \tag{6.3.6}$$

and

$$\sigma(t) = \theta + \mu R(1 - e^{-E(t - t_0)/\mu}) \tag{6.3.7}$$

The time t_1 is known from the given load history. The stress and strain at t_1 are given by Eqs. (6.3.7) and (6.3.6) as,

$$\sigma_1 = \theta + \mu R(1 - e^{-E(t_1 - t_0)/\mu}) \tag{6.3.8}$$

and

$$\varepsilon_1 = \varepsilon_0 + R(t_1 - t_0) \tag{6.3.9}$$

respectively.

For the range $t_1 < t < t_2$, the strain is,

$$\varepsilon(t) = \varepsilon_1 - R(t - t_1) \tag{6.3.10}$$

and the stress response given by,

$$\sigma(t) = \sigma_1 - ER(t - t_1) \tag{6.3.11}$$

The time t_2 is also known from the given load history. The stress and strain at t_2 are given by Eqs. (6.3.11) and (6.3.10)

$$\sigma_2 = \sigma_1 - ER(t_2 - t_1) \tag{6.3.12}$$

and

$$\varepsilon_2 = \varepsilon_1 - R(t_2 - t_1) \tag{6.3.13}$$

respectively.

During the interval $t_2 < t < t_2'$, the strain is given by,

$$\varepsilon(t) = \varepsilon_2 + R(t - t_2) \tag{6.3.14}$$

and stress response is,

$$\sigma(t) = \sigma_2 + ER(t - t_2) \tag{6.3.15}$$

The time, t_2', at which the elastic limit stress is reached during the second loading can be determined from Eq. (6.3.15) as,

$$t_2' = t_2 + \frac{\theta - \sigma_2}{ER} \tag{6.3.16}$$

and the strain at t_2' is determined from Eq. (6.3.14) as,

$$\varepsilon_2' = \varepsilon_2 + R(t_2' - t_2) \tag{6.3.17}$$

For the interval $t_2' < t < t_y$, the strain can be written as,

$$\varepsilon(t) = \varepsilon_2' + R(t - t_2') \tag{6.3.18}$$

and the stress response is,

$$\sigma(t) = \theta + \mu R(1 - e^{-E(t - t_2')/\mu}) \tag{6.3.19}$$

The strain at the maximum stress can be determined from Eq. (6.3.18) in the form,

$$\varepsilon_y = \varepsilon_2' + R(t_y - t_2') \tag{6.3.20}$$

where t_y is given by Eq. (6.3.19) as,

$$t_y = t_2' - \frac{\mu}{E} \text{en}\left\{\frac{Y - (\theta + \mu R)}{-\mu R}\right\} \qquad (6.3.21)$$

Above t_y the material is assumed to flow perfectly plastically to failure. For a number of cycles, the analysis proceeds in a similar manner to that above.

Metlbond 1113-2A and 1113A were tested for one and two cycles of constant strain rate loading and unloading, respectively, followed by constant strain rate to failure. The material properties observed during these tests are presented in Table 7. The modulus during loading was found to be that of the initial elastic modulus. However, the modulus during unloading was found to be lower than the initial elastic modulus. This phenomenon was observed for all unloading tests. As such, it is an interesting property of these materials. The reason for this behavior is not clearly understood at this time. It should, however, be a topic of future research. Values for the loading and unloading moduli are presented in Table 7.

Using the material properties presented in Table 7 and equations in the form of Eqs. (6.3.2) to (6.3.21), a value for the viscosity coefficient (given in Table 7) for each adhesive was determined which gave the best fit to the experimental results. The experimental and theoretical results are compared in Figs. 44 through 49. It can be observed that an accurate representation of the experimental results was achieved. It can also be observed that during subsequent loadings a finite value of strain is predicted theoretically for the zero state of stress. This is in agreement with the experimental results, and

Table 7. CONSTANT STRAIN RATE LOADING-UNLOADING PROPERTIES.

Adhesive	Specimen	Strain Rate $\lvert\dot{\varepsilon}\rvert_{avg}$ (m/m/sec)	Viscosity Co-efficient μ (MPa-sec)	Elastic Limit Stress θ (MPa)	Elastic Limit Strain ε_o (m/m)	Elastic Modulus During Loading E (MPa)	Elastic Modulus During 1st Unloading $\bar{E}_1$ (MPa)	Elastic Modulus During 2nd Unloading $\bar{E}_2$ (MPa)	Maximum Stress Y (MPa)
Metlbond 1113A	B-7-2	7.20×10^{-4}	3.22×10^{4}	27.5	0.0131	2100	--	--	47.0
	B-7-5	7.00×10^{-4}	3.50×10^{4}	27.5	0.0131	2100	2100	1975	47.5
Metlbond 1113-2A	A-8-2	6.95×10^{-4}	3.41×10^{4}	24.3	0.0122	2000	--	--	45.3
	A-8-4	6.93×10^{-4}	3.80×10^{4}	24.3	0.0123	1975	1680	--	45.5

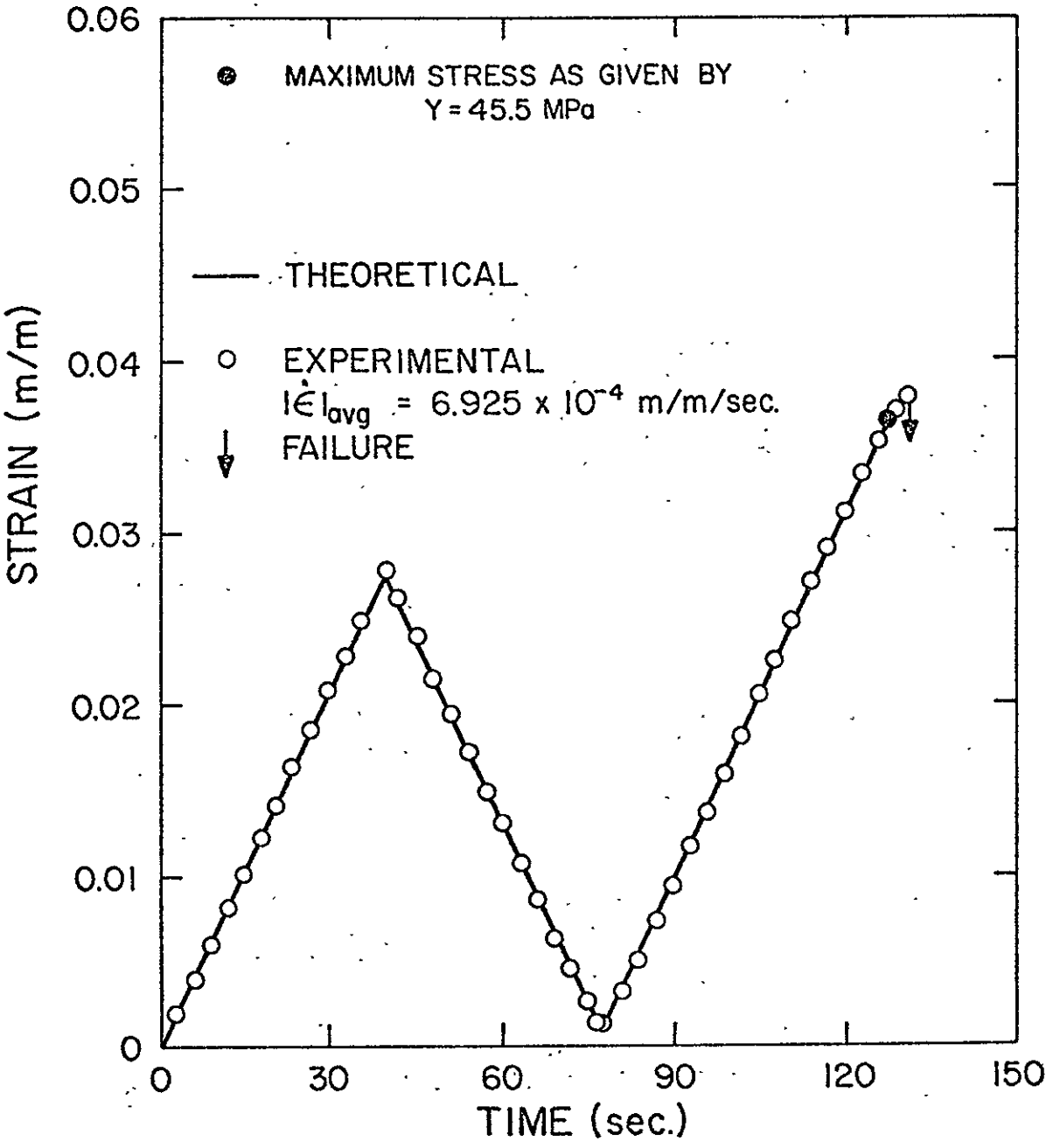

Figure 44. Strain History - 1 for Metlbond 1113-2A and Comparison to Theoretical Approximation .

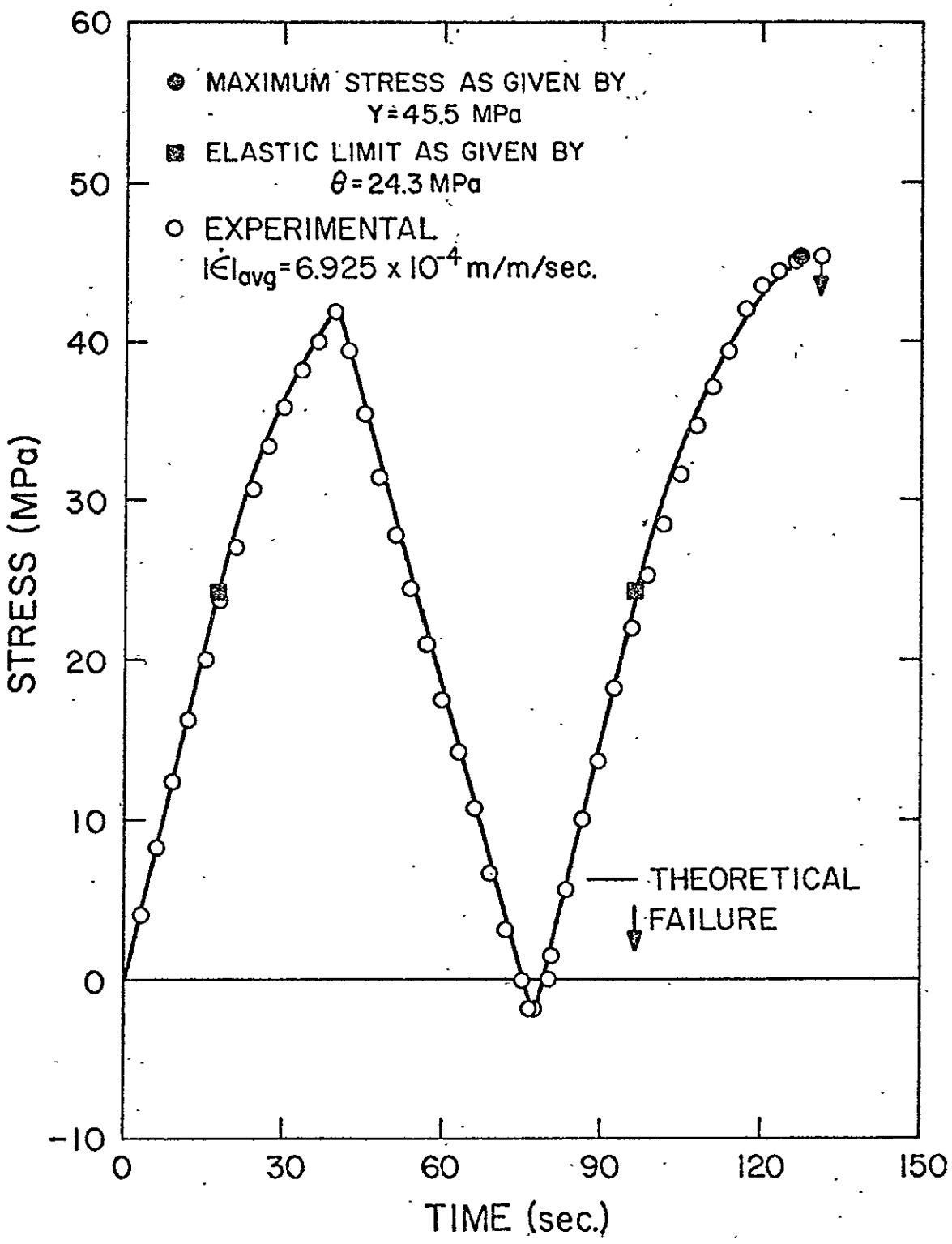

Figure 45. Theoretical and Experimental Stress-Time Response of Metlbond 1113-2A for Strain History - 1

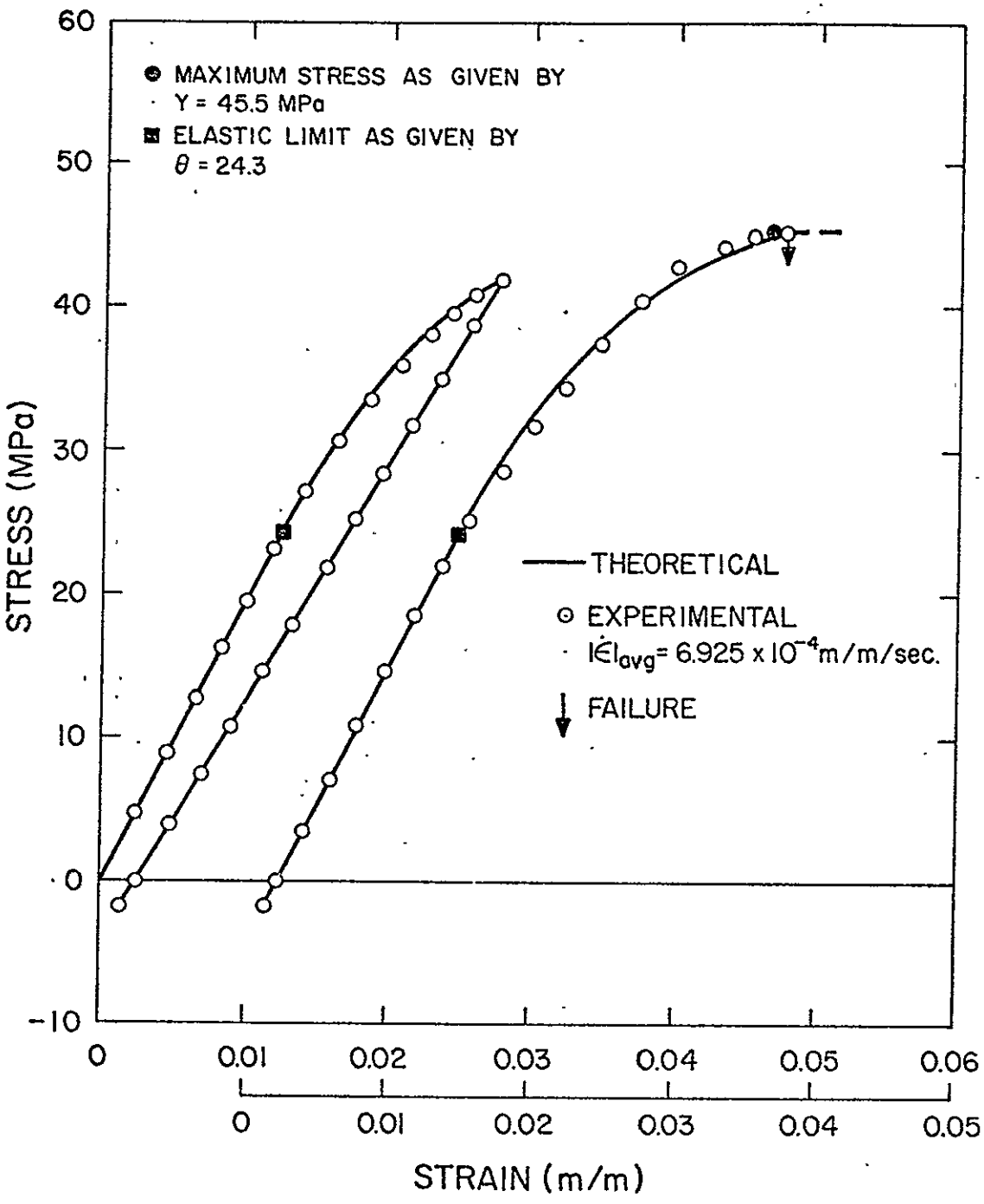

Figure 46. Theoretical and Experimental Stress-Strain Response of Metlbond 1113-2A for Strain History - 1

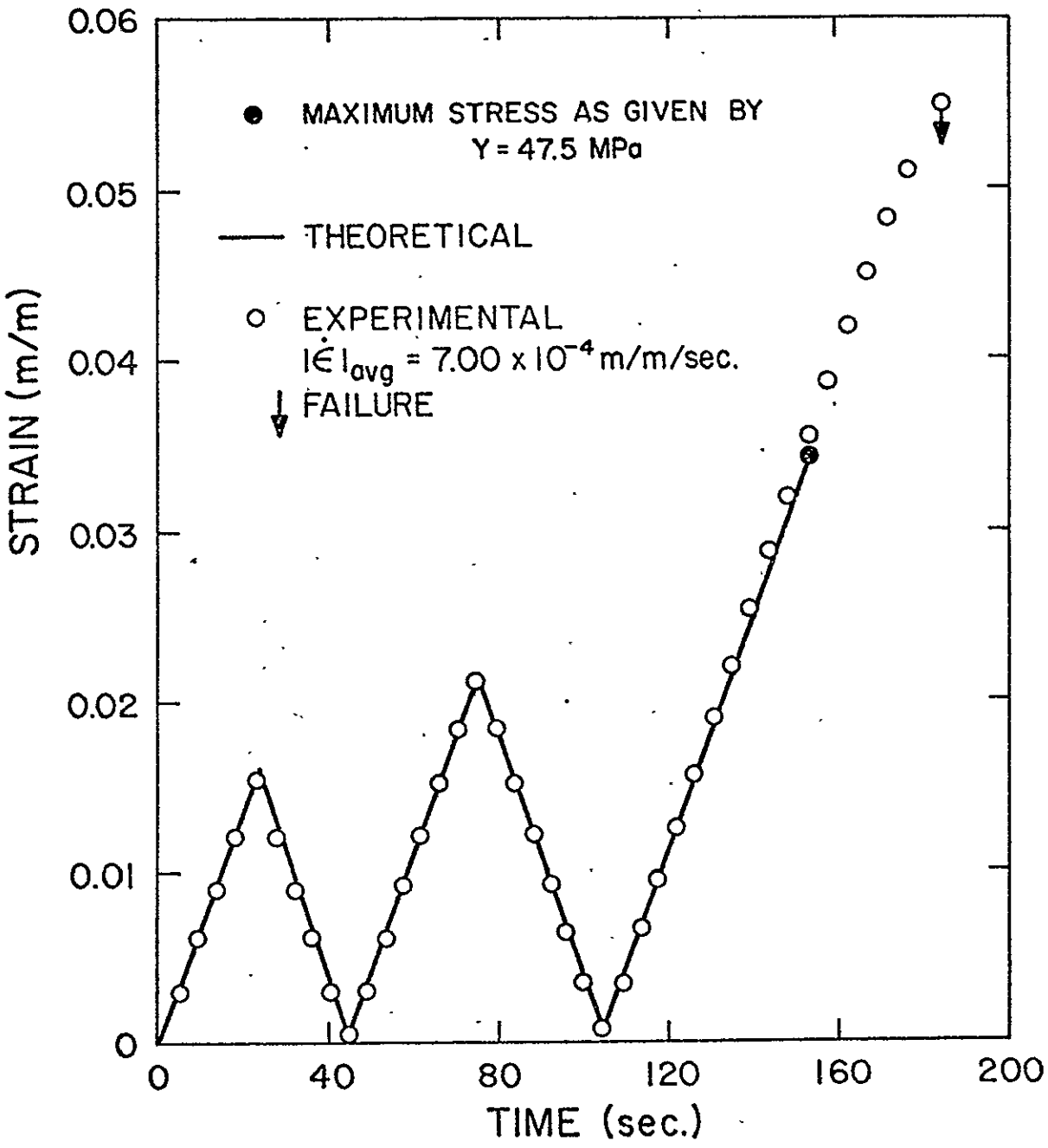

Figure 47. Strain History - 1 for Metlbond 1113A and Comparison to Theoretical Approximation

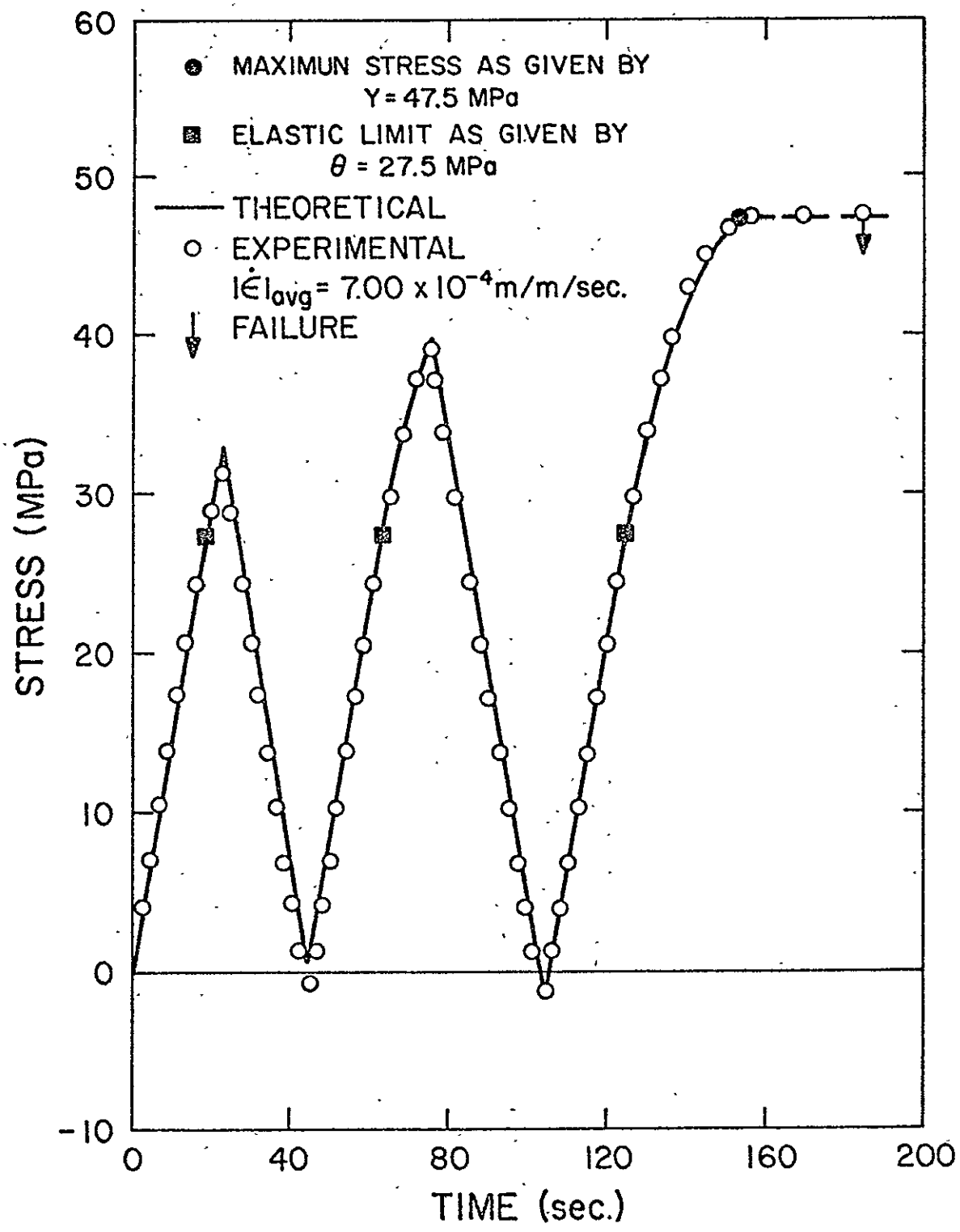

Figure 48. Theoretical and Experimental Stress-Time Response of Metlbond 1113A for Strain History - 1

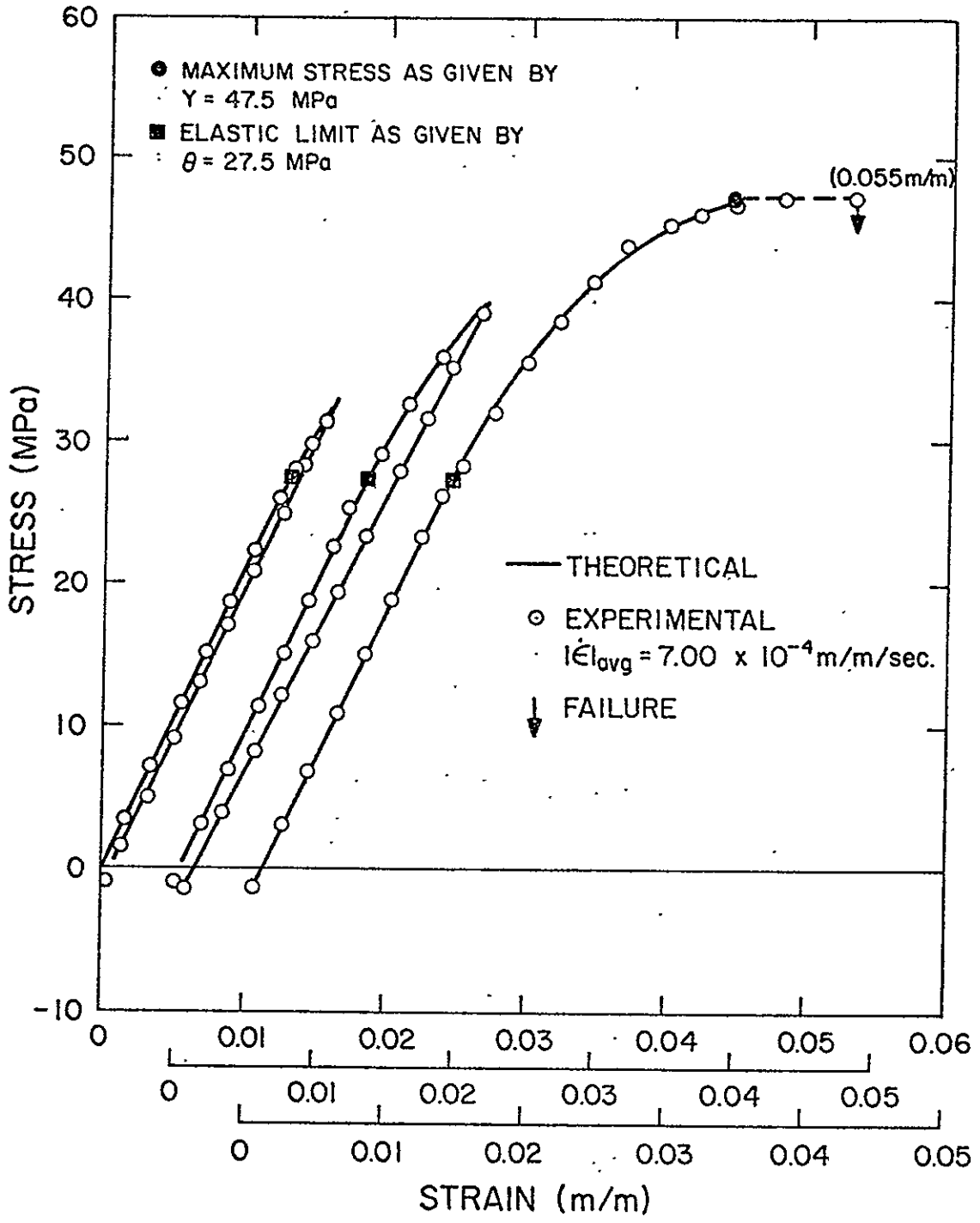

Figure 49. Theoretical and Experimental Stress-Strain Response of Metlbond 1113A for Strain History - 1

physically this can be attributed to the residual plastic strain produced during the previous loading cycle..

6.3.2 Strain History - 2

The second strain history considered is constant strain rate - constant strain cycles followed by constant strain rate to failure. Fig. 50 is a schematic representation of one cycle. The assumed stress response is also shown. The various times shown in Fig. 50 indicate the points in time where changes from elastic to viscoplastic behavior or from constant strain rate loading to constant strain loading occur. During constant strain rate segements, Eqs. (5.4.1) are solved according to the initial conditions generated at the end of the previous segment. During relaxation (constant strain) segements, Eq. (2.4.5) is solved according to the appropriate initial condition.

For the range $0 < t < t_1$, Eqs. (6.3.2) to (6.3.9) apply. In the interval $t_1 < t < t_2$, the strain is given by

$$\varepsilon(t) = \varepsilon_1 \tag{6.3.22}$$

and the stress response as,

$$\sigma(t) = \theta + (\sigma_1 - \theta)e^{-E(t - t_1)/\mu} \tag{6.3.23}$$

The time t_2 is known from the loading history. The values of stress and strain at t_2 are given by Eqs. (6.3.23) and (6.3.22) as,

$$\sigma_2 = \theta + (\sigma_1 - \theta)e^{-E(t_2 - t_1)/\mu} \tag{6.3.24}$$

and

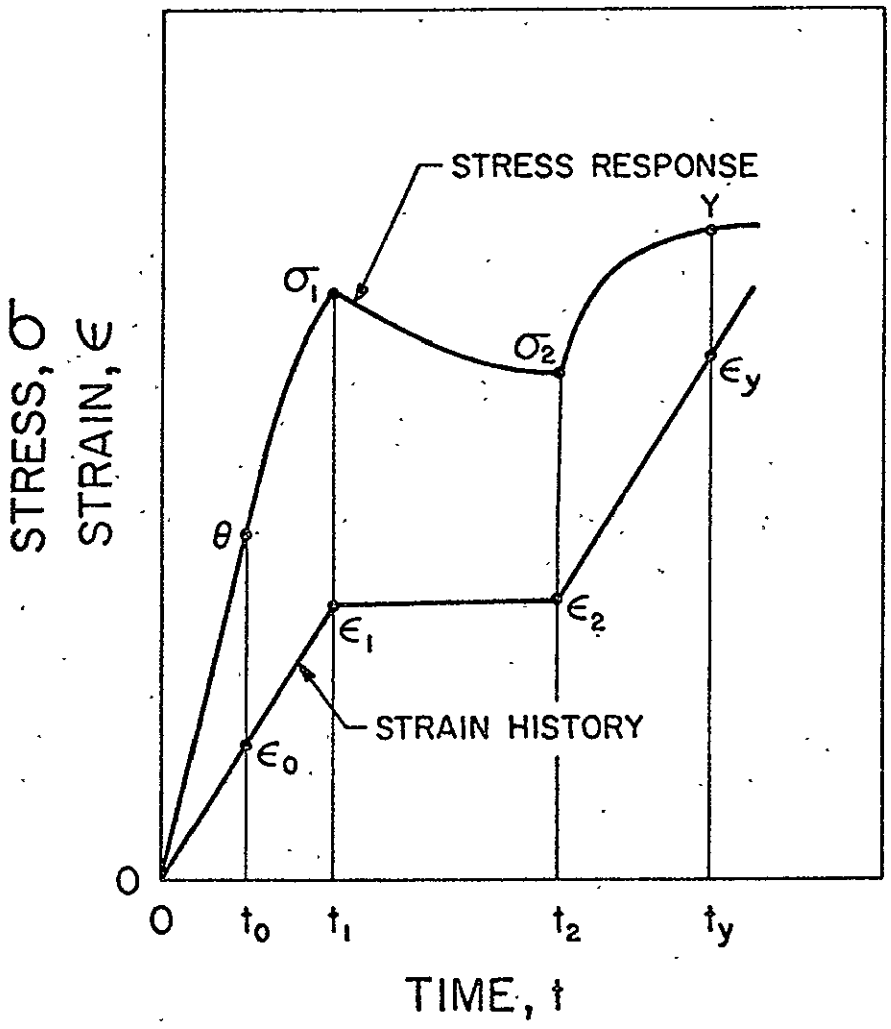

Figure 50. Strain History - 2 and Stress Response

$$\varepsilon_2 = \varepsilon_1 \tag{6.3.25}$$

respectively.

During the interval $t_2 < t < t_y$, the strain is,

$$\varepsilon(t) = \varepsilon_2 + R(t - t_2) \tag{6.3.26}$$

and the stress response is given by,

$$\sigma(t) = \theta + \mu R + (\sigma_2 - (\theta + \mu R))e^{-E(t - t_2)/\mu} \tag{6.3.27}$$

The strain, ε_y, corresponding to the maximum stress is given by Eq. (6.3.26) as,

$$\varepsilon_y = \varepsilon_2 + R(t_y - t_2) \tag{6.3.28}$$

where t_y is determined from Eq. (6.3.27) as,

$$t_y = t_2 - \frac{\mu}{E}\left[\frac{y - (\theta + \mu R)}{\sigma_2 - (\theta + \mu R)}\right] \tag{6.3.29}$$

Above t_y the material is assumed to flow perfectly plasticly to failure. For a number of cycles, the analysis proceeds in a similar manner to that above.

Metlbond 1113-2A and 1113A were tested for one cycle and two cycles of constant strain rate - constant strain, respectively, followed by constant strain rate to failure. The material properties observed during these tests are presented in Table 8.

Using the material properties presented in Table 8 and equations in the form of Eqs. (6.3.2) to (6.3.9) and (6.3.22) to (6.3.29), a value for the viscosity coefficient (given in Table 8) for each

Table 8. PROPERTIES FOR STRAIN HISTORY-2.

Adhesive	Specimen	Strain Rate $\dot{\varepsilon}_{avg}$ (m/m/sec)	Viscosity Co-efficient μ (MPa-sec)	Elastic Limit Stress θ (MPa)	Elastic Limit Strain ε_o (m/m)	Elastic Modulus E (MPa)	Maximum Stress Y (MPa)	θ During 1st Re-laxation (MPa)	θ During 2nd Re-laxation (MPa)
Metlbond 1113A	B-7-6	6.80×10^{-4}	3.70×10^{4}	27.5	0.0126	2180	47.0	22.0	36.0
Metlbond 1113-2A	A-8-5	6.85×10^{-4}	4.50×10^{-4}	24.3	0.0122	2000	46.3	34.0	--

adhesive was determined which gave the best fit to the experimental results. It was found that the value of μ determined during the constant strain rate loading can be used in the governing equations for the relaxation phases. The values of θ during the relaxation phase are then determined in order to give the best fit. As in the relaxation results, Section 6.2, this procedure yields the best approximation to the experimental results for short durations of time.

The experimental and theoretical results are compared in Figs. 51 through 56. The values of θ used in the governing equations during the relaxation phases are determined from the experimental results presented in Figs. 52 and 55. These values are taken to be the asymtotic value of stress approached if the relaxation curves are extrapolated beyond their time segment. The asymtotic values of θ are also recorded in Table 8. Since the relaxation times are short ($t < 2$ min) an accurate representation of the relaxation phases are represented using the above procedure. It can also be observed that overall agreement between theory and experiment is achieved.

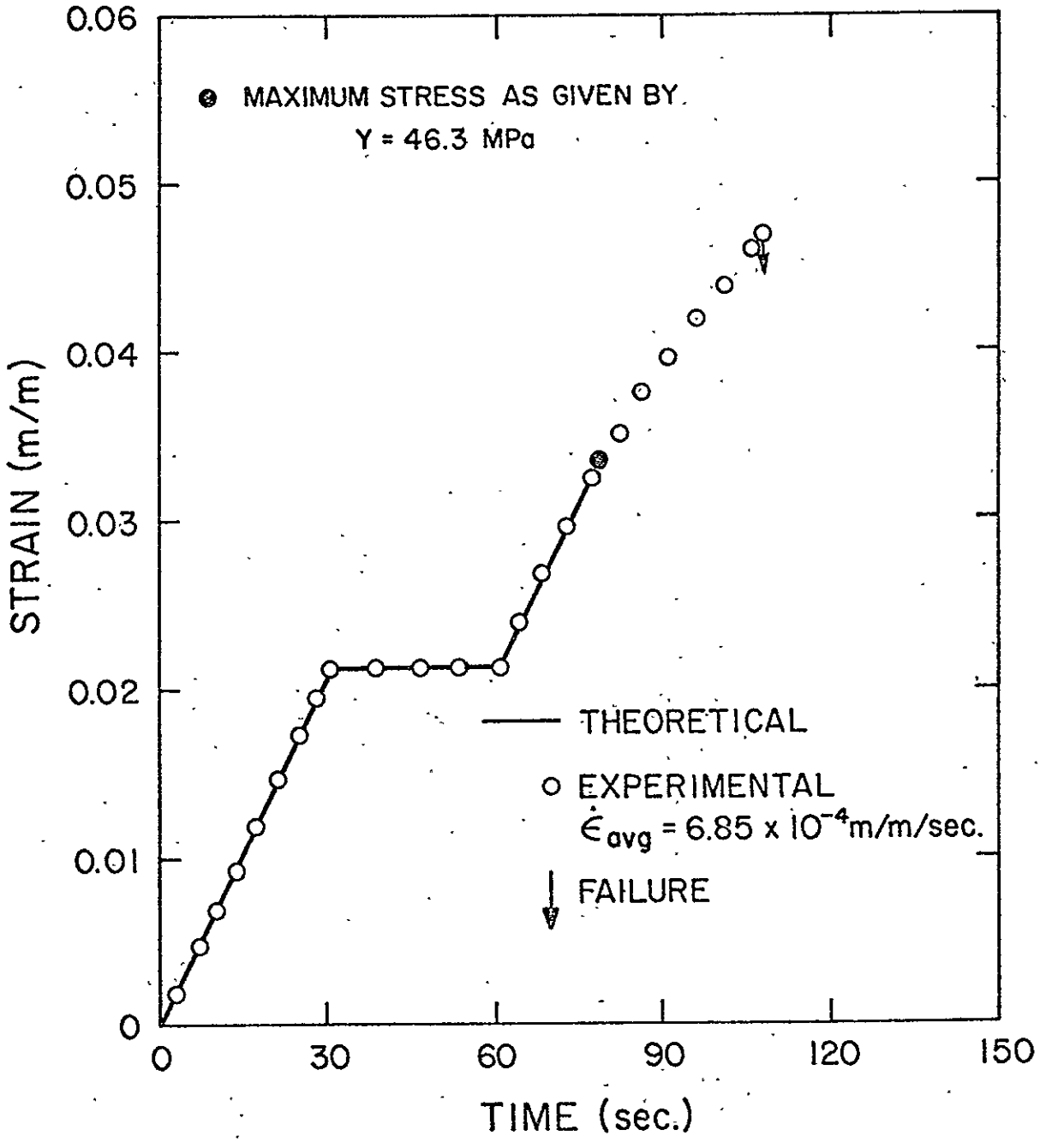

Figure 51. Strain History - 2 for Metlbond 1113-2A and Comparison to Theoretical Approximation

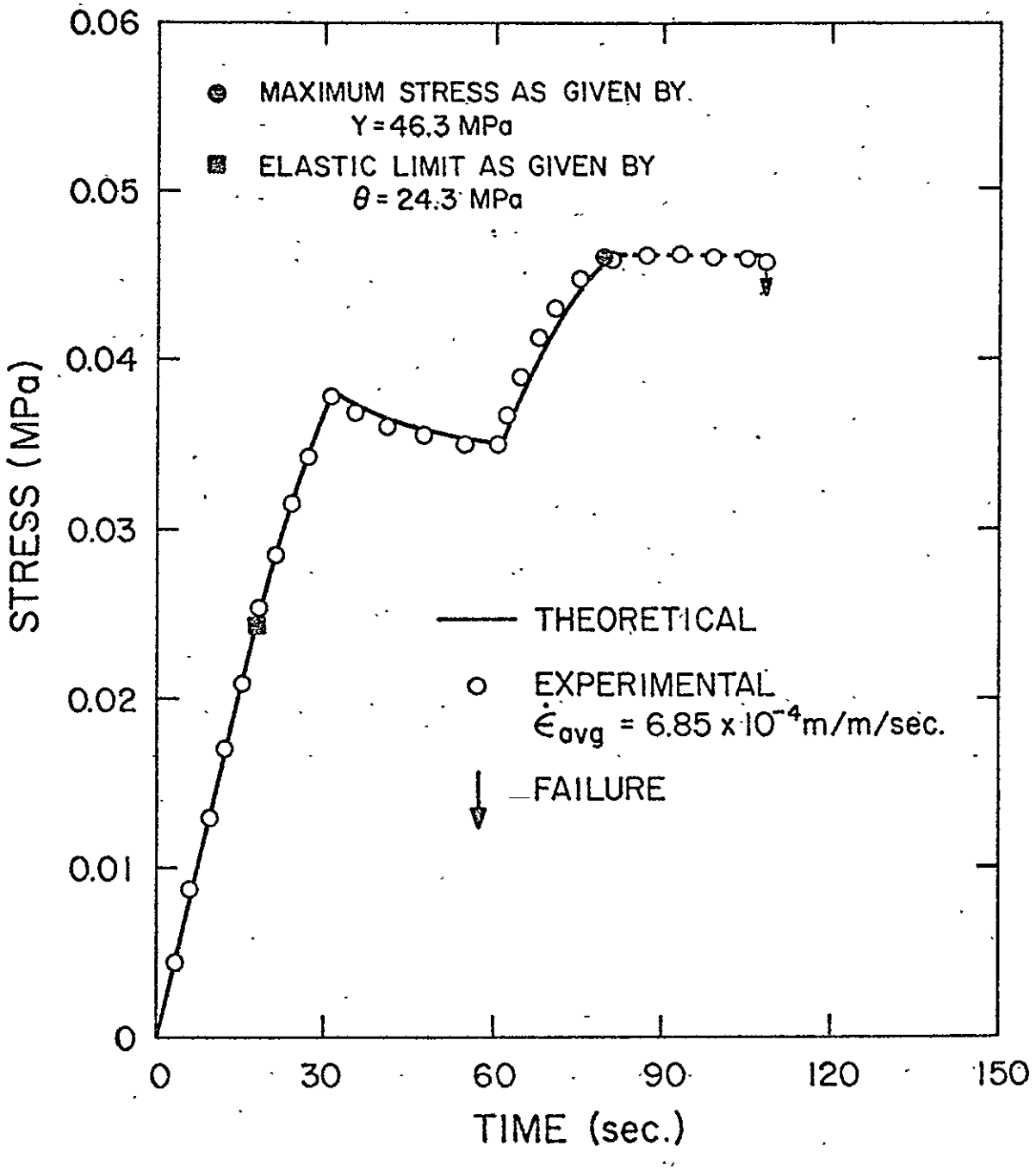

Figure 52. Theoretical and Experimental Stress-Time Response of Metlbond 1113-2A for Strain History - 2 .

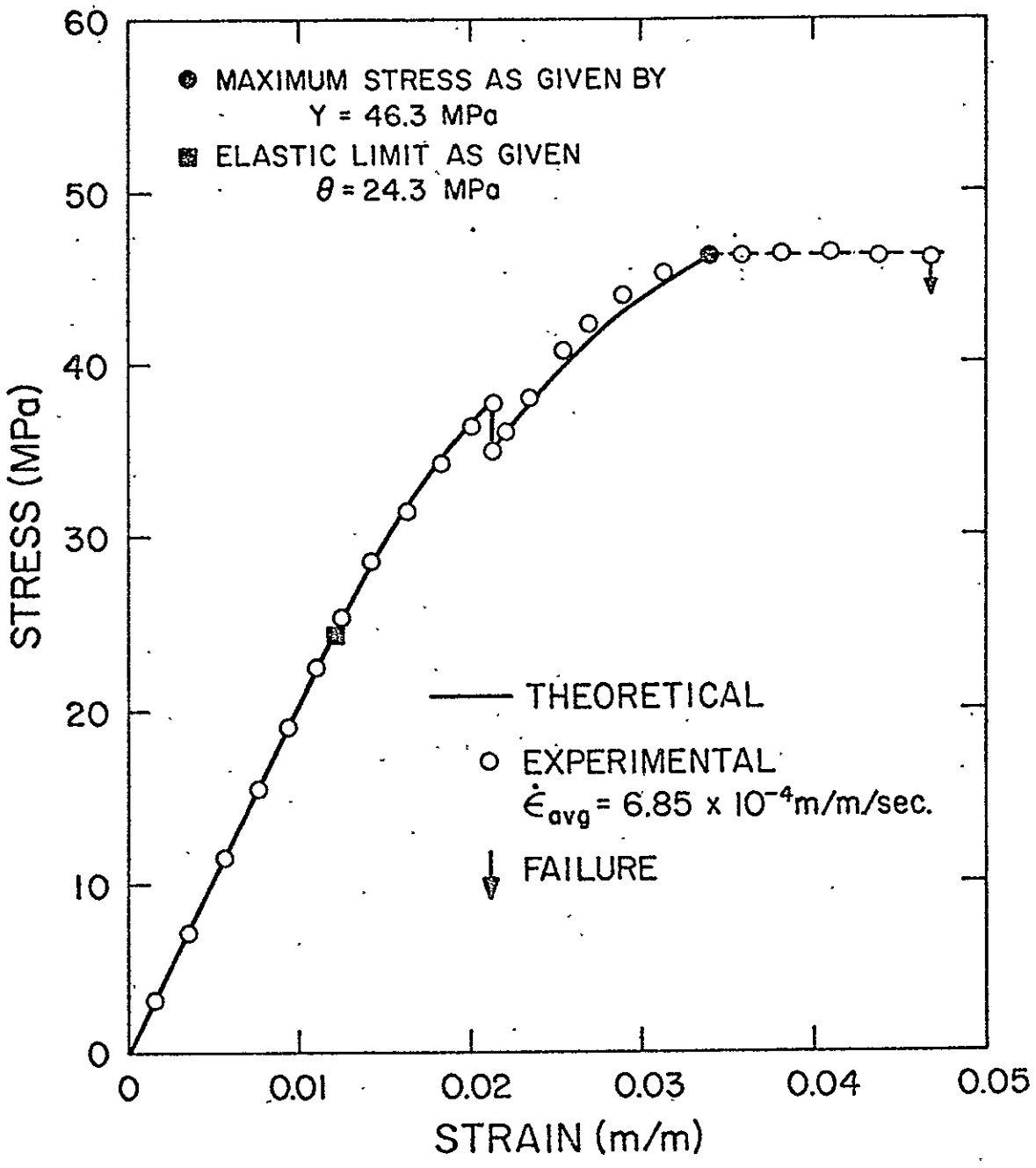

Figure 53. Theoretical and Experimental Stress-Strain Response of Metlbond 1113-2A for Strain History - 2

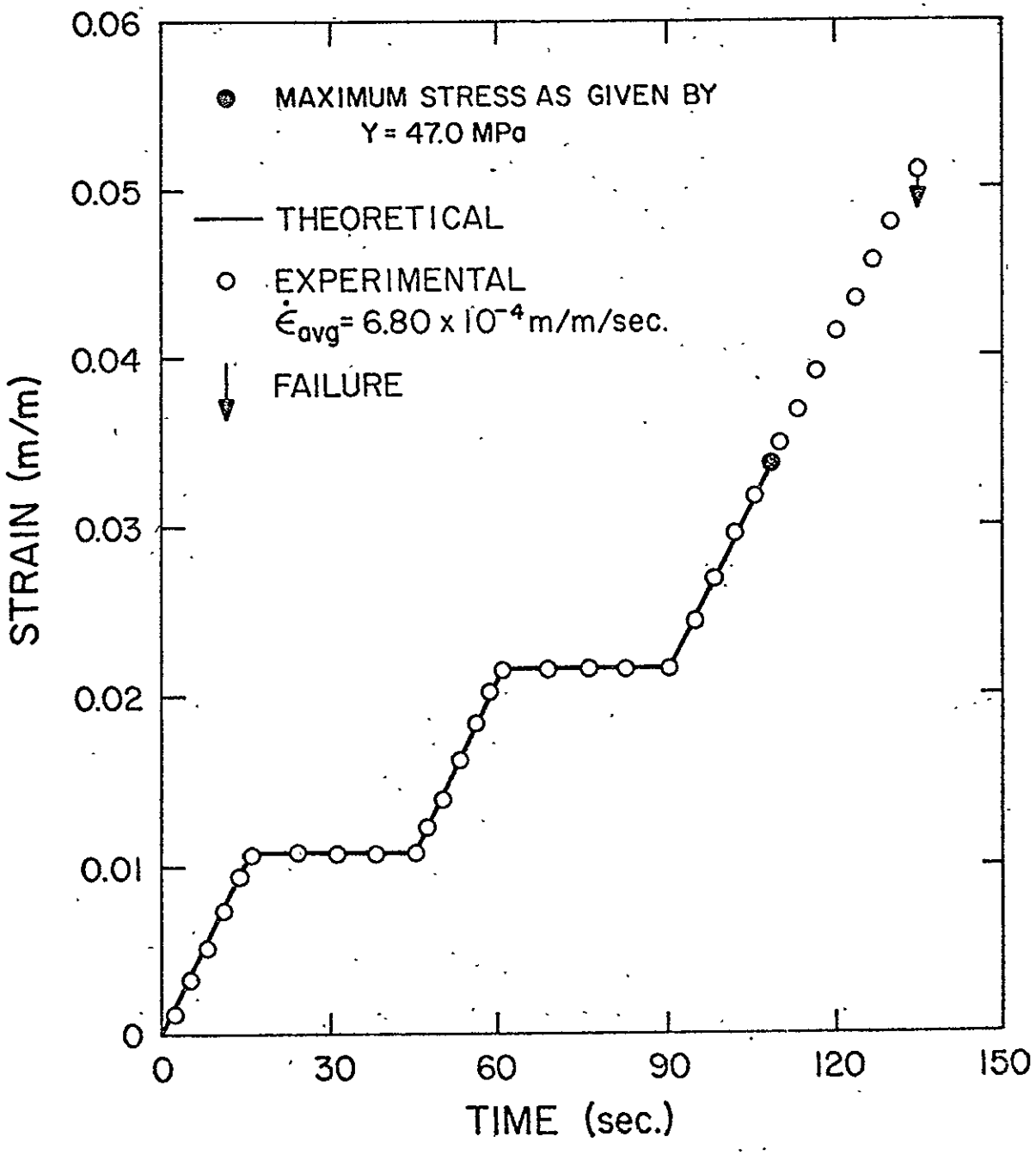

Figure 54. Strain History - 2 for Metlbond 1113A and Comparison to Theoretical Approximation

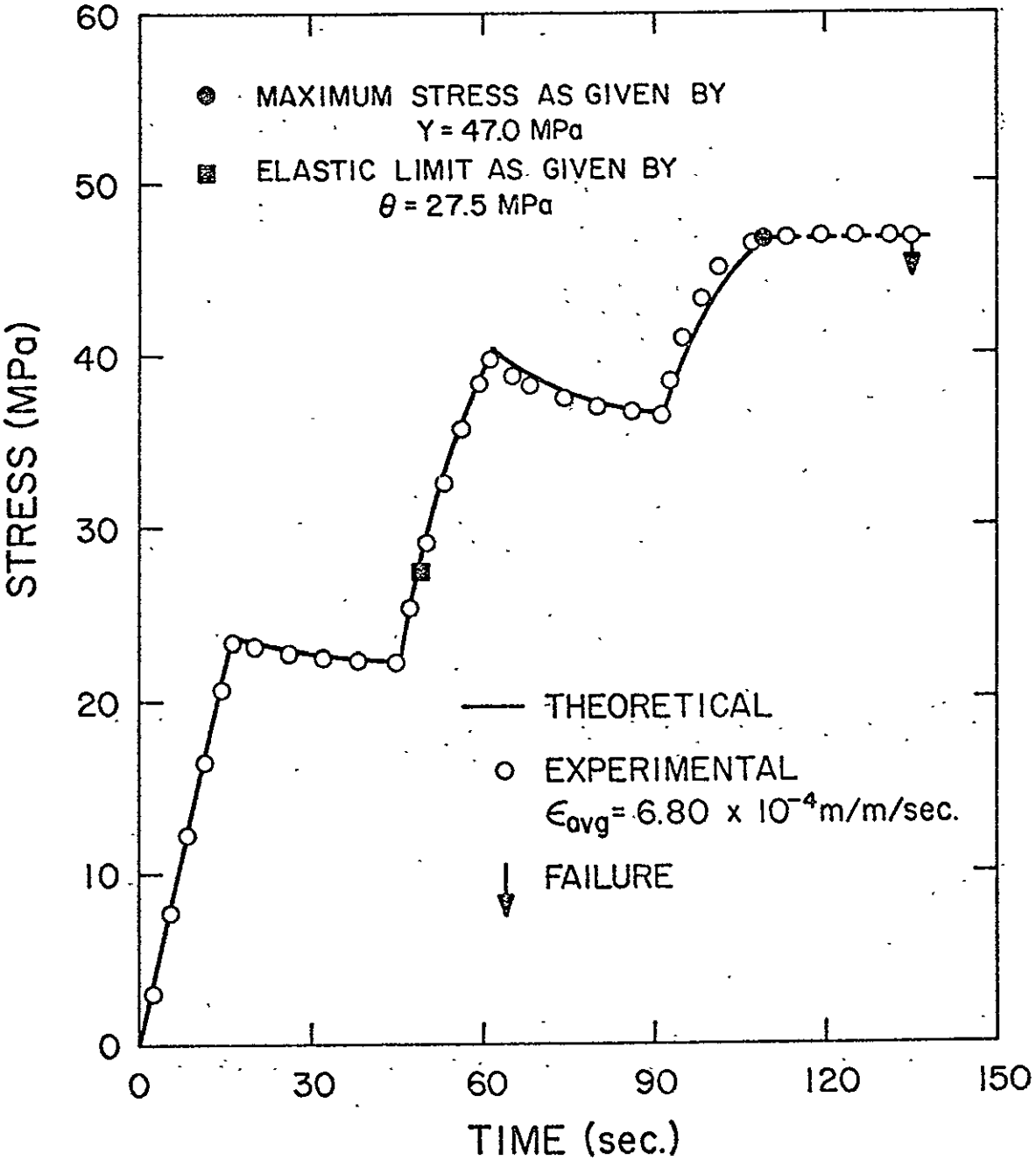

Figure 55. Theoretical and Experimental Stress-Time Response of Metlbond 1113A for Strain History - 2

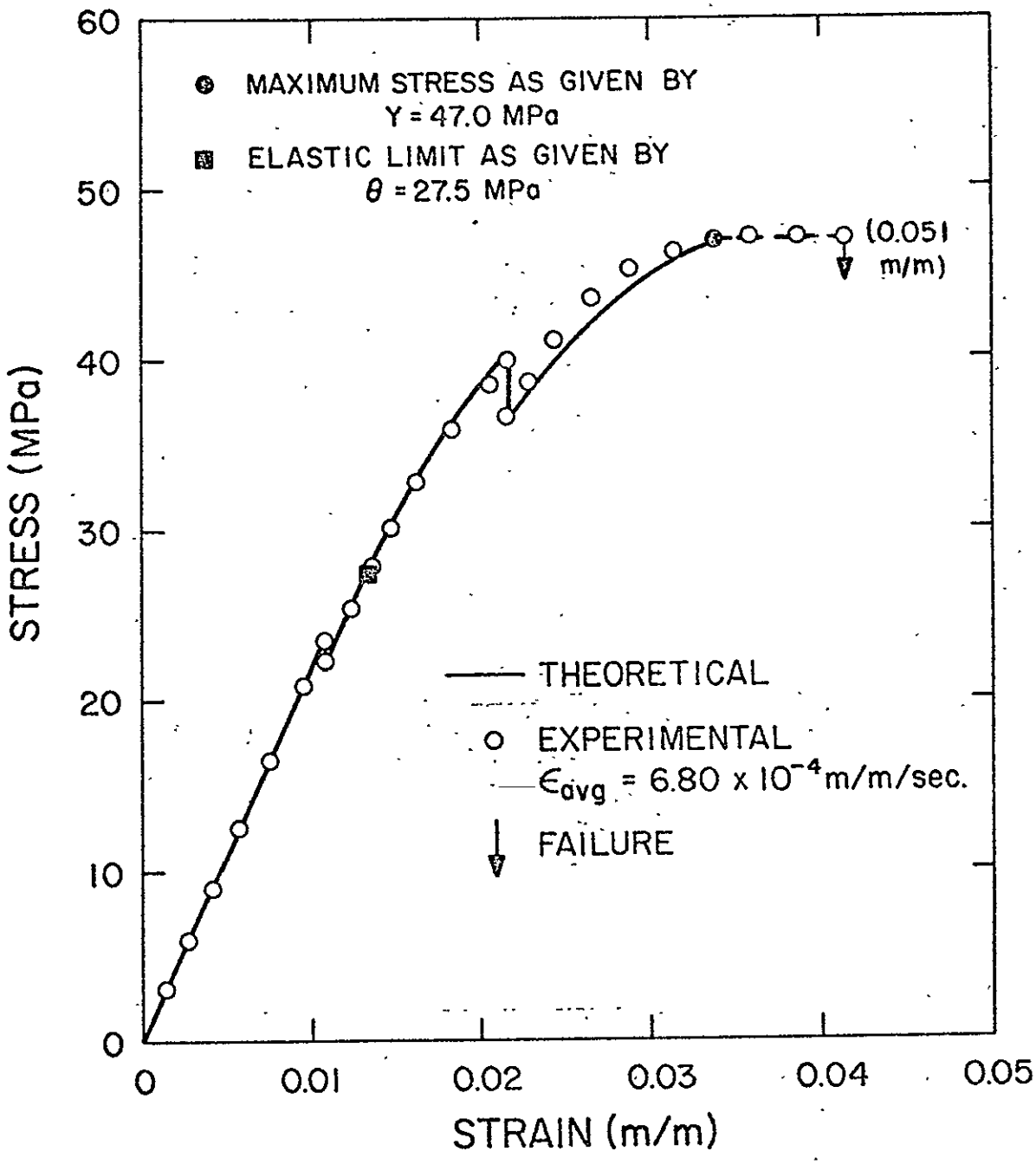

Figure 56. Theoretical and Experimental Stress-Strain Response of Metlbond 1113A for Strain History - 2

Chapter 7

ELEVATED TEMPERATURE BEHAVIOR

The mechanical properties of polymeric materials have a very strong dependence upon temperature. At least three distinct regions of behavior can be observed for a cross-linked polymer when the temperature is varied [31]. These are the glassy region, the transition region, and the rubbery plateau. The region which is of most interest in viscoelasticity is the transition zone, as time effects are especially pronounced in this region. Time effects are only observed over a long period of time (many decades of time) in the glassy range, whereas events occur so rapidly in the rubbery range that they are difficult to observe in an actual test.

The regions above can be established by conducting relaxation tests at various temperatures and then plotting the relaxation modulus versus temperature for a given time. For such tests, high-modulus glassy-type behavior will be characteristic of the glassy region, while low-modulus rubbery-type behavior will be characteristic of the rubbery region. Results for Metlbond 1113A and 1113-2A are presented in Figs. 57 and 58, respectively. It was found that both adhesives exhibited definite glassy and rubbery regions. It can be observed that these regions encompass the same temperature ranges for both adhesives. This indicates that the carrier cloth had little effect as to the temperature dependence of these regions.

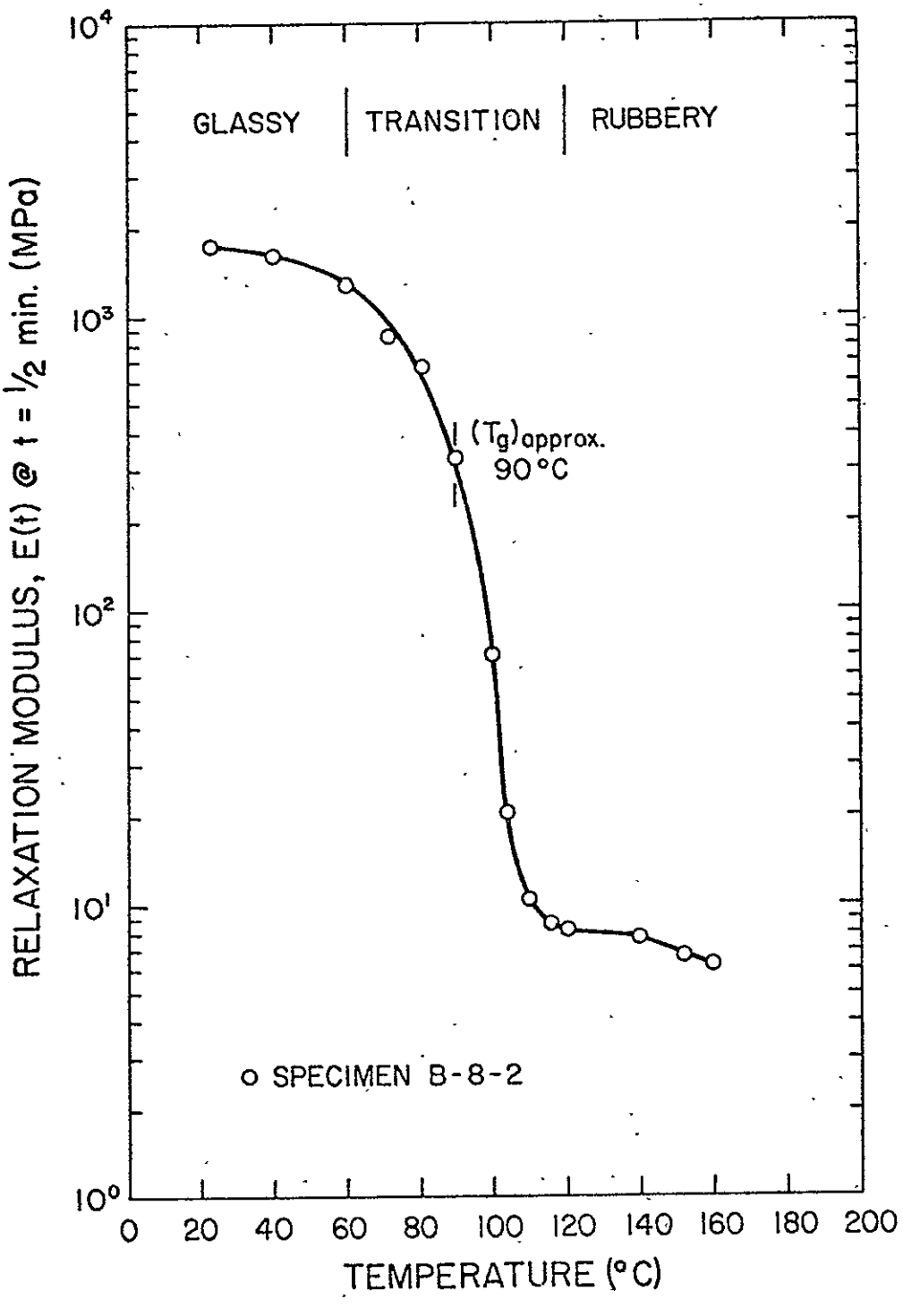

Figure 57. Variation in Relaxation Modulus with Temperature for Metlbond 1113A

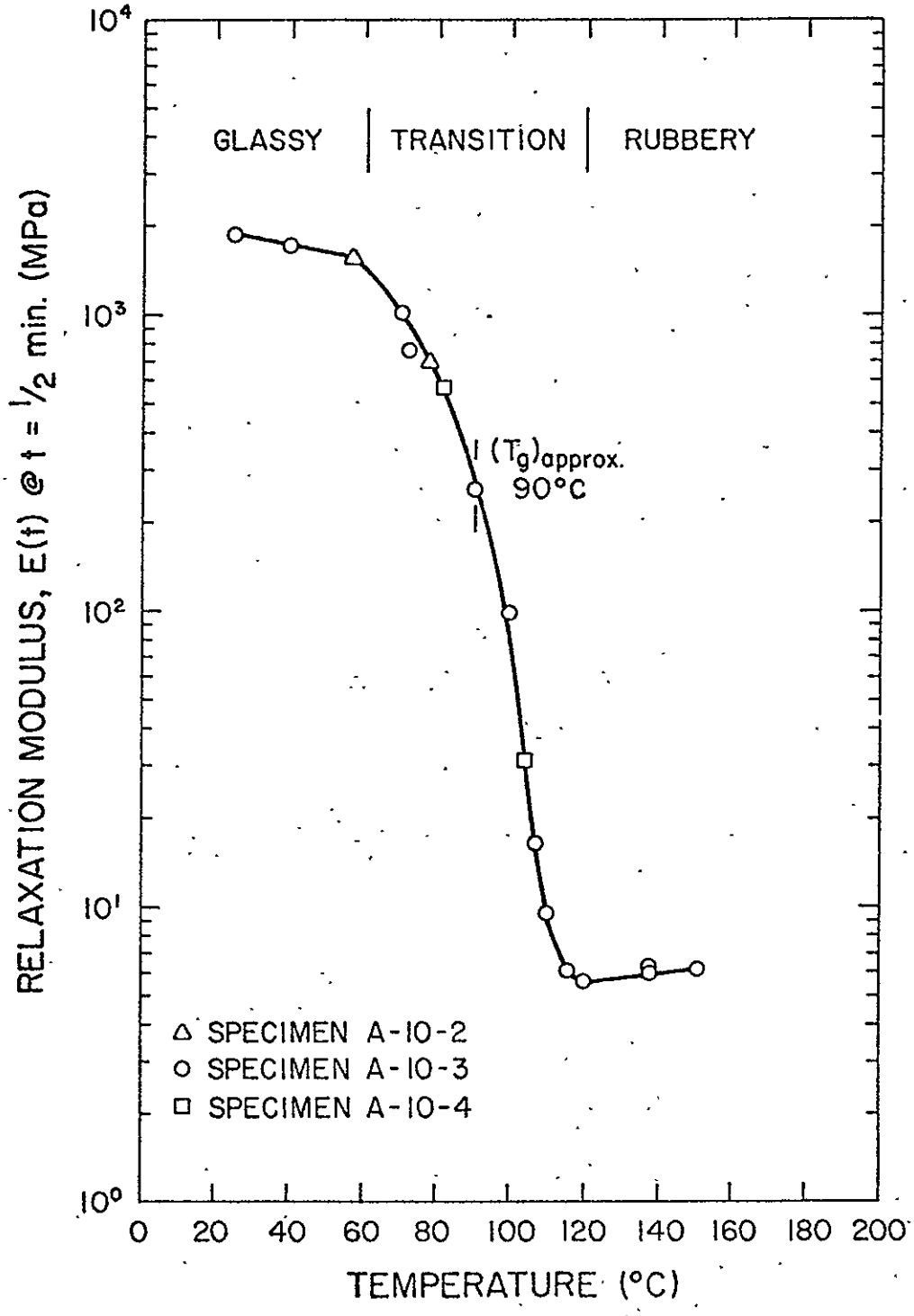

Figure 58. Variation in Relaxation Modulus with Temperature for Metlbond 1113-2A

The region where the modulus has the greatest dependence upon temperature (maximum magnitude of slope), is the transition region. Within this region a corresponding temperature, or narrow temperature range, is designated as the glass transition temperature T_g. The glass transition temperature is located near the beginning of the transition zone [32]. The value of T_g is approximately 90° C for both adhesives.

7.1 Time-Temperature Superposition

A statement of the time-temperature superposition principle is given by the equation [31],

$$E(t',T_0) = \frac{\rho_0}{\rho}\frac{T_0}{T} E(t = a_T t',T) \qquad (7.1.1)$$

where ρ represents the density of the material at temperature T and a_T is the "shift factor." This equation indicates that the relaxation modulus at the reference temperature T_0 and time t' can be obtained from the relaxation modulus measured at temperature T and time t. On a plot of modulus versus logarithmic time, this amounts to a vertical shift of the magnitude $\rho_0 T_0/\rho T$ and a horizontal shift of the magnitude log a_T. Although time-temperature superposition is applicable to other viscoelastic response (creep, dynamic, etc.), it is usually illustrated with stress relaxation, since most of the early development was done with stress relaxation [33].

The relaxation results were reduced by the factor T_0/T (the factor ρ_0/ρ was neglected as is frequently done in the literature [34]) and

are shown plotted in Figs. 59 and 60 for Metlbond 1113A and 1113-2A, respectively. The reduced curves were shifted laterally to obtain a master curve for a reference temperature of $T_o = T_g \simeq 90°$ C. It can be observed that this procedure yields a smooth continuous curve which represents the stress relaxation at 90° C over thirteen decades of time. Multiplication by the appropriate value of a_T then establishes the master curve at any other temperature and can thus be used to predict response at that temperature over the entire time scale.

7.1.1 WLF Equation

For many polymeric materials it has been found that if the polymer's glass transition temperature is chosen as the reference temperature, the shift factors are given, to a good approximation, by the Williams-Landel-Ferry (WLF) equation [31],

$$\text{Log } a_T = \frac{-C_1(T - T_g)}{C_2 + (T - T_g)} \qquad (7.1.2)$$

where $C_1 = 17.44$ and $C_2 = 51.6$. Eq. (7.1.2) is only valid from T_g up to approximately $T_g + 100°$ C since Eq. (7.1.1) cannot be proven to be valid for temperatures lower than T_g [31]. However, most researchers believe the time-temperature superposition principle is valid below the T_g--exactly how far below no one has ascertained [32]. For this reason, results for $T < 70°$ C are not shifted in Figs. 59 and 60.

The values of a_T used to superpose the various curves in Figs. 59 and 60 are compared with the WLF equation in Figs. 61 and 62, respectively. Although the WLF equation does not adequately fit the

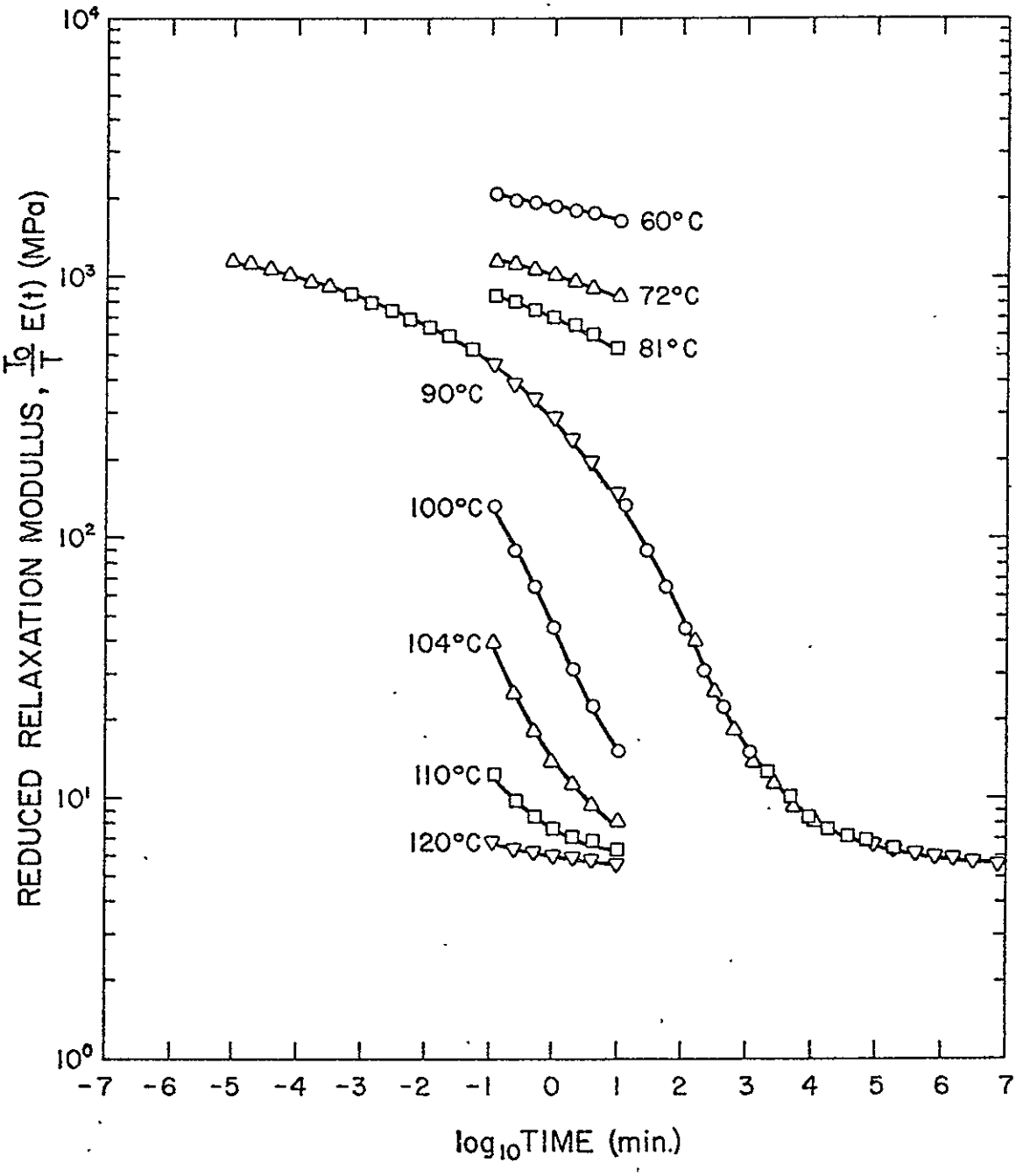

Figure 59. Master Curve of Relaxation Modulus for T_0 = 90° C for Metlbond 1113A

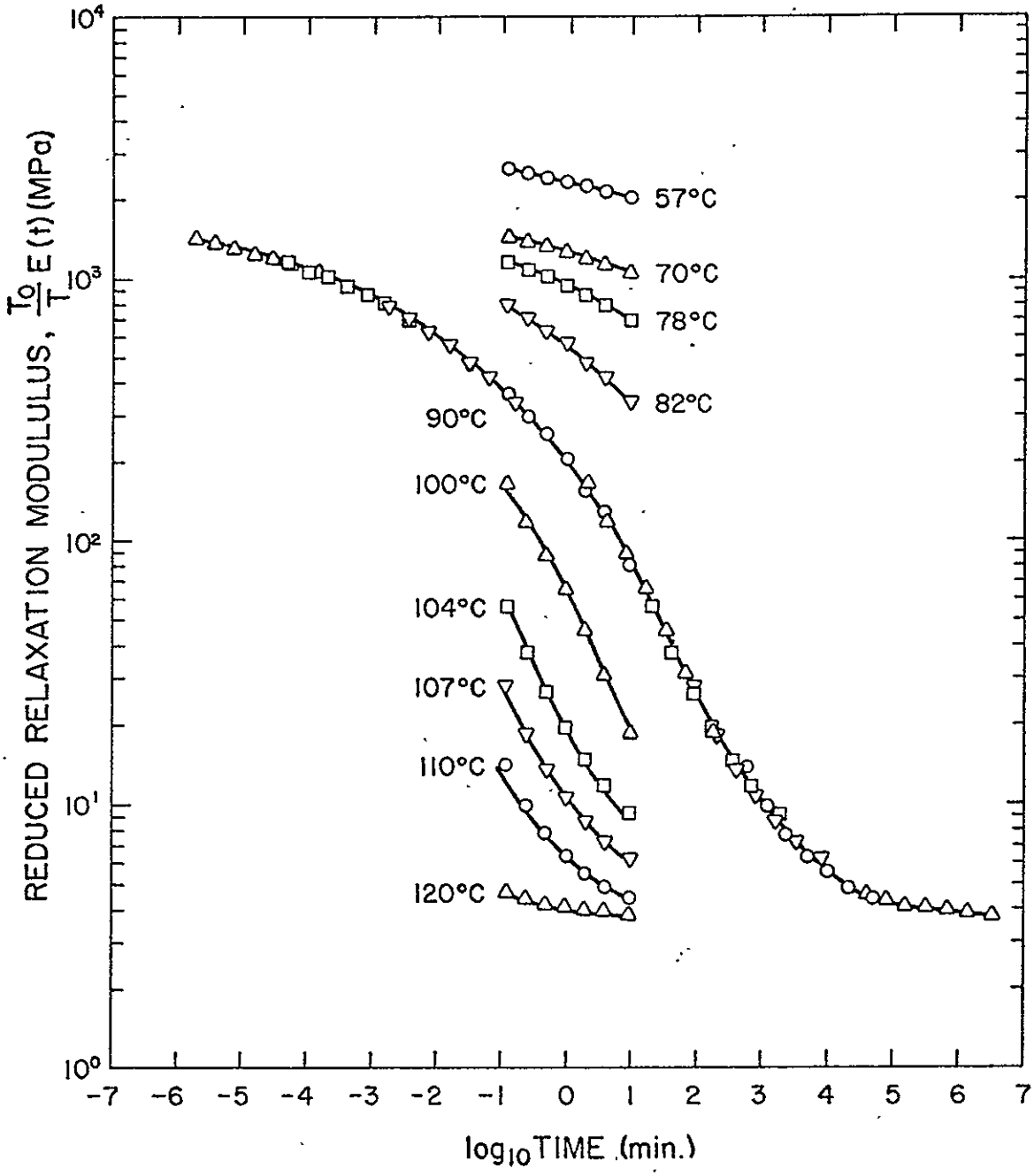

Figure 60. Master Curve of Relaxation Modulus for T_o = 90° C for Metlbond 1113-2A

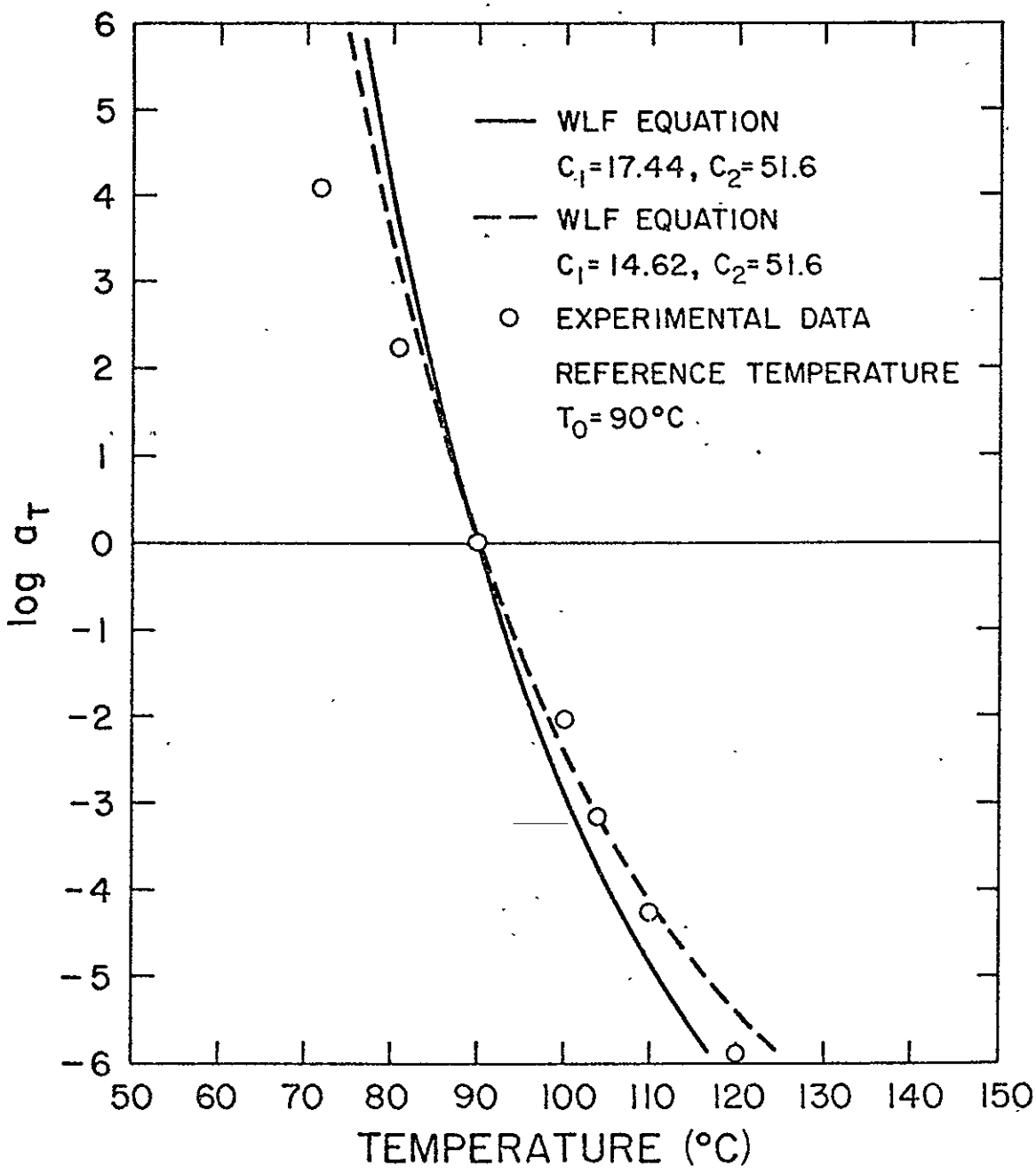

Figure 61. Comparison Between Experimental Data and WLF Equation for Metlbond 1113A

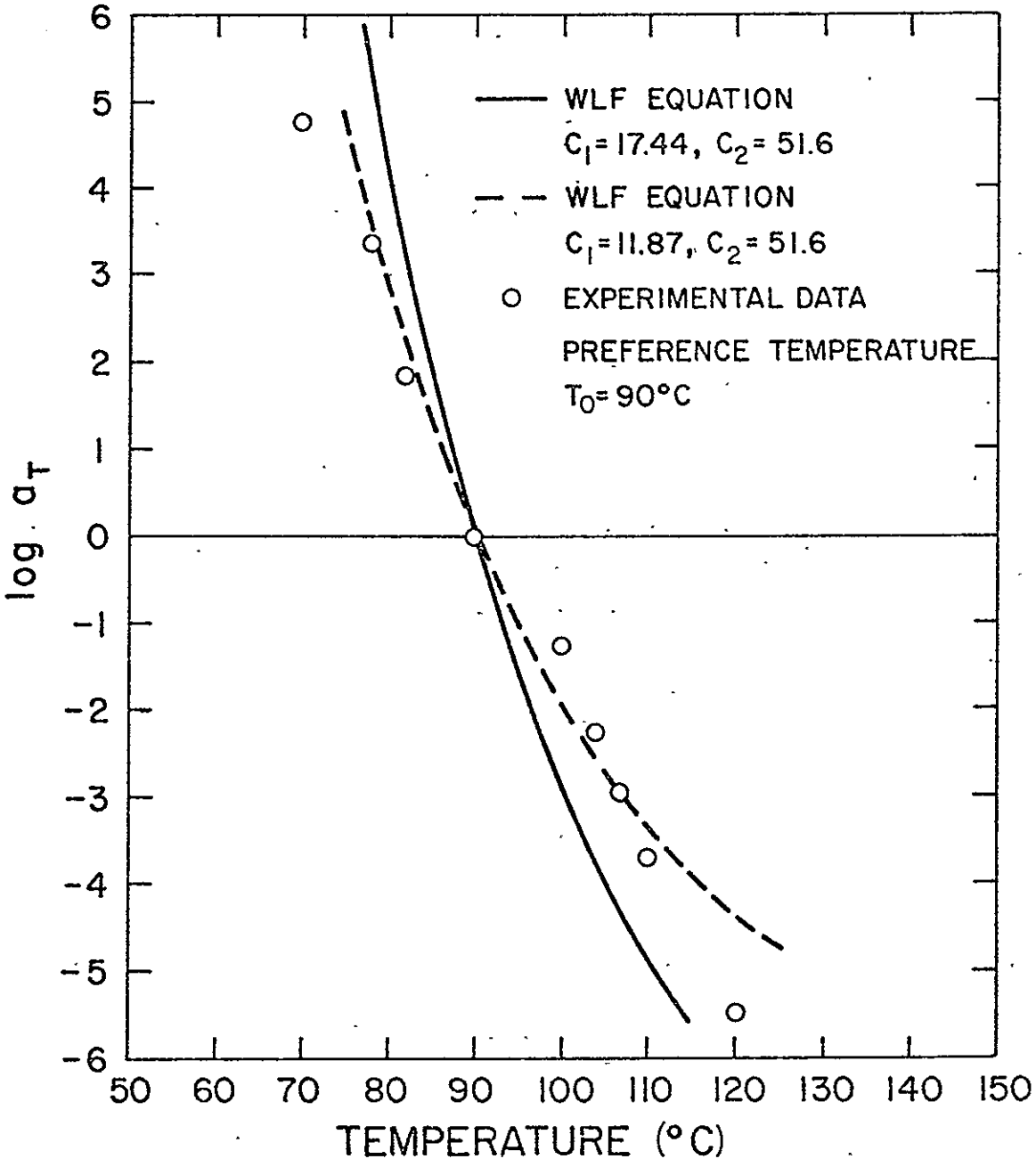

Figure 62. Comparison Between Experimental Data and WLF Equation for Metlbond 1113-2A

experimental results, the shapes of these curves are similar, indicating that C_1 in the WLF equation should not be taken as $C_1 = 17.44$. If the constant C_1 is adjusted for each adhesive (as given in Figs. 61 and 62), the curve for the WLF equation is brought into reasonably close agreement to the experimental results. For $t < 70°$ C and $t > 120°$ C the experimental shift factors begin to diverge considerably from the WLF equation, indicating that the WLF equation is invalid outside of these temperatures. It should be pointed out, however, that it is possible for a shift factor to exist even though the WLF equation is not satisfied [32].

Chapter 8

CONCLUSIONS

The present investigation has been concerned with the stress-strain, strain rate, creep, relaxation, yield and failure properties of two structural adhesives used in composite applications. Loading-unloading and elevated temperature behavior have also been studied.

In summary of the achievements of this study, the following conclusions can be made.

(1) Bulk form testing is a viable means of obtaining mechanical properties of structural adhesives.

(2) Metlbond 1113 and 1113-2 adhesives exhibit both rate and time dependent behavior. It was observed that the elastic limit stress and strain, and maximum stress are rate dependent; this behavior is accurately predicted using an equation proposed by Ludwik for yielding. The viscosity coefficient, μ, is also rate dependent. This phenomenon is indicated by the analogous constitutive form of the modified Bingham model derived from incremental theory, Eqs. (2.3.5).

(3) A stress-whitening phenomenon which is observed in the adhesives at high stress levels is attributed to crazing. The material in the crazed area is less dense than the virgin material. The properties of the adhesives are different after stress-whitening with a resulting increase in plastic flow and decrease in Poisson's ratio.

(4) Higher strength is observed in Metlbond 1113 as compared to Metlbond 1113-2 due to the presence of the carrier cloth. This carrier cloth also tends to stabilize Metlbond 1113 as failure strains during the rate tests are less random and Poisson's ratios above the stress-whitening level are relatively constant.

(5) It is shown that constitutive equations postulated by early investigators based on experimental results can be derived from existing theories and mechanical models.

(6) The proposed bilinear forms of the Ramberg-Osgood model, Eqs. (5.3.5) and (5.3.9), accurately predict the rate behavior of the adhesives. These models indicate that the material coefficients are different before and after stress-whitening due to changes in the material properties. The bilinear forms predict an accurate representation of the slope of the stress-strain curves which is essential when incremental formulations are used in advanced analyses.

(7) The modified Bingham model, Eqs. (5.4.1), accurately predicts the rate behavior of the adhesives. This model gives an accurate representation of the slope without having to change material coefficients before and after the stress-whitening point. This model also has the advantage of predicting perfectly plastic flow once the maximum stress is reached; such behavior is exhibited by the experimental results. It is felt, therefore, that of all models

investigated, the modified Bingham model is the preferred one for representing the rate behavior of the adhesives.

(8) The nonlinear form of the modified Bingham model, Eqs. (5.4.3), indicates that the coefficients of the linear model may vary due to the change in material properties before and after the stress-whitening point. The nonlinearities present, however, are small and thus the variations in the coefficients would also be small.

(9) A creep to failure phenomenon is observed that can be predicted using a technique proposed by Crochet coupled with the modified Bingham model.

(10) The proposed form of the loading-unloading equations for the modified Bingham model, Eqs. (3.3.3), predicts the loading-unloading behavior of the adhesives reasonably well.

(11) Initial results of relaxation tests at elevated temperatures indicate that the adhesives follow the time-temperature superposition principle.

(12) This study should give insight into rate and time dependent behavior of other adhesives and polymeric matrix materials used in advanced composites as they are frequently similar in composition to the adhesives investigated herein.

Future work may be to compare the bulk properties of structural adhesives to those in the bonded state. An initial step would be to compare properties for single lap shear specimens to those for bulk shear specimens. Future endeavors in the area of loading-unloading

behavior should be very worthwhile. The effect of temperature on the rate properties should also prove to be an interesting area of future research. Results from these tests could be correlated to those from the relaxation tests conducted at elevated temperatures herein.

BIBLIOGRAPHY

1. Bowers, R. C. and Zisman, W. A., "Surface Properties," Engineering Design for Plastics, (E. Baer, Ed.), Reinhold Book Corp., New York, 1964, p. 689-741.

2. Lee, L. H. (ed.), Recent Advances in Adhesion, Gordon and Breach, New York, 1973.

3. Brinson, H. F., Renieri, M. P., and Herakovich, C. T., "Rate and Time Dependent Failure of Structural Adhesives," Fracture Mechanics of Composites, ASTM STP 593, American Society for Testing and Materials, 1975, pp. 177-199.

4. Davis, J. L., "An Elementary Theory of Nonlinear Viscoelasticity," Journal of Polymer Science, Part A, Vol. 2, pp. 1311-1320, 1964.

5. Perzyna, P., "Fundamental Problems in Viscoplasticity," Adv. in Applied Mechanics, 9, pp. 243-377, 1966.

6. Hencky, H. Z., "Zur Theorie Plastischer Deformationen und der hiedurch im Material hervorgerufenen Nachspannungen," Z. Angew. Math: Mech., 4, 1924, pp. 323-334.

7. Kachanov, L. M., Foundations of the Theory of Plasticity, North-Holland Publishing Co., Amsterdam, 1971.

8. Hill, R., The Mathematical Theory of Plasticity, Oxford University Press, London, 1956.

9. Ramberg, W. and Osgood, W. R., "Description of Stress-Strain Curves by Three Parameters," NACA TN 902, April, 1943.

10. McLellan, D. L., "Constitutive Equations for Mechanical Properties," AIAA, Vol. 5, No. 3, 1966.

11. McLellan, D. L. and Eichenberger, T. W., "A Description of Strain Rate Effects on the Compressive Behavior of Pure Aluminum," Applied Polymer Symposia, No. 5, pp. 185-204, 1967.

12. McLellan, D. L., "Prediction of Stress-Strain Behavior at Various Strain Rates and Temperatures," Applied Polymer Symposia, No. 12, pp. 137-163, 1969.

13. Zabora, R. F., Clinton, W. W., and Bell, J. E., "Adhesive Property Phenomena and Test Techniques," AFFDL-TR-71-68, July 1971.

14. Prandtl, L., "Spannungsverteilung in plastichen Koerpern," Proceedings of the 1st International Congress on Applied Mechanics, Delft, Technische Boekhandel en Druckerij, J. Waltman, Jr., pp. 43-54, 1925.

15. Reuss, E., "Beruecksichtigung der elastischen Formae nderungen in der Plastizitaetstheorie," Z. Angew. Math. Mech., pp. 266-274, 1930.

16. Mendelson, A., Plasticity: Theory and Application, MacMillan Company, New York, 1968.

17. Hohenemser, K. and Prager, W., "Uber die Ansatze der Mechanik isotroper Kontinua," Zeitschrift f. angew. Math. u. Mech. 12, pp. 216-226, 1932.

18. Freudenthal, A. M., "The Mathematical Theories of the Inelastic Continuum," Handbuch der Physik VI, Springer-Verlag, Berlin, 1958.

19. Perzyna, P., "The Constitutive Equations for Rate Sensitive Plastic Materials," Quarterly of Applied Mathematics, Vol. 20, p. 321, 1963.

20. Malvern, L. E., "The Propagation of Longitudinal Waves of Plastic Deformation in a Bar of Material Exhibiting a Strain-Rate Effect," Journal of Applied Mechanics, Vol. 18, pp. 203-208, 1951.

21. Sokolovsky, V. V., "The Propagation of Elastic-Viscous-Plastic Waves in Bars," Prikladnaia Mathematika i Mekhanika, Vol. 12, pp. 261-280, 1948 (Russian).

22. Chase, K. W. and Goldsmith, W., "Mechanical and Optical Characterization of an Anelastic Polymer at Large Strain Rate and Large Strains," Experimental Mechanics, Jan. 1974, pp. 10-18.

23. Brinson, H. F., "The Viscoelastic-Plastic Behavior of a Ductile Polymer," Deformation and Fracture of High Polymers, (H. H. Kaush, et al., eds.), Plenum Press, New York, 1973, p. 397.

24. Brinson, H. F. and DasGupta, A., "The Strain Rate Behavior of Ductile Polymers," SESA Paper No. 2256, presented at the SESA Fall Meeting, Indianapolis, Ind., Oct. 16-19, 1973.

25. Metlbond 1113 Adhesive Product Information Brochure, Narmco Materials Division, Whittaker Corporation, Costa Mesa, California.

26. Wilson, III, G. H. and Herakovich, C. T., "Application of a Dedicated Micro-processor for Automatic Data Acquisition of Load, Strain, and Acoustic Emission Data," Experimental Mechanics, March 1976, pp. 111-115.

27. Ludwik, P. G., Elemente der Technologischen Mechanik, J. Springer, Berlin, 1909, p. 9.

28. Hashin, Z., Bagchi, D., and Rosen, B. W., "Non-linear Behavior of Fiber Composite Laminates," NASA CR-2313, 1973.

29. Kibler, J. J., "Nolin--A Nonlinear Laminate Analysis Program," NASA-CR-2410, 1974.

30. Renieri, G. D., Present work on Ph.D. dissertation; and communication.

31. Ferry, J. D., Viscoelastic Properties of Polymers, John Wiley and Sons, Inc., New York, 1961.

32. Brinson, H. F., "Mechanical and Optical Viscoelastic Characterization of Hysol 4290," Experimental Mechanics, December, 1968.

33. Rosen, S. L., Fundamental Principles of Polymeric Materials for Practicing Engineers, Barnes and Noble, Inc., New York, 1971.

34. Nielsen, L. E., Mechanical Properties of Polymers, Reinhold Publishing Corp., New York, 1962.

APPENDICES

See: M. P. Renieri, "Rate and Time Dependent Behavior of Structural Adhesives", Ph.D. Dissertation, Virginia Polytechnic Institute and State University, June, 1976.

DISTRIBUTION LIST

Professor David M. Barnett
Dept. of Materials Science
Stanford University
Standford, CA 94305

Dr. Lynn Ebert
Case Western Reserve University
10900 Euclid Avenue
Cleveland, OH 44106

Professor Fazil Erdogan
Lehigh University
Dept. of Mechanical Engr. & Mechanics
Bethlehem, PA 18015

Dr. Melvin F. Kanninen
Battelle
Columbus Laboratories
505 King Avenue
Columbus, OH 43210

Dr. Anthony Kelly
Imperial Chemical Industries, Ltd.
Research and Development Dept.
Imperial Chemical House
Millbank London SW1P 3JF

Dr. Edward J. McQuillen
Structures Division
Air Vehicle Technology Dept.
Naval Air Development Center
Warminster, PA 18974

Dr. Nicholas J. Pagano
WPAFB/MBM
Wright Patterson Air Force Base
OH 45433

Dr. R. Byron Pipes
Dept. of Mechanical and Aerospace Engr.
107 Evans Hall
University of Delaware
Newark, DE 19711

Dr. Alan R. Rosenfield
Battelle
Columbus Laboratories
505 King Avenue
Columbus, OH 43201

Dr. Edmund F. Rybicki
Battelle
Columbus Laboratories
505 King Avenue
Columbus, OH 43201

Dr. E. Scala
Cortland Advanced Products
P.O. Box 1362
Cortland, NY 13045

Dr. George P. Sendeckyj
Structures Division
Air Force Flight Dynamics Lab.
Wright-Patterson Air Force Base
OH 45433

Professor George C. Sih
Dept. of Mechanical Engineering &
Mechanics
Lehigh University
Bethlehem, PA 18015

Dr. William J. Walker
Airforce Office of Scientific Res.
1400 Wilson Boulevard
Arlington, VA 22209

Dr. Dell P. Williams
Materials Science Branch
Mail Stop 240-1
NASA-Ames Research Center
Moffett Field, CA 94035

Dr. Carl H. Zweben
Textile Fibers Dept.
E. I. DuPont de Nemours & Company, Inc.
Experimental Station/B262
Wilmington, DE 19898

Dr. B. W. Rosen
Materials Science Corporation
Blue Bell Office Campus
Blue Bell, PA 19422

Dr. S. V. Kulkarni
Materials Sciences Corporation
Blue Bell Office Campus
Blue Bell, PA 19422

Dr. S. W. Tsai
Nonmetallic Materials Division
Air Force Materials Laboratory
Wright-Patterson Air Force Base
Ohio

Dr. J. M. Whitney
Nonmetallic Materials Division
Air Force Materials Laboratory
Wright-Patterson Air Force Base
OH

Prof. R. A. Schapery
Civil and Aerospace Engineering Dept.
Texas A & M University
College Station, TX 77840

Dr. John G. Davis, Jr.
Mail Code No. 188A
Langley Research Center
Hampton, VA 23665

Mr. Herbert F. Hardrath
Mail Code 188M, Bldg. No. 1205
Materials Division
Langley Research Center
Hampton, VA 22065

Dr. I. M. Daniel, Manager
IIT Research Institute
10 West 35 Street
Chicago, IL 60616

Mr. Sidney J. Green, President
Terra Tale, Inc.
420 Wakara Way
Salt Lake City, UT 84108

Dr. Roger Heimbach
Metals Engr. Department
G. M. Manufacturing & Development
Warren, MI 48090

Mr. R. H. Marloff
Research & Development
1310 Beulah Road
Pittsburgh, PA 15230

Mr. Clayton A. May
Lockheed Missiles & Space Company
1111 Lockheed Way
Orgn 4201 Bldg. 150
Sunnyvale, CA 94088

Dr. R. Williams
Scientific Analysis Group
Draft & Whitney Aircraft
Division of United Aircraft Corp.
East Hartford, CT 06118

NASA Scientific and Technical
Inforamtion Facility
P.O. Box 8757
Baltimore/Washington International
Airport
Baltimore, MD 21240

Dr. Larry Roderick
Langley Research Center
Mail Stop 188E
Hampton, VA 23665

Dr. Frank Crossman
Lockheed Research Lab
Org. 52-41, Bldg. 204
3251 Hanover Street
Palo Alto, CA 94034

Mr. M. E. Waddoups
General Dynamics Corp.
Fort Worth, Texas 76101

Dr. J. C. Halpin
Flight Dynamics Lab.
Wright-Patterson Air Force Base
OH 45433

Prof. D. H. Morris Drawer ME
Mississippi State
State College, MS 39762

Professor J. W. Dally
Dept. of Mech. Engr.
U. of Maryland
College Park, MD 20742

Dr. Longin B. Greszczuk
McDonnell Douglass Astronautics Co.
5301 Bolsa Avenue
Huntington Beach, CA 92647

Professor R. E. Rowlands
Dept. of Engineering Mechanics
University of Wisconsin
Madison, WI 53706

Dr. R. L. Foye
U.S. Army Mobility Res. & Dev. Laboratory
Langley Research Center, Mail Stop 188A
Hampton, VA 22065

Dr. John R. Davidson
Mail Code 188E
MD-Structural Integrity Branch
Langley Research Center
Hampton, VA 23665

Dr. Darrell R. Tenney
Mail Code 188M
MD-Materials Research Branch
Langley Research Center
Hampton, VA 22065

Dr. T. A. Cruse
Scientific Analysis Group
Pratt & Whitney Aircraft
Division of United Aircraft Corp.
East Hartford, CT 06118

Professor Donald F. Adams
Dept. of Mechanical Engineering
University of Wyoming
Larmie, WY 82070

Professor Phil Hodge
107 Aeronautical Engineering Bldg.
University of Minnesota
Minneapolis, Minnesota 55455

Mr. Glenn C. Grimes, Engr. Specialist
Structures R & T, Dept. 3780/62
Northrop Corp., Aircraft Div.
3901 W. Broadway
Hawthorne, CA 90250

Dr. Martin M. Mikulas
Mail Stop 190
NASA-Langley
Hampton, VA 23665

Dr. Paul A. Cooper
Mail Stop 208
NASA-Langley
Hampton, VA 23665

Mr. Dale Black
NARMCO Materials Division
Whittaker Corporation
600 Victoria Street
Costa Mesa, CA 92627

Mr. Edward L. Hoffman
Mail Stop 188A
NASA-Langley Research Center
Hampton, VA 23665

Dr. N. J. Johnson
Mail Stop 226
NASA-Langley Research Center
Hampton, VA 23665

Dr. Michael F. Card
Mail Stop 190
NASA-Langley Research Center
Hampton, VA 23665